

2

AD A 074310

THE ⁽¹¹⁾B(p,n)⁽¹¹⁾C REACTION: MEASUREMENTS OF DIFFERENTIAL CROSS SECTIONS AT PROTON ENERGIES BETWEEN 3.1 AND 4.5 MeV, AND APPLICATIONS TO DEPTH PROFILING,

Captain Richard Philip Ebright
HQDA, MILPERCEN (DAPC-OPP-E)
200 Stovall Street
Alexandria, VA 22332

DDDC
RECEIVED
SEP 26 1979
E

9
Final report, 24 August 1979

11 24 Aug 79

Approved for public release; distribution unlimited.

12 109p.

A thesis submitted to University of Oregon, Eugene, Oregon, in partial fulfillment of the requirements for the degree of Master of Science in Physics.

This document has been approved for public release and sale; its distribution is unlimited.

79 09 24 133

391 191

PII Redacted

JP

REPORT DOCUMENTATION PAGE		READ INSTRUCTIONS BEFORE COMPLETING FORM
1. REPORT NUMBER	2. GOVT ACCESSION NO.	3. RECIPIENT'S CATALOG NUMBER
4. TITLE (and Subtitle) THE $^{11}\text{B}(p,n)^{11}\text{C}$ REACTION: MEASUREMENT OF DIFFERENTIAL CROSS SECTIONS AT PROTON ENERGIES BETWEEN 3.1 AND 4.5 MeV, AND APPLICATIONS TO DEPTH PROFILING		5. TYPE OF REPORT & PERIOD COVERED FINAL REPORT, 24 AUGUST 1979
7. AUTHOR(s) Cpt. Richard Philip Ebright		6. PERFORMING ORG. REPORT NUMBER
9. PERFORMING ORGANIZATION NAME AND ADDRESS Student, HQDA MILPERCEN (DAPC-OPP-E) 200 Stoval street Alexandria Va 22332		8. CONTRACT OR GRANT NUMBER(s)
11. CONTROLLING OFFICE NAME AND ADDRESS HQDA MILPERCEN, ATTN: DAPC-OPP-E 200 Stoval street Alexandria Va 22332		10. PROGRAM ELEMENT, PROJECT, TASK AREA & WORK UNIT NUMBERS
14. MONITORING AGENCY NAME & ADDRESS (if different from Controlling Office)		12. REPORT DATE 24 August 1979
		13. NUMBER OF PAGES 102
		15. SECURITY CLASS. (of this report) UNCLASSIFIED
		15a. DECLASSIFICATION/DOWNGRADING SCHEDULE
16. DISTRIBUTION STATEMENT (of this Report) APPROVED FOR PUBLIC RELEASE; DISTRIBUTION UNLIMITED		
17. DISTRIBUTION STATEMENT (of the abstract entered in Block 20, if different from Report)		
18. SUPPLEMENTARY NOTES THESIS SUBMITTED TO UNIVERSITY OF OREGON		
19. KEY WORDS (Continue on reverse side if necessary and identify by block number) NUCLEAR PHYSICS, NUCLEAR CROSS SECTIONS, ANGULAR DISTRIBUTIONS - 2008 BORON - 0702 , NEUTRON SPECTROMETRY - 0804 CONCENTRATION - 0704 , DEPTH, PROFILING -1407		
20. ABSTRACT (Continue on reverse side if necessary and identify by block number) Thick target neutron time-of-flight techniques have been used to study the $^{11}\text{B}(p,n)^{11}\text{C}$ reaction at proton energies from threshold to 4.5 MeV. Neutron time-of-flight spectra were obtained at laboratory angles of $0^\circ, 20^\circ, 31^\circ, 50^\circ, 69.8^\circ, 80.3^\circ, 90^\circ, 100^\circ, 114^\circ, 138.2^\circ, 155^\circ$, and converted to cross sections averaged over 10 KeV intervals in proton energy. Targets of polycrystalline boron and B_2O_3 were used. Boron concentrations in Si and SiO_2 targets of otherwise known composition		

were determined using the $^{11}\text{B}(p,n)^{11}\text{C}$ reaction with neutron time-of-flight techniques. The concentration was determined by taking the ratio of neutron time-of-flight spectra from a pure B metal target and a target of unknown boron content. This technique was applied to a Si wafer implanted in the $\langle 100 \rangle$ direction with 200 KeV atoms.

Less than
or
More than
100

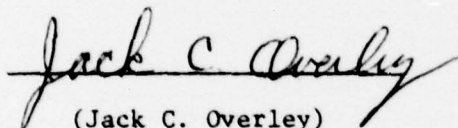
79 09 24 133

An Abstract of the Thesis of

Richard Philip Ebricht for the degree of Master of Science
in the Department of Physics to be taken September 1979

Title: The $^{11}\text{B}(p,n)^{11}\text{C}$ Reaction: Measurement of Differential Cross
Sections at Proton Energies Between 3.1 and 4.5 MeV, and
Applications to Depth Profiling

Approved:


(Jack C. Overley)

Thick target neutron time-of-flight techniques have been used to study the $^{11}\text{B}(p,n)^{11}\text{C}$ reaction at proton energies from threshold to 4.5 MeV. Neutron time-of-flight spectra were obtained at laboratory angles of 0° , 20° , 31° , 50° , 69.8° , 80.3° , 90° , 100° , 114° , 138.2° , and 155° , and converted to cross sections averaged over 10 KeV intervals in proton energy. Targets of polycrystalline boron and B_2O_3 were used.

Boron concentrations in Si and SiO_2 targets of otherwise known composition were determined using the $^{11}\text{B}(p,n)^{11}\text{C}$ reaction with neutron time-of-flight techniques. The concentration was determined by taking the ratio of neutron time-of-flight spectra from a pure B metal target and a target of unknown boron content. This technique was applied to a Si wafer implanted in the $\langle 100 \rangle$ direction with 200 KeV ^{11}B atoms.

THE $^{11}\text{B}(p,n)^{11}\text{C}$ REACTION: MEASUREMENT
OF DIFFERENTIAL CROSS SECTIONS AT PROTON ENERGIES
BETWEEN 3.1 AND 4.5 MeV, AND APPLICATIONS TO DEPTH PROFILING

by
RICHARD PHILIP EBRIGHT

A THESIS

Presented to the Department of Physics
and the Graduate School of the University of Oregon
in partial fulfillment
of the requirement for the degree of
Master of Science

September 1979

Approved/Editor	
Reviewed/Editor	
DDO/Editor	
Unannounced	
Justification	
By	
Distribution/	
Availability Codes	
Dist	
Avail and/or special	

A

Approved: Jack C. Overley
(Jack C. Overley)

VITA

NAME OF AUTHOR: Richard Philip Ebright

PII Redacted

UNDERGRADUATE AND GRADUATE SCHOOLS ATTENDED:

California State University at San Jose, San Jose, California
University of Oregon, Eugene, Oregon

DEGREES AWARDED:

Bachelor of Science, 1973, California State University, San Jose
Master of Science, 1979, University of Oregon, Eugene

AREA OF SPECIAL INTEREST:

Nuclear Physics and Chemistry

PROFESSIONAL EXPERIENCE:

Research Assistant, Department of Physics, University of Oregon
Eugene, Oregon, 1977-1979

PUBLICATIONS:

"Concentration Profiling of Boron in Solids by Neutron Time-of-Flight,"
IEEE Transactions on Nuclear Science, NS-26, 1624, (1979).

ACKNOWLEDGEMENTS

I would like to thank Dr. Jack C. Overley for his assistance, guidance and support throughout all aspects of this project. Without his help this thesis would not have been possible. I would also like to thank Dr. H. W. Lefevre for his assistance in data collection and stimulating comments, Greg Sieger for his advice and help in drawing the diagrams, Hsiao-Yuan Wu for her comments, Dr. R. M. Sealock and Dr. C. A. Burke for computer programs and J. D. MacDonald for his technical assistance. I would like to thank Dr. D. Dean Casey of Tektronics, Inc. for providing us with the boron implanted silicon targets.

I especially wish to thank my wife and family for enduring the stress of the long hours I have spent away from them over the past two years, and for providing the essential moral support.

I would like to acknowledge the support I have received from the United States Army Chemical Corps who made it possible for me to study Nuclear Physics.

This work was supported in part by the United States Department of Army and the National Science Foundation.

R. P. E.

DEDICATED

TO

Kathy, Shawn, Shannon, and David

TABLE OF CONTENTS

	<u>Page</u>	
Chapter I	Introduction	1
Chapter II	Experimental Methods	4
	A. Thick Target Kinematics	4
	B. Transformation Equations	5
Chapter III	Experimental Detail	8
	A. Hardware	8
	B. Data Acquisition	12
Chapter IV	Data Analysis for Cross section	17
	A. Determination of Neutron Detector Efficiency	17
	B. Conversion of Time-of-Flight Spectra to Cross Section	21
Chapter V	Cross Section Analysis	23
	A. Results and Discussion	23
	B. Uncertainties	30
	C. Summary	33
Chapter VI	Profiling	35
	A. Theory	35
	B. Resolution Analysis	39
	C. Sensitivity	42
	D. Conclusions	53

TABLE OF CONTENTS (continued)

	<u>Page</u>
Appendix A Differential Cross Sections and Associated Statistical Uncertainty for the $^{11}\text{B}(p,n)^{11}\text{C}$ Reaction	56
Appendix B Legendre Power Series Coefficients and Associated Statistical Errors	65
Appendix C Program TOF-NE	69
Appendix D Program B11PNX, Subroutines KINSUB and FIT2	72
Appendix E Program LSQFT3, Subroutines CBFIT8, LEGPOL and MINV7	78
Appendix F Program SIBPRP and Subroutine HISTO	87
References	90

LIST OF FIGURES

<u>Figure</u>		<u>Page</u>
1	Energy level diagram of the ^{12}C compound nucleus.	2
2	Block diagram of the electronics used in the determination of the $^{11}\text{B}(p,n)^{11}\text{C}$ cross section.	11
3	Time-of-flight spectrum for the $^{11}\text{B}(p,n)^{11}\text{C}$ reaction at zero degrees with an incident proton energy of 4.517 MeV.	14
4	Time-of-flight spectrum for the $^{18}\text{O}(p,n)^{18}\text{F}$ reaction at 0° with proton energy equal to 4.517 MeV.	15
5	Neutron detector efficiency.	20
6	Ratio of Burke to Liskien and Paulsen published zero degree ground state neutron production cross sections.	22
7	Zero degree $^{11}\text{B}(p,n)^{11}\text{C}$ differential cross sections.	24
8	$^{11}\text{B}(p,n)^{11}\text{C}$ differential cross sections for laboratory angles of 0° through 155° .	25
9	Total cross sections for the $^{11}\text{B}(p,n)^{11}\text{C}$ reaction.	27

LIST OF FIGURES (continued)

<u>Figure</u>		<u>Page</u>
10	Legendre polynomial expansion coefficients A_1 , A_2 , A_3 , and A_4 .	29
11	$^{11}\text{B}(p,n)^{11}\text{C}$ angular distributions in the center of mass system.	31
12	Neutron time-of-flight spectra for the $^{11}\text{B}(p,n)^{11}\text{C}$ reaction.	36
13	Depth resolution versus depth in Si and SiO_2 targets.	41
14	Concentration of boron atoms versus depth in the boro-silicate glass target.	43
15	Block diagram of electronics used in sensitivity profiling.	46
16	Time-of-flight spectrum for boron profiling.	49
17	Background time-of-flight spectrum for a silicon target.	50
18	Concentration of boron atoms versus depth for silicon implanted with boron.	52

LIST OF TABLES

<u>Table</u>		<u>Page</u>
1	Published Cross Sections for the $^{11}\text{B}(p,n)^{11}\text{C}$ Reaction	34
A.1	Differential Cross Sections and Associated Statistical Uncertainty for the $^{11}\text{B}(p,n)^{11}\text{C}$ Reaction (0° - 80.3°)	56
A.2	Differential Cross Section and Associated Statistical Uncertainty for the $^{11}\text{B}(p,n)^{11}\text{C}$ Reaction (90° - 155°)	61
B.1	Legendre Power Series Coefficients and Associated Statistical Errors	65

I. INTRODUCTION

This thesis has two objectives. The first is to resolve discrepancies in previously measured cross sections for the $^{11}\text{B}(p,n)^{11}\text{C}$ reaction. The second is to determine the extent to which this reaction can be used to measure boron concentrations in solids.

The $^{11}\text{B}(p,n)^{11}\text{C}$ reaction was studied using protons in the energy range from threshold (3.016 MeV) to 4.6 MeV. In this range only the ground state of ^{11}C can be produced by this reaction. The $^{11}\text{B}(p,n)^{11}\text{C}$ reaction has a nuclear disintegration energy (Q value) of -2.763 MeV and forms a compound nucleus of ^{12}C . A partial energy diagram¹ of the compound nucleus is shown in Figure 1. Two other decay modes of ^{12}C , which are not studied here, are: the production of $^8\text{Be} + \alpha$, with a center of mass energy of 7.367 MeV with respect to the ground state ^{12}C compound nucleus, and $^{12}\text{C} + \gamma$.

The cross section for $^{11}\text{B}(p,n)^{11}\text{C}$ reaction has been studied in the past.²⁻¹⁰ Discrepancies by as much as a factor of four exist in published total cross sections. Thin target techniques, involving the evaporation of a thin layer of boron on a surface have been extensively used in the past. The discrepancies in past measurements were probably caused by uncertainties in composition or thickness of these thin targets. We have tried to avoid the first problem by using thick targets.

The $^{11}\text{B}(p,n)^{11}\text{C}$ reaction is an interesting candidate for boron depth profiling experiments. The cross section for production of neutrons

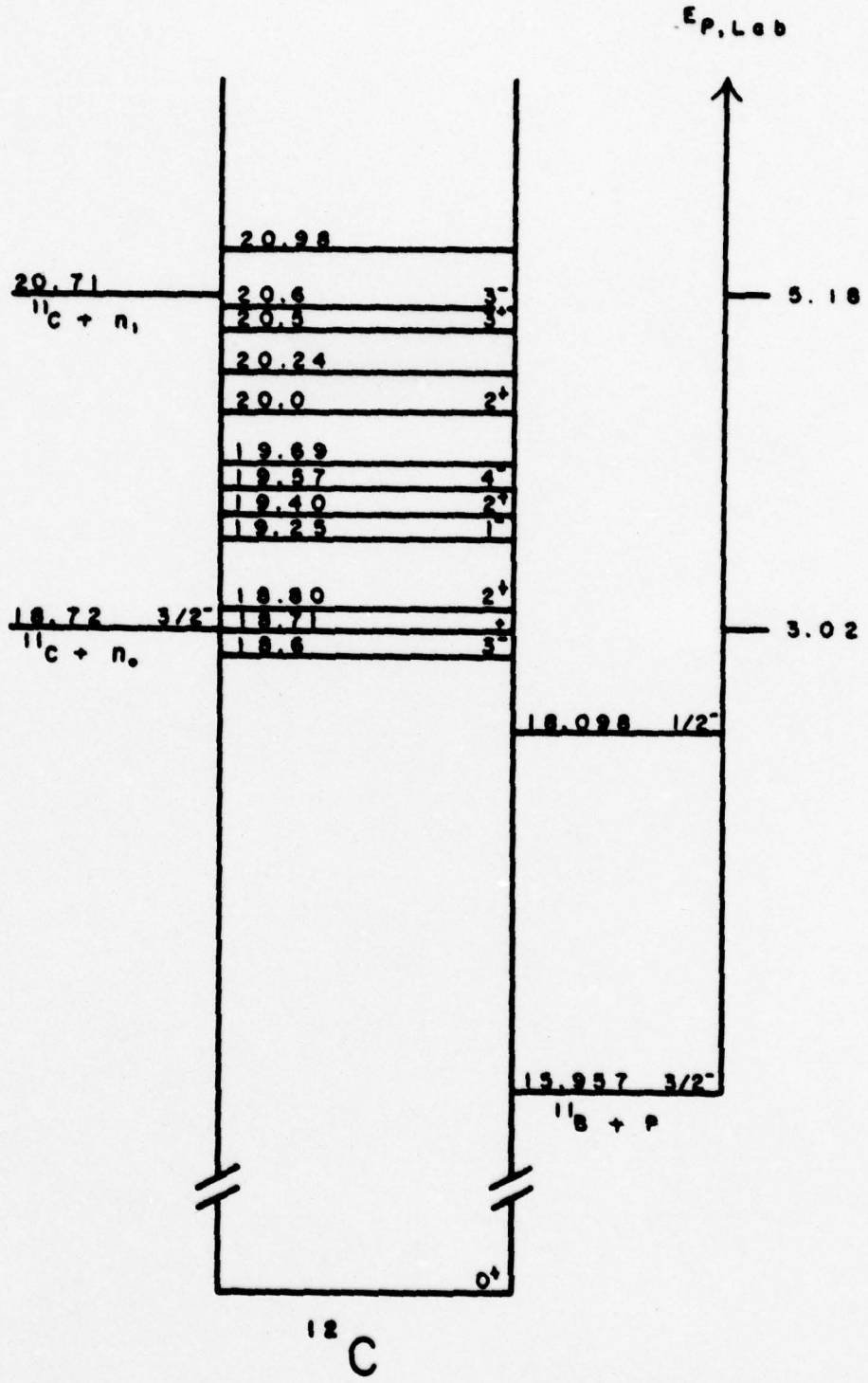


Fig. 1. Energy level diagram of the ¹²C compound nucleus.
 Levels are identified by energy (MeV), spin and parity.

is relatively large, in the ten millibarn/steradian region, and varies slowly with proton energy. Only ground state neutrons can be produced at proton energies below 5.2 MeV. The reaction leads to reasonable sensitivity and resolution for profiling, as discussed in detail in Chapter VI. From an applied physics point of view, boron profiling could be used by the semiconductor industry, where boron is used in making p-type materials by implanting specific concentrations of boron at specific depths in intrinsic or n-type materials.

The first objective was accomplished by studying neutron yields from thick B_2O_3 and B metal targets through neutron Time-of-Flight (TOF) techniques, after carefully determining the neutron detector efficiency. After resolving the cross section discrepancies, the second objective was met by profiling known amounts of boron implanted in silicon at known depths. The feasibility of the reaction technique for profiling was then determined by comparing the experimental resolution and sensitivity to theoretical expectations.

II. EXPERIMENTAL METHODS

A. Thick Target Kinematics.

Thick boron targets of about 1 mm thickness were bombarded with a nanosecond-pulsed proton beam. The thickness of the target is important, because the proton beam, after striking the target with an incident energy, must be degraded in energy to below the reaction threshold prior to exiting the target.

The main advantage of the thick target technique is that the cross section for the production of neutrons as a function of proton energy (E_p) can be obtained from only the one incident proton beam energy. This technique also has the advantage that targets made from bulk material should be more easily reproduced than thin targets.

A proton beam incident on a thick boron target will interact and slow down in accordance with the stopping power of the target material. Therefore, a continuum of proton energies from incident to below threshold is produced. Because there is a possibility of a nuclear reaction at all energies above threshold there will also be a continuum of neutron energies produced. Considering the $^{11}\text{B}(p,n)^{11}\text{C}$ nuclear reaction as a two body process, conservation of energy and of momentum give rise to "kinematic restrictions" of the reaction. The resulting energy of the neutron (E_n) is a function of its emission angle (θ), energy of the proton and masses of the four interacting particles.

As a result of the negative Q value the $^{11}\text{B}(p,n)^{11}\text{C}$ nuclear reaction has the following kinematic restrictions. The reaction has a kinematic

threshold value of $E_p = 3.016$ MeV where neutrons are emitted with $E_n = 20$ KeV only at $\theta_{lab} = 0^\circ$. As E_p increases neutrons are emitted at greater angles until finally a "cone opening" energy of 3.042 MeV is reached. Neutrons are then emitted at all angles in the lab frame. Values for E_p from threshold to cone opening can give rise to double values of E_n in the lab frame corresponding to forward- and backward-emitted neutrons in the center of mass frame. The backward-emitted neutrons will have a lab $E_n = 20$ KeV at threshold and zero energy at the cone opening energy. At E_p greater than cone opening energy only one E_n is allowed for a given θ_{lab} and E_p . For example, at $E_p = 4.5$ MeV and $\theta_{lab} = 0^\circ$, $E_n = 1.69$ MeV while at the same E_p with $\theta_{lab} = 180^\circ$, $E_n = 0.87$ MeV.

B. Transformation Equations.

A neutron TOF spectrometer was used and the number of neutrons detected as a function of their flight time t from the target was measured. More precisely, the number of neutrons detected $N_{det}(t)\Delta t$ is the number of neutrons detected at time t , summed over time interval Δt . Knowing the experimental time of flight and the flight path from the target to the detector the corresponding neutron energy can be calculated. Nonrelativistically the kinetic energy of the neutron is $\frac{1}{2} mX^2 / t^2$, where X is the flight path and m is the mass of the neutron. The neutron energy interval ΔE_n which corresponds to Δt is related to a proton energy interval ΔE_p through the kinematic equations.

A continuous neutron TOF spectrum can be transformed to a neutron energy spectrum,¹¹

$$N(E_n, \theta) = \frac{N_{\text{det}}(t)\Delta t}{N_p \cdot \Delta E_n \cdot \Delta \Omega \cdot \epsilon(E_n)}, \quad 2.1$$

where $N(E_n, \theta)$ is the number of neutrons emitted at angle θ per incident proton, unit neutron energy interval and solid angle. The neutron detector subtends solid angle $\Delta \Omega$ at the target, N_p is the number of incident protons that strike the target and $\epsilon(E_n)$ is the neutron detector efficiency.

The detector efficiency is defined as the number of neutrons detected divided by the number of neutrons that strike the detector. In present work, $\epsilon(E_n)$ is experimentally determined using the ${}^7\text{Li}(p,n){}^7\text{Be}$ nuclear reaction as the standard. The experimental neutron detector efficiency is discussed in detail in Chapter IV.

Once $\epsilon(E_n)$ is experimentally determined the differential cross section $\sigma(\theta)$ can be calculated from¹¹

$$\sigma(\theta) = \frac{N_{\text{det}}(t)\Delta t \cdot \left(\frac{1}{n} \frac{dE_p}{dx}\right)}{N_p \cdot \Delta E_p \cdot \Delta \Omega \cdot \epsilon(E_n)}, \quad 2.2$$

where $\frac{1}{n} \frac{dE_p}{dx}$ is the stopping cross section per ${}^{11}\text{B}$ atom.

The stopping cross section per ${}^{11}\text{B}$ atom is a function of the total target composition. For a molecule containing two elements, it is given by¹²

$$\frac{1}{n} \frac{dE_p}{dx} = \frac{b \cdot \left(\frac{1}{\rho} \frac{dE_p}{dx}\right)_B \cdot M_B + a \left(\frac{1}{\rho} \frac{dE_p}{dx}\right)_A \cdot M_A}{b \cdot (0.8022) \cdot \Gamma}, \quad 2.3$$

where "b" denotes the number of atoms of boron (B) in the target molecule and "a" is the number of atoms of the other element (A) in the molecule. For example, a B_2O_3 target would have $b = 2$ and $a = 3$. The stopping power of the given element is given by $\frac{1}{\rho} \frac{dE_p}{dx}$ as compiled by Janni,¹³ M is the corresponding element's molecular weight and Γ is Avogadro's number. The number 0.8022 accounts for the fact that boron is 80.22% ^{11}B and 19.88% ^{10}B .

The stopping cross section per ^{11}B atom must be calculated at some energies because Janni only gives the stopping power for each element at 200 KeV intervals. The interpolation formula used is a generalized form of the Bethe-Bloch equation,¹⁴

$$\frac{1}{n} \frac{dE_p}{dx} = C_1 \cdot [\ln(E_p) + C_2] / E_p. \quad 2.4$$

The constants C_1 and C_2 were obtained by solving the above equation simultaneously using values of $\frac{1}{n} \frac{dE_p}{dx}$ from Eq. 2.3 at proton energies of 3.0 and 4.6 MeV. Values of $\frac{1}{n} \frac{dE_p}{dx}$ at intermediate energies agree within 0.1% with the values obtained from Eq. 2.3 and Janni's tabulated stopping powers over the proton energy range from 3.0 to 4.6 MeV. For B_2O_3 , values of constants are $C_1 = 5.525 \times 10^{-21}$ $\text{MeV}^2 \text{cm}^2 / ^{11}B \text{ atom}$, $C_2 = 2.839$ while for elemental boron, $C_1 = 1.644 \times 10^{-21}$ $\text{MeV}^2 \text{cm}^2 / ^{11}B \text{ atom}$ and $C_2 = 2.982$.

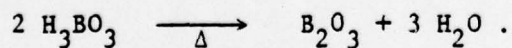
III. EXPERIMENTAL DETAIL

A. Hardware.

The same experimental set up as described by Burke¹¹ was used in the determination of the $^{11}\text{B}(p,n)^{11}\text{C}$ cross section. A more detailed discussion of the following areas can be found in his thesis: pulsed beam mechanism, target holder, target chamber, neutron shielding, neutron detector, and electronic set up.

The University of Oregon Van de Graaff accelerator was used to produce a 4.6 MeV pulsed, klystron bunched, proton beam. Deflection and focussing magnets were used to direct the beam through three collimators to the target on the 32° East beam line. The resulting beam size was approximately 3 mm in diameter and had a beam pulse repetition period of 4 to 16 μsec depending on the type of target used. An overall time resolution of 1.5 nsec was obtained. Time average beam currents were about 0.5 microamperes. The beam line vacuum near the target was $\sim 5 \times 10^{-6}$ torr.

Two types of targets were used in the determination of the cross section: B_2O_3 and B metal. Analytical reagent grade Boric Acid* was used to make the B_2O_3 targets, through the following reaction,



*Mallinckrodt Chemical works, Boric Acid granular, Heavy metal to 0.01% max impurity.

Boric acid was heated in a stainless steel target holder to a red heat in a partial vacuum. As the sample was heated, the pressure inside the bell jar was decreased slowly to ≈ 25 microns. Extreme care had to be taken to insure most of the water was driven off, resulting in a clear, colorless, glass-like solid. Boron metal was commercially purchased from Alfa Ventron* as a polycrystalline solid. Because boron metal has a hardness rating of 9.5 (MOHS)¹⁵ a diamond toothed saw had to be used to cut the boron chunks into target thicknesses of 1 mm. Two different types of targets were prepared. One target had the front surface untouched, the other was sanded smooth using a diamond impregnated sanding disk. Both targets were mounted on tantalum target holders using epoxy glue.

Two different types of target holders were used. The closed end stainless steel "top hat" used in the preparation of the B_2O_3 targets, had an inside diameter of 1 cm, wall thickness of 0.25 mm and an overall length of 5 cm. The boron metal targets were mounted in tantalum dishes, 0.64 mm thick and 1.4 cm inside diameter. Both target holders were hermetically sealed to the evacuated target chamber by an "o-ring" and held in place by atmospheric pressure.

The target chamber was a stainless steel tube with an inside diameter of 1.27 cm and an overall length of 16.5 cm. The chamber was electrically isolated from the target holder by a 1 cm long glass tube and also from the grounded beam pipe by a non-conducting pipe-

* Alfa Division, Ventron Corp. Boron pieces crystalline, 5 cmx down 99.8% pure with respect to metallic impurities.

coupling flange. The target chamber was biased at -300 volts with respect to the target holder for secondary electron suppression.

The neutron shielding which surrounded the target was made by Lunnon¹⁶ and designed to reduce room background. The system consisted of two metal tanks, 1 meter in diameter, containing a lithium carbonate - water slurry and nine paraffin - lithium carbonate wedge-shaped sections. The pie sections were mounted between the two tanks on a horizontal plane parallel to the target chamber. One of the pie sections was made of high density polyethylene and had a horizontal conical hole cut in its center with half angle of $1/2^\circ$, allowing neutrons emitted from the target to strike the detector unobstructed.

The neutron detector consisted of a cylindrical Naton 136 plastic scintillator, 1.27 cm thick and 6.2 cm in diameter, optically coupled to a RCA C70133 B photomultiplier. The neutrons were detected through the hydrogen and carbon atom recoils in the plastic scintillator. The entire assembly was magnetically shielded to decrease the angular dependence of the photo tube gain to less than the 1% level.

A diagram of the electronics used in the measurement is shown in Fig. 2. The analog to digital conversion of the Time-to-Amplitude Converter (TAC) output pulses was done by a dual twelve bit Nuclear Data 161F Analog to Digital Converter (ADC).

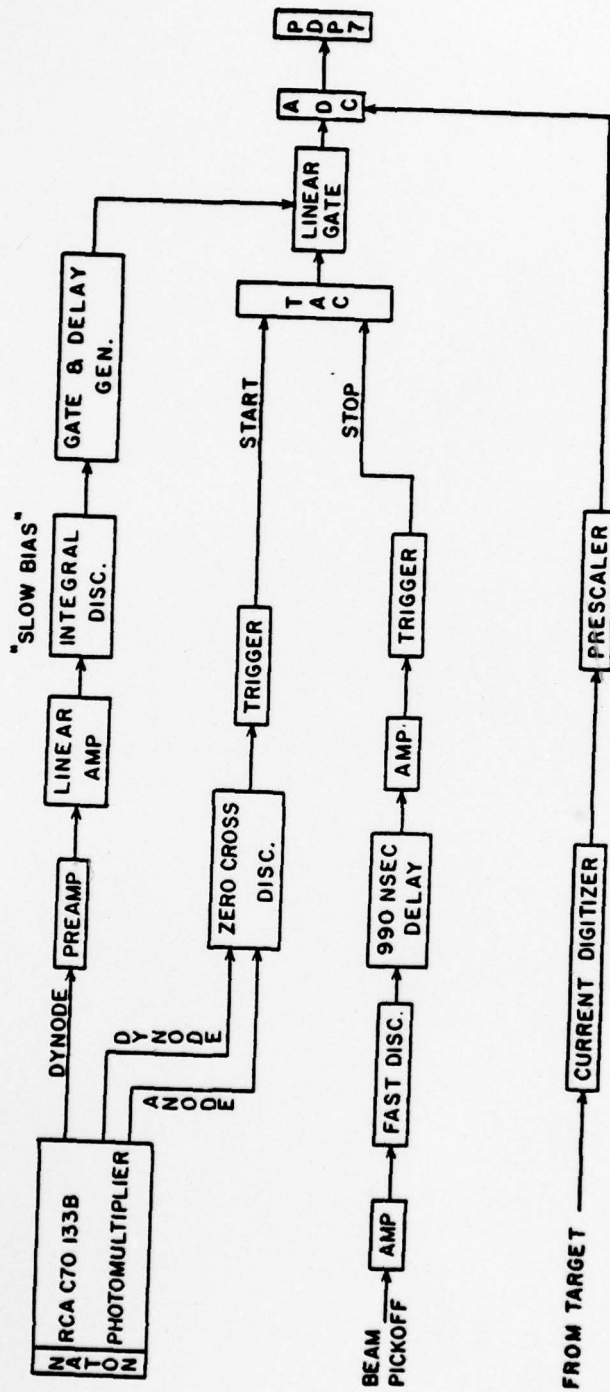


Fig. 2. Block diagram of the electronics used in the determination of the $^{11}\text{B}(p,n)^{11}\text{C}$ cross section.

B. Data Acquisition.

The pulse-height electronics were standardized to a pulse height spectrum of ^{241}Am γ rays prior to each day's run. The electronics were checked several times during the day's run and corrected for any drift. The detection (or "slow") bias was set to 1/17 of the ^{241}Am 60 KeV γ ray full energy peak. The timing (or "fast") bias was set below this level. The fast bias was always adjusted such that a pulse height spectrum gated with only this bias matched the spectrum gated only by the slow bias for pulse heights above the level of the slow bias.

Neutron TOF spectra were taken in three groups over a one year period. The B_2O_3 targets were used to measure the neutron yields at the following eleven angles: 0° , 20° , 31° , 50° , 69.8° , 80.3° , 90° , 100° , 114° , 138° and 155° . The flight path varied depending on the room geometry. The TOF spectra at 0° to 31° were taken at 2.19 meters while those taken at 50° to 155° were at 1.91 meters. Boron metal targets were also used to measure TOF spectra at 0° . No appreciable difference was noticed between the two types of B metal targets. The ADC TOF processing dead time was $\sim 8\%$ for B_2O_3 targets and $\sim 16\%$ for B metal targets. This dead time effect was compensated for by using the external clock input port of the ADC, which timed each run for a pre-selected amount of beam charge. The number of incident protons that struck the target was derived from the resulting total integrated charge. This charge was an experimental variable and was chosen to give counting statistics of $\sim 1\%$ with $\sim 10^6$ counts above the fast bias. The integrated charge for the B_2O_3 targets was 200 μc at each angle and for the B

metal targets it was 100 μc .

The resulting TOF spectra were stored in a 1024 channel array of number of counts versus flight time in a PDP-7 computer. After completion of each run the spectrum was written on magnetic DEC tape.

A TOF spectrum for the $^{11}\text{B}(p,n)^{11}\text{C}$ reaction with a B_2O_3 target, with an incident proton energy equal to 4.517 MeV and laboratory angle equal to zero degrees, is shown in Fig. 3. The flight time is measured from right to left with channel 880.5 corresponding to zero flight time. The prompt γ ray peak is located in channel 873. The sharp leading edge of the neutron production is located in channel 755 and corresponds to the maximum neutron energy of 1.69 MeV. The neutron energy corresponding to a given channel number C is

$$E_n = \left[\frac{163}{880.5 - C} \right]^2, \quad 3.1$$

where the constant 163 incorporates a flight path of 2.197 meters and a channel calibration of 0.9756 nsec per channel.

In contrast to previous TOF spectrum, a TOF spectrum from the same target taken with an incident proton beam below the threshold energy revealed a completely flat background with a similar prompt γ ray peak, and the same smaller peak at channel 810. The smaller peak is thought to be a result of a higher beam mass or an unlikely gating difficulty visible only when γ rays are intense. The flat background indicates that no reactions with higher Q values contaminate the spectrum. Background effects from the $^{18}\text{O}(p,n)^{18}\text{F}$ reaction were investigated at

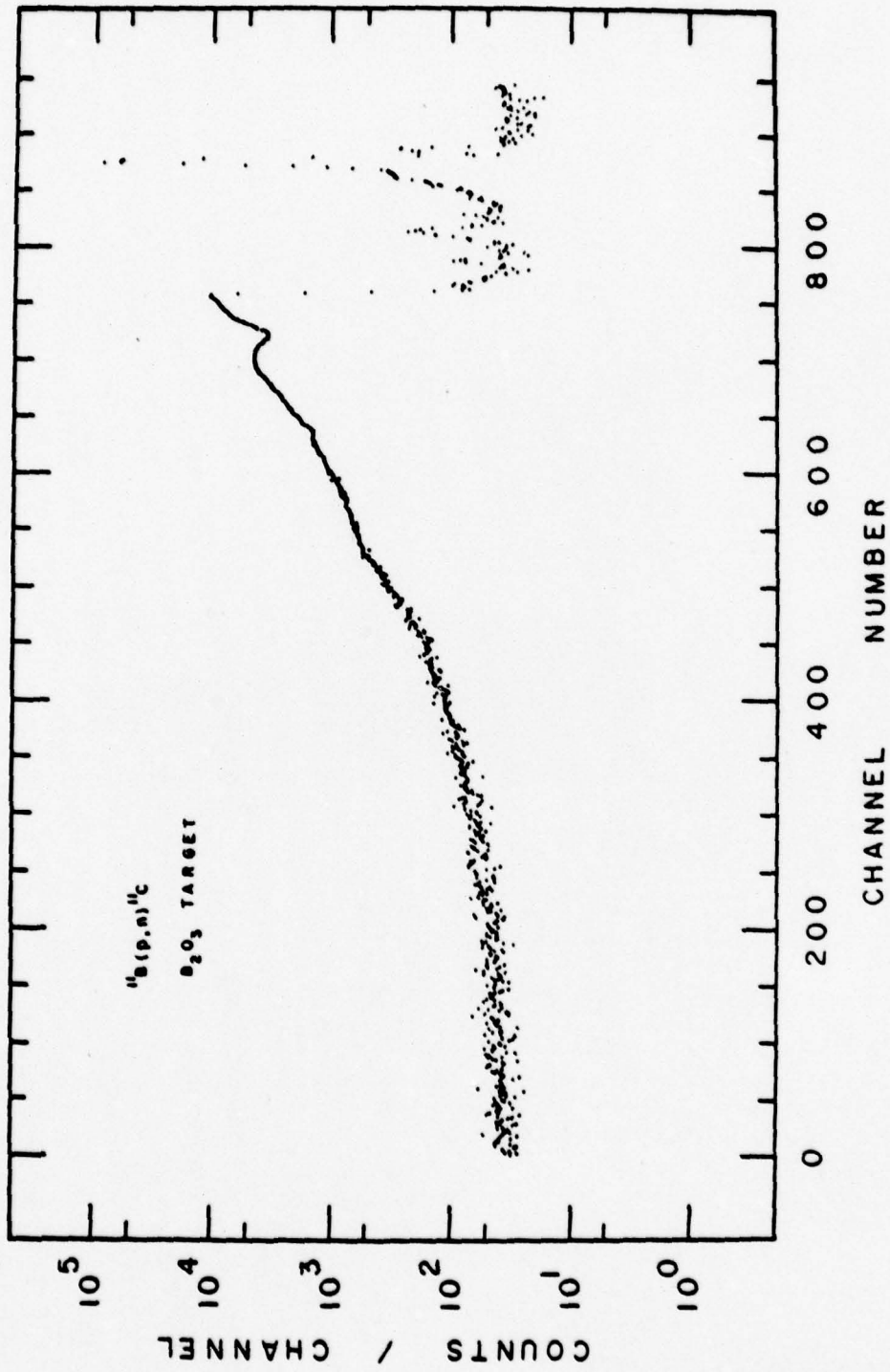


Fig. 3. Time-of-flight spectrum for the $^{11}\text{B}(p,n)^{11}\text{C}$ reaction at zero degrees with incident energy of the proton equal to 4.517 MeV, a flight path of 2.197 meters and an integrated beam current of 200 μc .

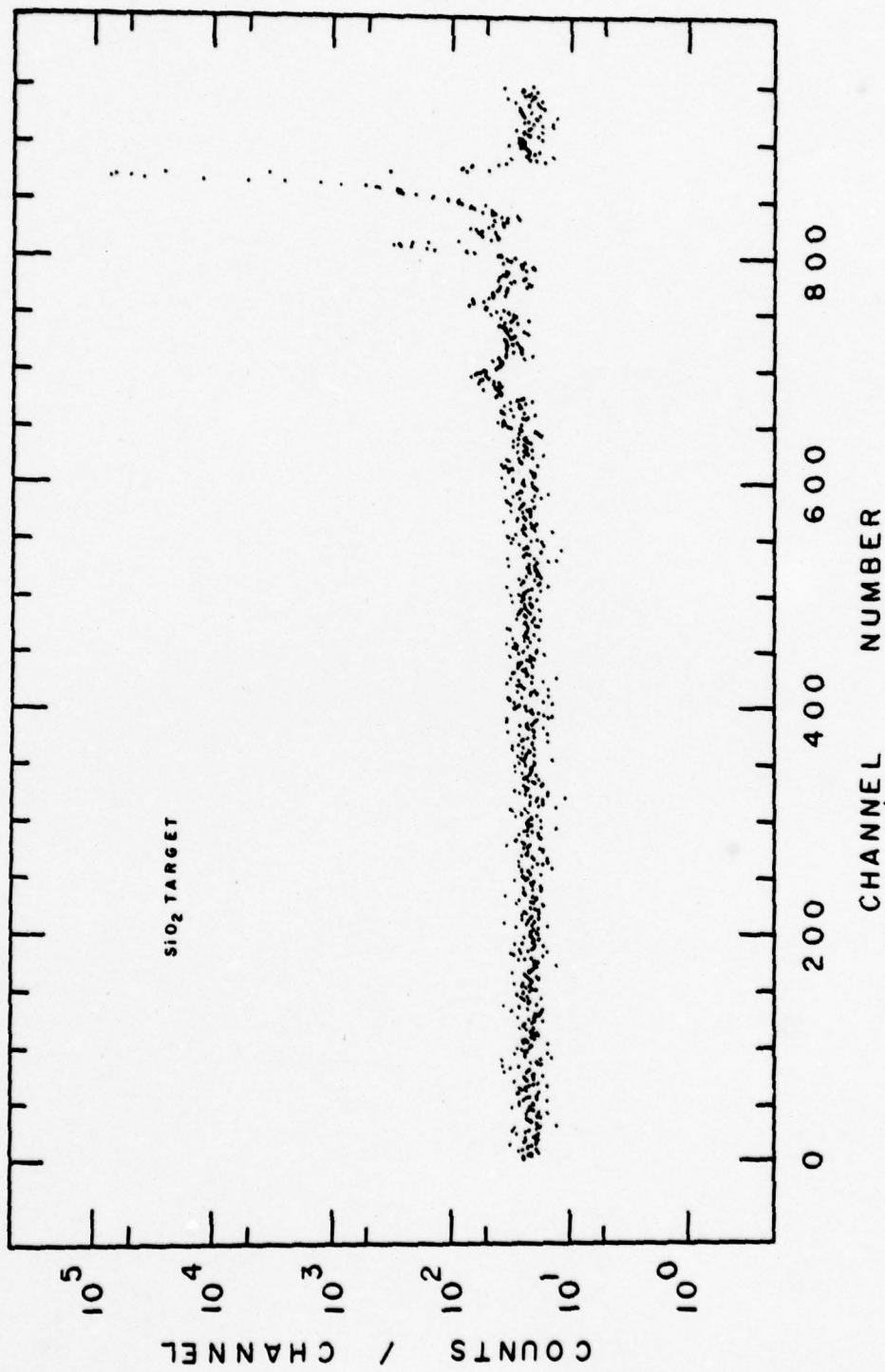


Fig. 4. Time-of-flight for the $^{18}\text{O}(p,n)^{18}\text{F}$ reaction at 0° with energy proton equal to 4.517 MeV, flight path of 2.233 meters, integrated beam current of 100 μc and an SiO_2 target.

$E_p = 4.517$ MeV, $\theta_{lab} = 0^\circ$ with an SiO_2 target. The resulting TOF spectrum is shown in Fig. 4. Again the same two γ ray peaks are seen in channels beyond 800. Some structure is seen in the region from channels 650 to 800, with a maximum value of 70 counts and a background level of ~ 30 counts. Comparing this spectrum to the B_2O_3 TOF spectrum one can see that the statistical uncertainty in the number of counts from the B_2O_3 target is approximately equal to the number of counts from the SiO_2 target. Thus the effect of ^{18}O in the B_2O_3 target is very small and is neglected in this experiment.

A total of fifteen $^7\text{Li}(p,n)^7\text{Be}$ neutron TOF spectra were taken on two days, three months apart. These TOF spectra were used to determine the neutron detector efficiency, which is discussed in detail in the next chapter. Lithium metal targets were prepared as described by Burke¹¹ and mounted in the top hat target holder. The same electronic set up was used with a flight path of 2.14 meters, total integrated charge of 25 μc and an ADC dead time of 20%.

The time per channel calibration was taken each day upon completion of the day's run, using an Ortec 462 Time Calibrator. Several spectra were taken at various dead times corresponding to the experimental dead times noted during the B_2O_3 , B metal or Li targets run on that day. The average channel width was ~ 0.97 nsec per channel.

IV. DATA ANALYSIS FOR CROSS SECTION

A. Determination of Neutron Detector Efficiency.

The neutron detector efficiency, as defined in Chapter II, can be expressed by rewriting Eq. 2.1,

$$\epsilon(E_n) = \frac{N_{\text{det}}(t)\Delta t}{N(E_n, \theta) \cdot \Delta E_n \cdot \Delta \Omega \cdot N_p} \quad 4.1$$

The neutron detector efficiency has been studied by Burke¹¹ utilizing the same electronic set up. The detector efficiency is subject to experimental conditions and as such should be experimentally determined. For example, the efficiency of the detector is a function of the signal processing bias settings (fast and slow), the quality of the optical coupling between the scintillator and the photomultiplier and sometimes the age of the scintillator.

The ${}^7\text{Li}(p,n){}^7\text{Be}$ nuclear reaction is used to determine $\epsilon(E_n)$ by experimentally determining N_{det} , ΔE_n , $\Delta \Omega$ and N_p . The number of neutrons emitted in the ${}^7\text{Li}(p,n){}^7\text{Be}$ reaction, $N(E_n, \theta)$, can be calculated if the (p,n) cross sections and atomic stopping cross sections are known. The number of neutrons emitted can be solved from Eq. 2.1 and 2.2,

$$N(E_n, \theta) = \frac{\sigma}{(1/n)(dE_p/dx)} \frac{dE_p}{dE_n}, \quad 4.2$$

where the transformation derivative dE_p/dE_n is determined through the kinematic relationships for the ${}^7\text{Li}(p,n){}^7\text{Be}$ reaction and $\frac{1}{n} \frac{dE_p}{dx}$ is the

atomic stopping cross section per ${}^7\text{Li}$ atom. The case of the ${}^7\text{Li}(p,n){}^7\text{Be}$ reaction is more complicated than implied by Eq. 4.2 because two groups of neutrons can be emitted if E_p is above 2.378 MeV.

The cross section for the ${}^7\text{Li}(p,n){}^7\text{Be}$ reaction at $\theta_{\text{lab}} = 0^\circ$ has been studied extensively and has been reported in detail.^{11,17-19} Lefevre²⁰ has used Eq. 4.2, the ground state cross sections of Burke¹¹ and the first excited state cross sections inferred from the measurements of Bevington¹⁷ and Borchers¹⁸ to calculate $N_o(E_n, 0^\circ)$ for ground state neutrons and $N_1(E_n, 0^\circ)$ for first excited state neutrons.

The number of detected neutrons N_{det} in a time-of-flight experiment is converted to a modified energy spectrum

$$N_{\text{exp}}(E_n, 0^\circ) = \frac{N_{\text{det}}(\tau)\Delta t}{N_p \cdot \Delta E_n \cdot \Delta \Omega} \quad 4.3$$

This is just Eq. 2.1 with the efficiency $\epsilon(E_n) = 1$. The detector efficiency can now be determined from

$$\epsilon(E_n) = \frac{N_{\text{exp}}(E_n, 0^\circ)}{N_o(E_n, 0^\circ) + N_1(E_n, 0^\circ)} \quad 4.4$$

Lithium TOF spectra for incident proton energies from 2.9 MeV to 5.1 MeV were transformed to $N_{\text{exp}}(E_n, 0^\circ)$ spectra using the program TOF-NE, written by Burke¹¹ (Appendix C). Utilizing Eq. 4.4, an efficiency table was calculated for each transformed Li TOF spectra. The number of neutrons emitted $N_o(E_n, 0^\circ) + N_1(E_n, 0^\circ)$ was calculated separately at each incident energy from Lefevre's tables. Efficiencies were calculated for each of the two separate days and averaged, taking into account the target front surface contamination effects. Average

efficiencies for each day were within the experimental statistical errors, but the two days differed by $\pm 5\%$ from the overall average or by somewhat more than the statistical uncertainties.

Extreme care must be exercised in the steering of the pulsed proton beam onto the target. Once the beam is properly steered onto the center of the target, over or under focusing of the beam will have little effect on the resulting TOF spectrum. The preparation of the Li is also very important. Target front surface contamination effects extending as far as 300 KeV in proton energy loss were noted in efficiencies determined for 3.0 and 5.1 MeV protons incident on the same target.

The resulting overall efficiency for the neutron detector and that calculated by Burke¹¹ are shown in Fig. 5. The two sets of efficiencies agree to $\pm 4\%$ for E_n greater than 0.4 MeV. For E_n less than this, Burke's values are lower by more than 7%. In the neutron energy interval of 0.2 MeV to 0.4 MeV the ${}^7\text{Li}(p,n){}^7\text{Be}$ cross section at $\theta_{\text{lab}} = 0^\circ$ has a very sharp minimum. It is possible, in this region, that neutron scattering could lead to significant effects in the efficiency calculation. The dip in the efficiency table at 250 KeV is due to Li resonance scattering at that energy. Burke's results were corrected for this effect.

The efficiency table used in this work was based on Burke's¹¹ measured cross section values. Because Burke used the same experimental set up it is hoped that experimental systematic errors will tend to cancel. A comparison of Burke's published zero degree ground state

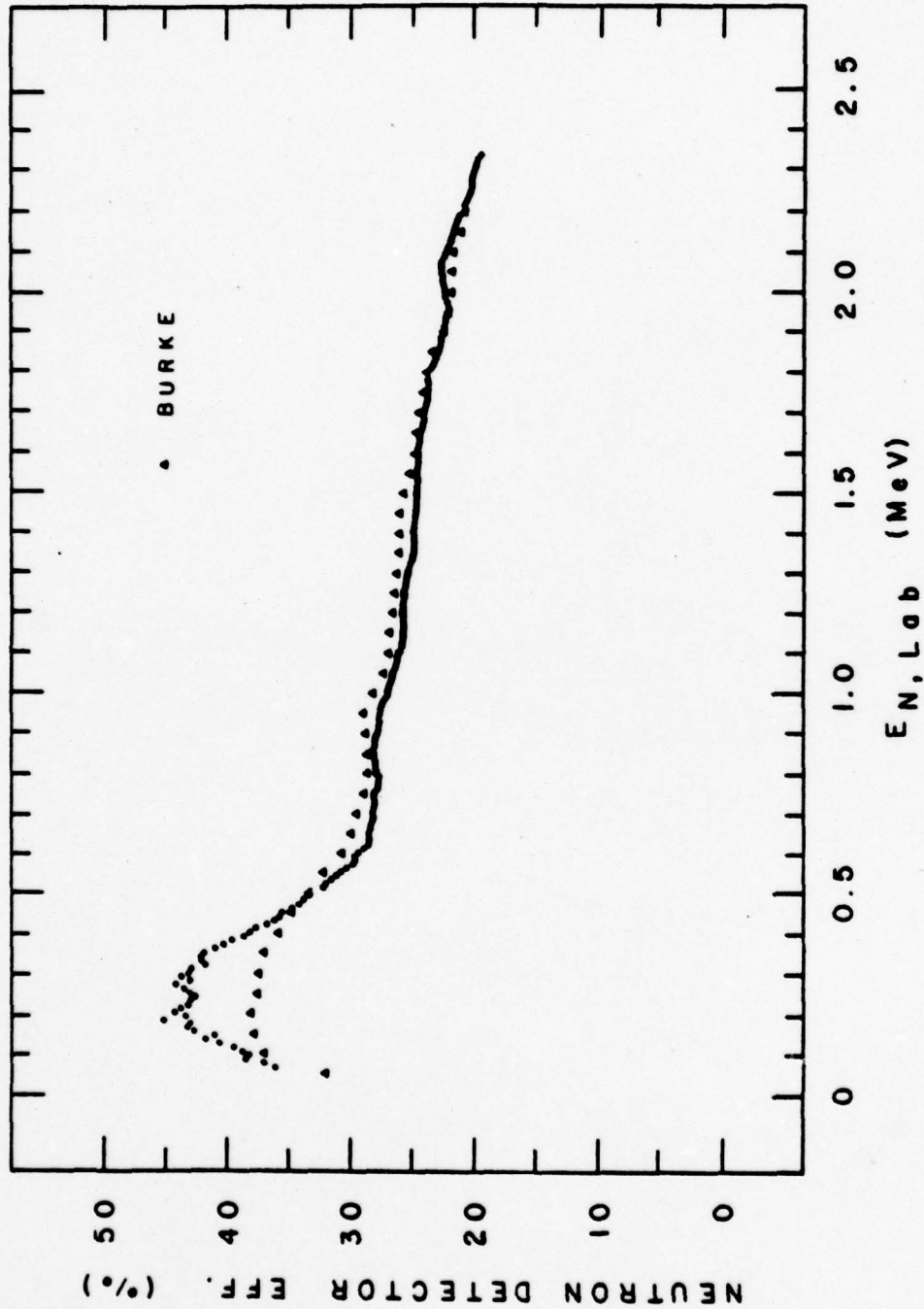


Fig. 5. Neutron detector efficiency. The circles represent present results. The triangles represent the detector efficiency as determined by Burke¹¹ over seven years ago.

cross sections and those tabulated by Liskien and Paulsen¹⁹ are shown in Fig. 6. Burke's values are not included in those reported by Liskien and Paulsen and are ~10% higher.

The neutron detector efficiency used through the remainder of this work has an estimated overall accuracy of ±7%. If the cross section values by Liskien and Paulsen were used the efficiencies would be larger by ~10%. Thus, there is a possible systematic error of ~10% in the efficiencies used.

B. Conversion of Time-of-Flight Spectra to Cross Section.

A constant flat background was subtracted from each $^{11}\text{B}(p,n)^{11}\text{C}$ neutron TOF spectrum. Each spectrum was then smoothed to increase counting statistics by using a three channel running average. The TOF spectrum was then labeled in channel 0-5 with experimental parameters that are used in the transformation computer programs.

The prepared TOF spectra were transformed to laboratory differential cross sections versus proton energy by the program B11PNX (Appendix D). The computer program was a modified version of LITPN1 written by Burke.¹¹ The program uses Eq. 2.2 and efficiencies described in the previous section. Time-of-flight spectra for both B_2O_3 and B metal targets were transformed using the B11PNX program where, of course, appropriate atomic stopping cross sections were used for each target.

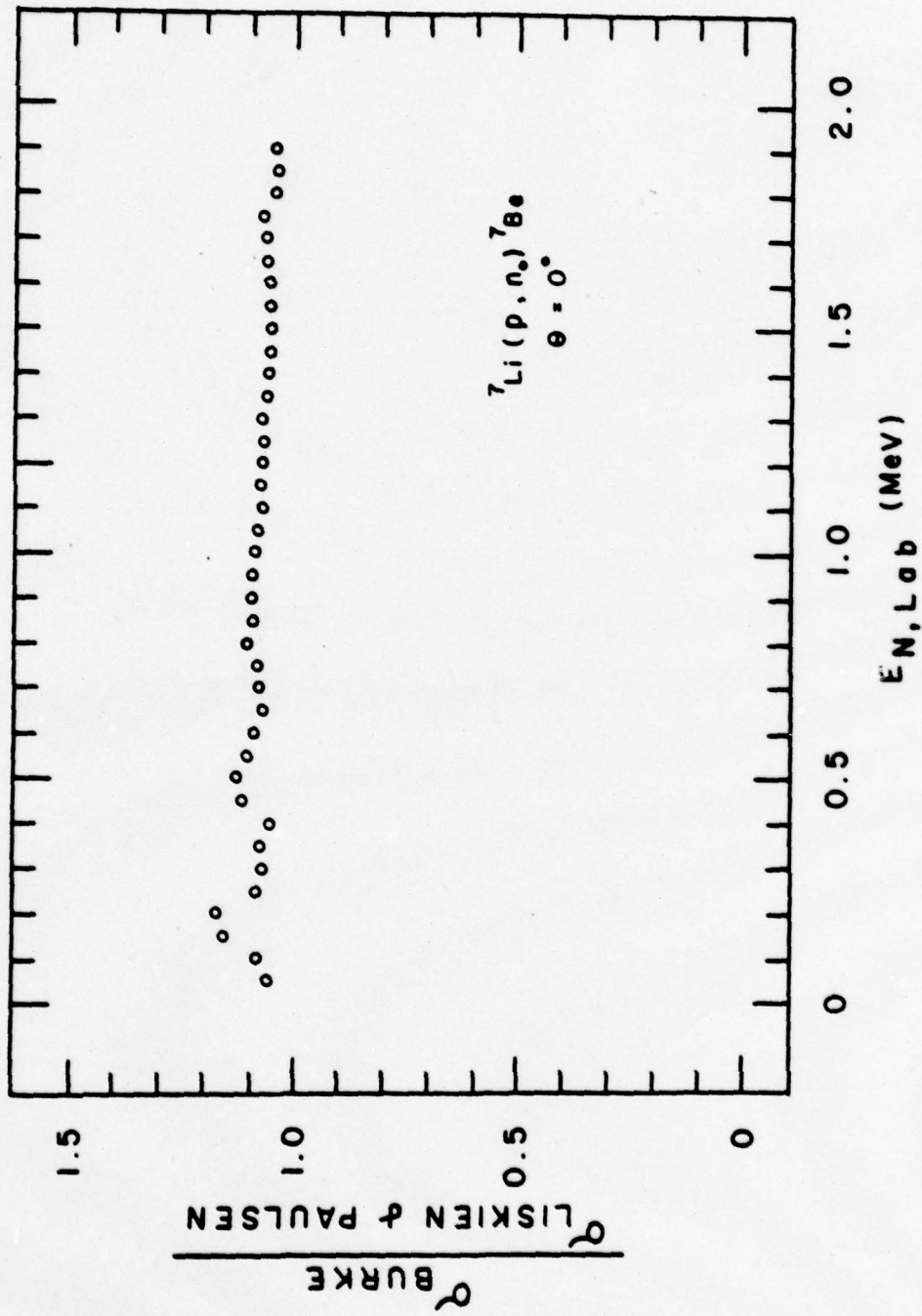


Fig. 6. Ratio of Burke¹¹ to Liskien and Paulsen¹⁹ published zero degree ground state neutron production cross sections.

V. CROSS SECTION ANALYSIS

A. Results and Discussion.

The $^{11}\text{B}(p,n)^{11}\text{C}$ zero degree differential cross section for B_2O_3 and B metal targets are compared to the published results by Van der Zwan and Gieger⁹ in Fig. 7. The B_2O_3 target was bombarded with 4.517 MeV incident protons, while 4.618 MeV protons were used for the B metal target. The disagreement between the two boron targets is less than $\pm 4\%$ but is larger than uncertainties due to counting statistics. The fact that the B_2O_3 target's cross section was lower at high energies and larger near 4.1 and 3.5 MeV could be due to two types of target impurities. The B_2O_3 target could have absorbed water molecules on its front surface during transportation of the target from the bell jar to the target chamber. The B metal target, a polycrystalline solid, could have had slight impurities on the surface or internal crystals. Therefore, as the proton beam penetrated further into the target it could have passed through pockets of impurities, thereby giving lower cross section results. Both the B_2O_3 and B metal target gave cross section values larger than those reported by Van der Zwan and Gieger.⁹ An experimental error bar for the latter's work is shown in Fig. 7 at 3.58 MeV.

The $^{11}\text{B}(p,n)^{11}\text{C}$ differential cross sections measured at lab angles of 0° , 20° , 31° , 50° , 69.8° , 80.3° , 90° , 100° , 114° , 138.2° , and 155° are shown in Fig. 8. These cross sections were obtained from bombarding a B_2O_3 target with a 4.517 MeV incident proton beam. The

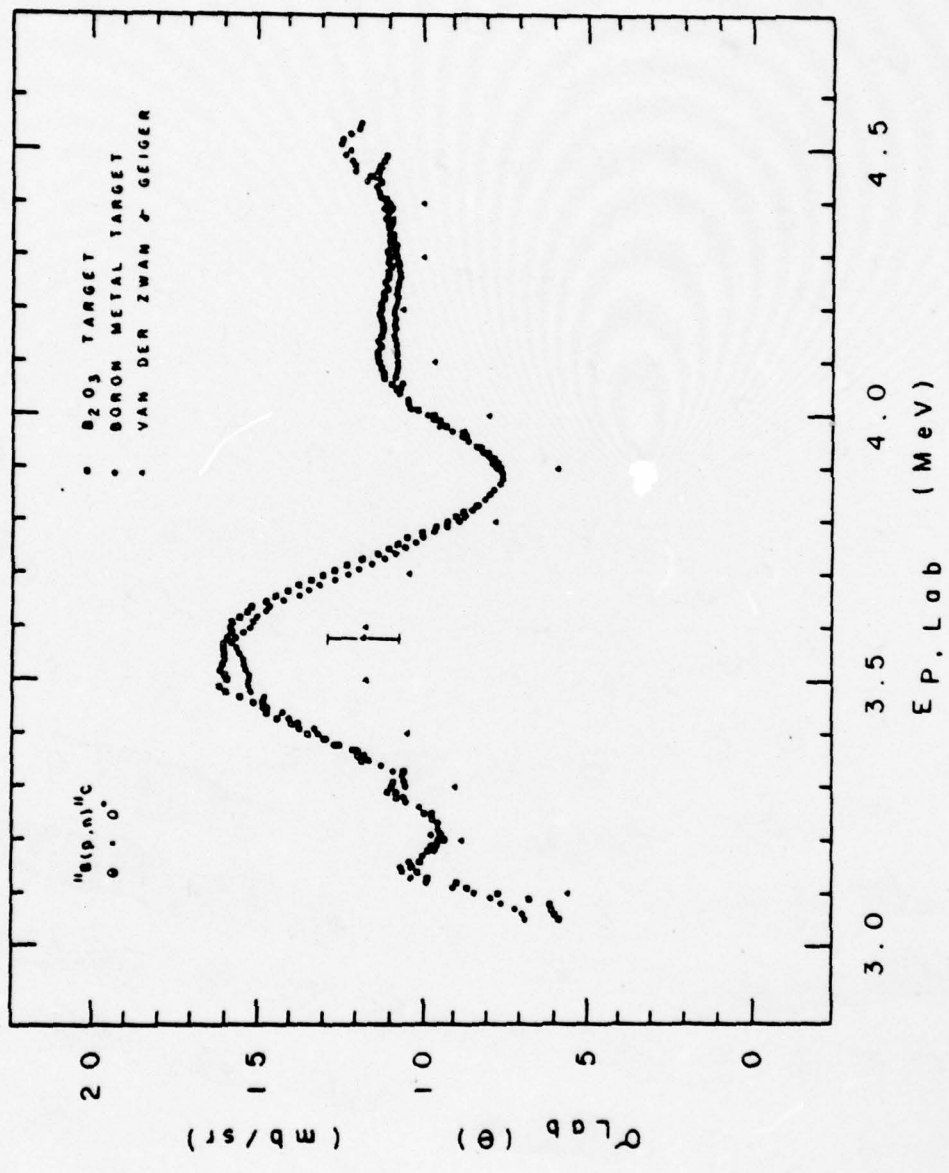


Fig. 7. Zero degree $^{11}\text{B}(p,n)^{11}\text{C}$ differential cross sections. The squares and circles represent the present results. The triangles represent values published by Van der Zwan and Gieger.

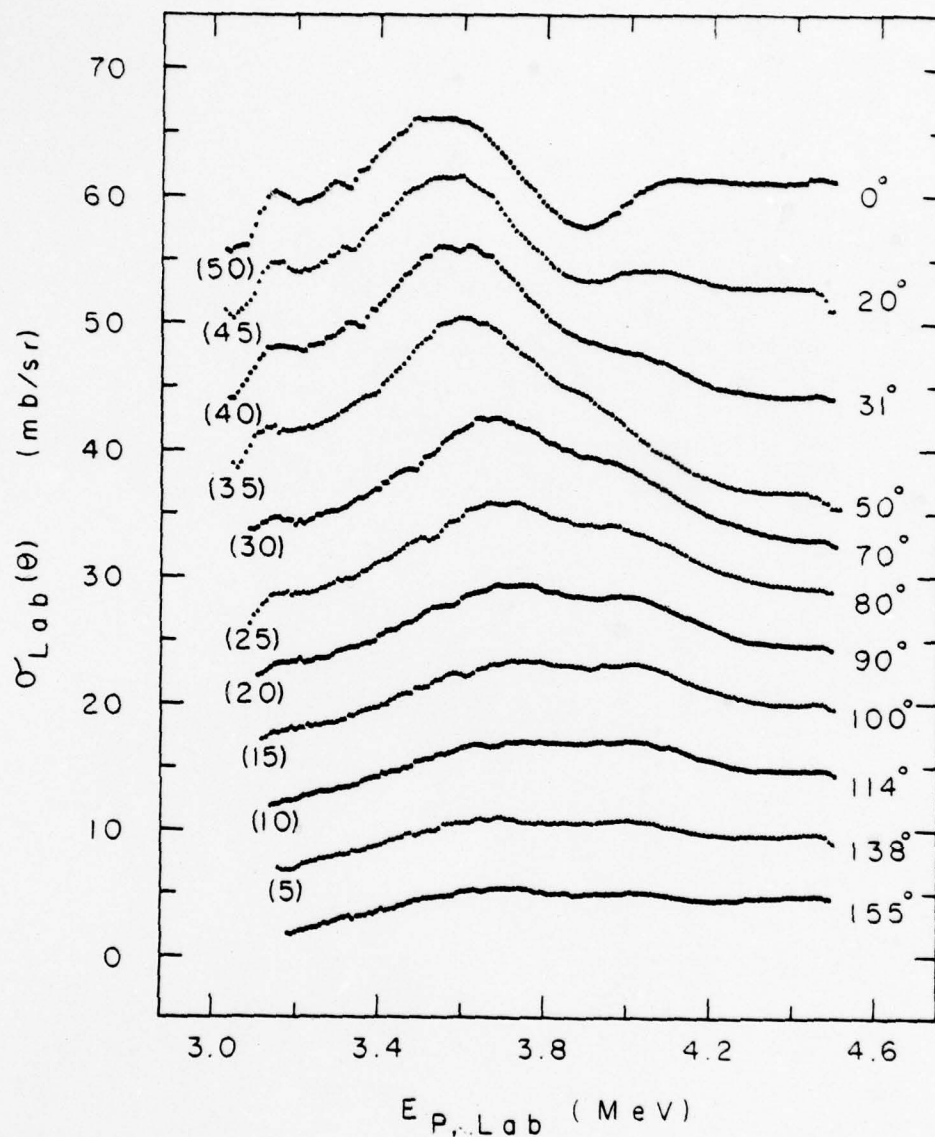


Fig. 8. $^{11}\text{B}(p,n)^{11}\text{C}$ differential cross sections for laboratory angles of 0° through 155° . The reaction angle of each curve is labeled on the right. Each curve is labeled on the left side with a vertical offset (in parentheses) to be subtracted from the ordinate to obtain the cross section at that angle. The reaction threshold is at 3.015 MeV.

numerical values of the cross section and their statistical uncertainties are given in Appendix A. The pronounced dip in the cross section at 3.33 MeV at 0° , increasing in proton energy to 3.62 MeV at 100° , corresponds to a neutron energy of 0.433 MeV. Because this dip was always at the same neutron energy, it is probably due to resonance scattering by the B_2O_3 target ^{16}O nuclei.²¹ A closer look at results from the B_2O_3 and B metal targets in Fig. 7 shows that the B metal target values do not exhibit such a drastic dip. A comparison of the eleven curves in Fig. 8 shows that the zero degree cross section is the largest.

Angular distributions in the center of mass system were fitted with a series of Legendre polynomials;

$$\sigma_{cm}(\theta) = \sum_{L=0}^N A_L P_L(\cos\theta_{cm}) .$$

The conversion to the center of mass system and calculation of the Legendre polynomial coefficients was done using the program LSQFT3 (Appendix E). This program was a modified version of Burke's¹¹ LTHM3. The LSQFT3 program allows the operator to input at the teletype computer interface the masses and Q value of the two body reaction under study, the number of Legendre polynomials coefficients to be calculated (up to 6) and the number of differential laboratory cross sections to be used as a basis for calculations (up to 15).

The total cross section, $4\pi A_0$, for the $^{11}B(p,n)^{11}C$ reaction is compared to results published by Van der Zwan and Geiger⁹ and to normalized results of Gibbons and Macklin⁴ in Fig. 9. Because the

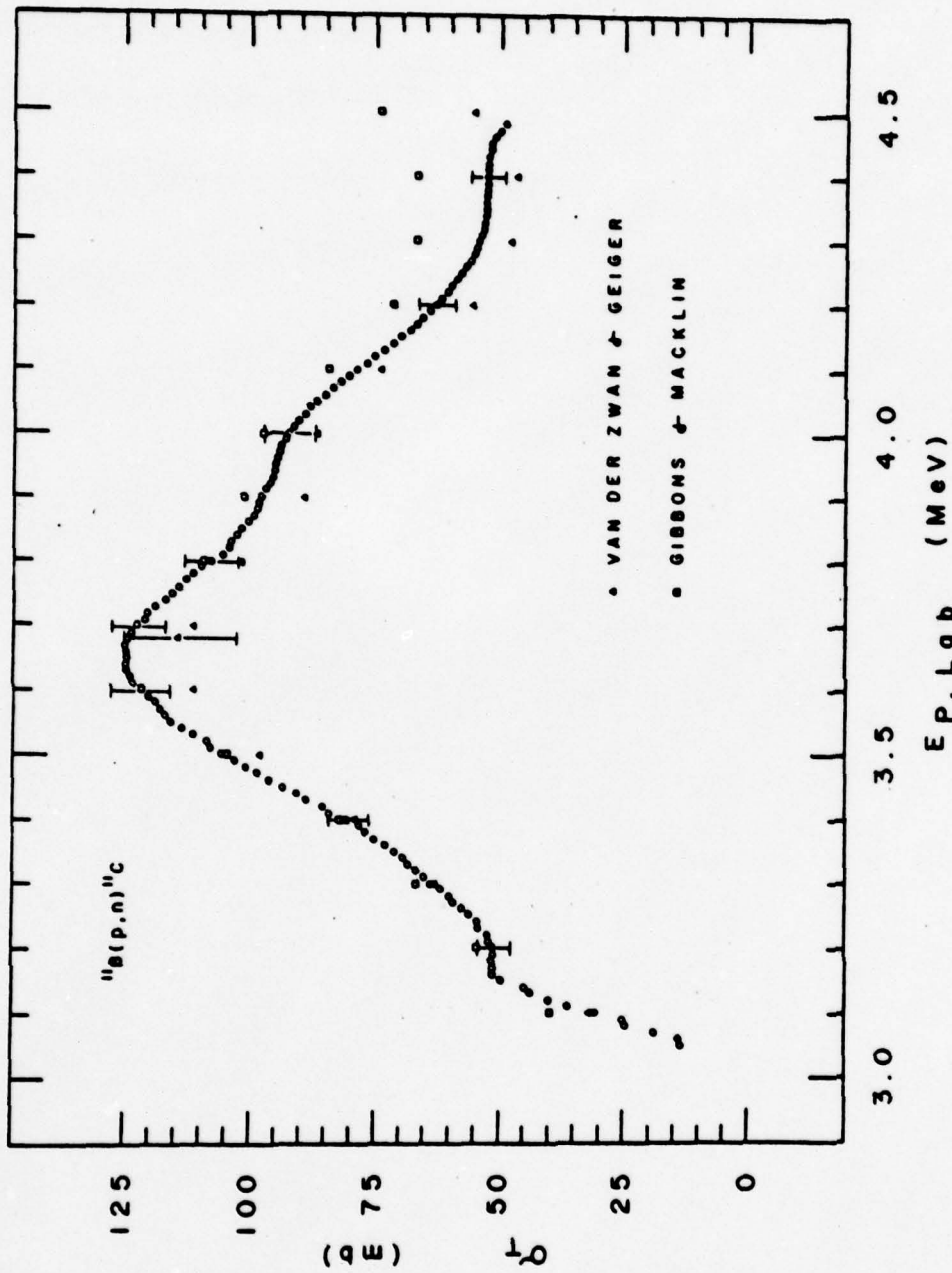


Fig. 9. Total cross sections for the $^{11}\text{B}(p,n)^{11}\text{C}$ reaction. The circles represent the present results with error bars representing the statistical uncertainties.

latter authors were unable to determine their target thickness, their published results were normalized to results published by Blaser et al.² Thus the results of Gibbons and Macklin were multiplied by a factor of 1.99 to normalize them to the present work near the 3.6 MeV peak. Statistical uncertainties for the present work are shown with error bars. Van der Zwan and Geiger's results are plotted at 100 KeV intervals and show a peak value at 3.58 MeV. Their experimental uncertainty is shown by an error bar at this energy. Within the uncertainties, there is agreement between Van der Zwan and Geiger's results and the present work. The numerical values of the total cross section and the associated uncertainties are given in Appendix B.

The Legendre polynomial power series coefficients A_1 through A_4 for the present work and the values reported by Van der Zwan and Geiger⁹ are shown in Fig. 10. The coefficients and associated statistical errors for the present work are tabulated in Appendix B. The error bars in Fig. 10 represent the statistical uncertainty for the present work. Van der Zwan and Geiger's values are plotted at 100 KeV intervals starting at 3.5 MeV. They report an isotropic behavior from threshold to 3.5 MeV, but five polynomials were required to fit their data between 3.5 and 4.5 MeV. The present results agree with a fit of five polynomials at higher energies but do not show the isotropic behavior at low energies. Increasing the number of polynomials to six did not improve the quality of the fit. Due to the kinematic restrictions in the $^{11}\text{B}(p,n)^{11}\text{C}$ reaction, the coefficients calculated below 3.2 MeV are not reliable because the back angle data does not exist

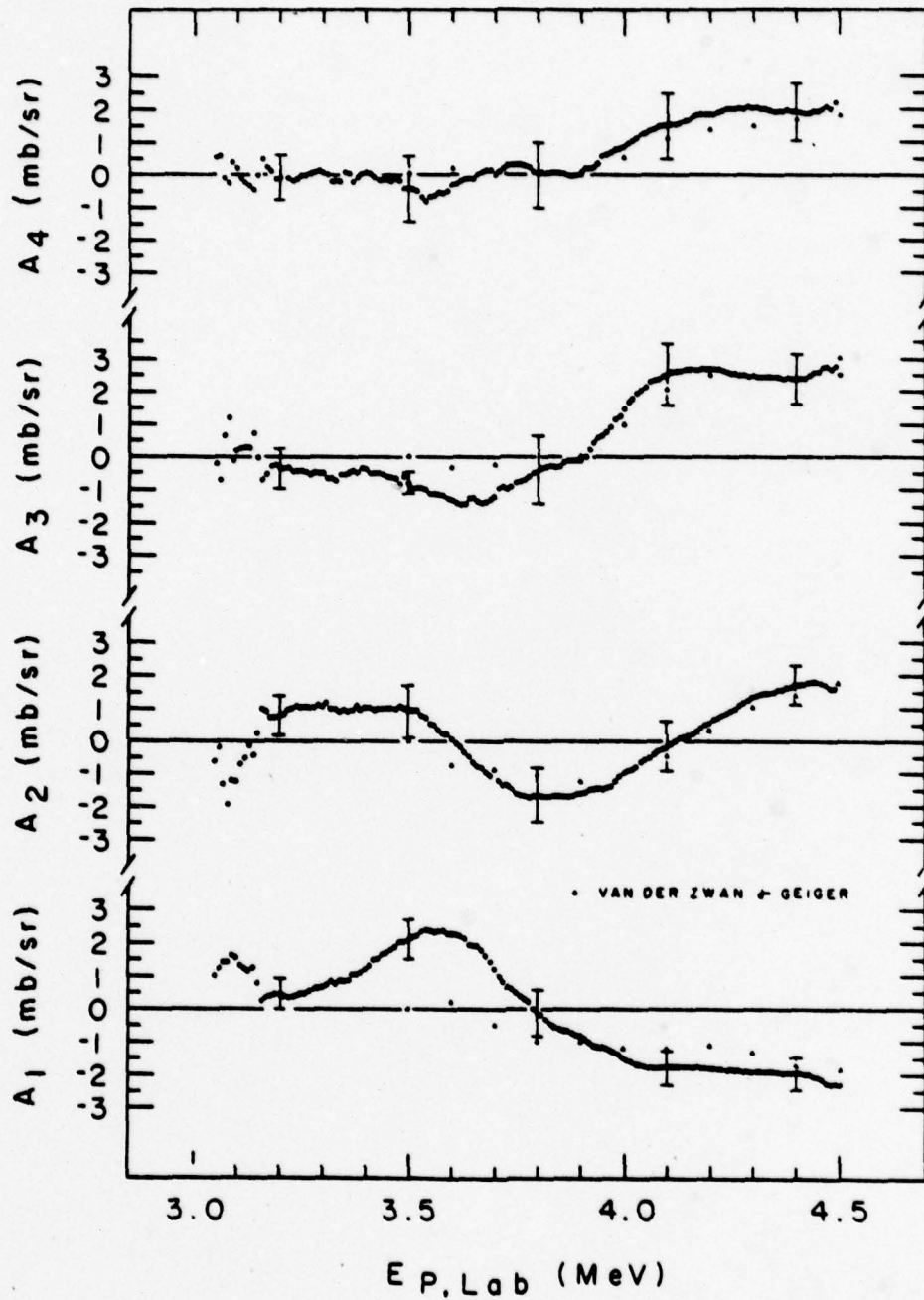


Fig. 10. Legendre polynomial expansion coefficients A_1 , A_2 , A_3 , and A_4 . The circles represent the results of the present work with error bars representing the statistical uncertainties. The triangles represent Van der Zwan and Gieger⁹ published results. The latter authors reported an isotropic behavior from threshold to 3.5 MeV.

or there are large uncertainties due to the low neutron detector efficiency. At values greater than 3.8 MeV the present data show a general agreement with those of Van der Zwan and Geiger.

The center-of-mass cross sections as a function of center-of-mass angle for selected laboratory proton energies are shown in Fig. 11. The solid curves represent calculated cross sections based on the five polynomial coefficients shown in Figs. 9 and 10. The cross sections appears to be forward peaked at higher proton energies.

B. Uncertainties.

The uncertainties in this experiment can be divided into two areas: those associated with the cross section and those associated with the proton energy.

The uncertainty in the cross section can be determined from Eq. 2.2 by taking the square root of the sum of the square of the uncertainties in each of the terms. The number of neutrons detected was subject to statistical uncertainties in the number of counts (\sqrt{N} —which is a function of the flight time) and in the time correlated background (\sqrt{N}). The resulting uncertainty for N_{det} was about 1.4%. The remainder of the uncertainties in the other terms were due to systematic errors. The stopping cross section had an overall uncertainty of 6%. This value was due in part to Janni's¹³ elemental $\frac{1}{\rho} \frac{dE_p}{dx}$ ($\sqrt{4}$ %) and possible target impurities that could give rise to another 4% error. The efficiency of the neutron detector has an associated uncertainty of 7%, although the uncertainty is probably lower at higher

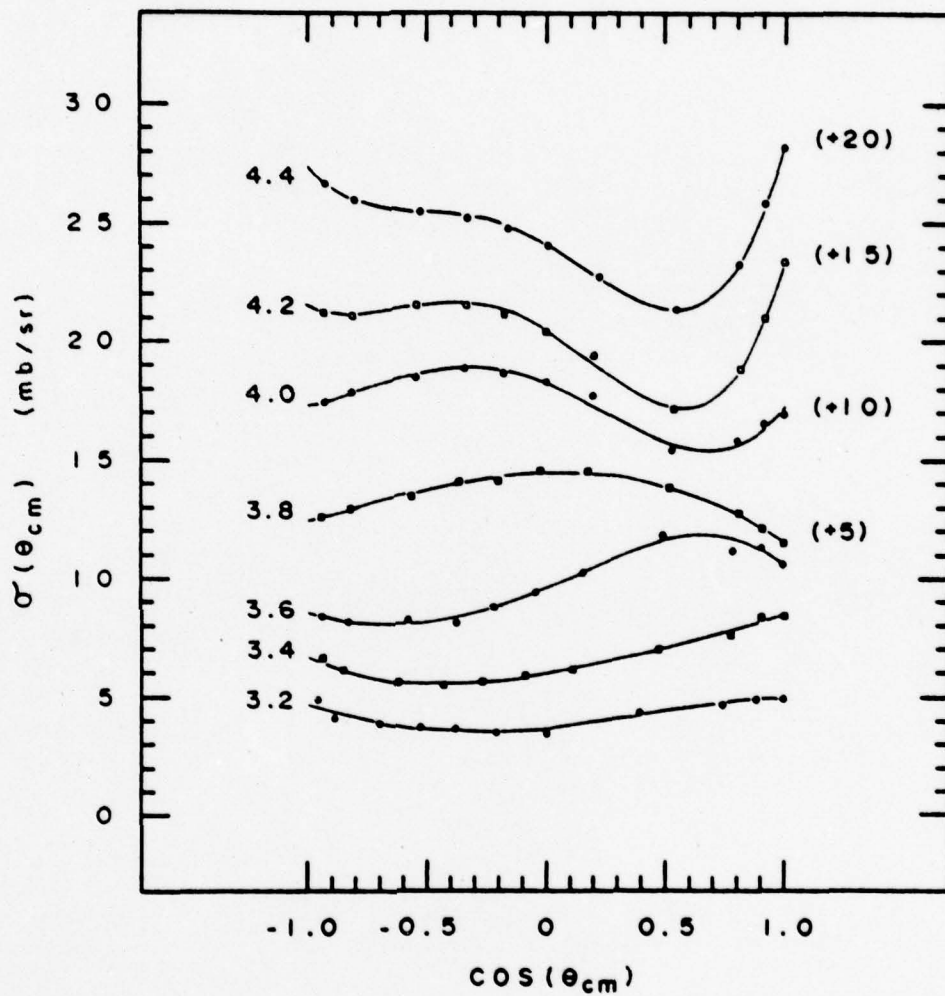


Fig. 11. $^{11}\text{B}(p,n)^{11}\text{C}$ angular distributions of the center of mass system. The laboratory proton energy of each curve is labeled on the left. The top four curves here are labeled on the right side with a vertical offset (in parentheses) to be subtracted from the ordinate to obtain the cross section at the given energy. The solid curves represent the calculated cross section as determined from the Legendre polynomials.

energies as discussed in Chapter IV. The number of incident protons had an associated uncertainty of 0.3% due in part to beam current integration uncertainty. The solid angle uncertainty was due to the combined effects of the area of the scintillator and the flight path which gave a 0.9% uncertainty. Finally the uncertainty in dE_n was $\sim 2\%$ due mainly to the channel width uncertainty.

Combining the uncertainties as mentioned above, a 9.6% uncertainty would be associated with the determination of the cross section. If the neutron efficiency were measured with respect to Liskien and Paulsen's¹⁹ data, as discussed in Chapter IV, results would be consistently lower by about 10%.

Uncertainties associated with the proton energy axis of the cross section curves depend on flight path and flight time uncertainties, and kinematic transformation of the flight time to proton energy. The flight path had an uncertainty of 0.6% due mainly to the thickness of the scintillator. The flight time uncertainty was a function of the overall timing resolution (FWHM = 1.5 nsec) and the Ortec time mark generator which gave the number of nsec per channel. At neutron energies greater than the bias settings, $\frac{dE_n}{dE_p} \approx 1$, which meant that the uncertainty for both the neutron and proton energy were about the same. Taking all this into account, uncertainties in proton energy at 3.2 and 4.5 MeV were ± 3 KeV and ± 21 KeV respectively.

C. Summary.

The first objective of this thesis has been satisfactorily met. Table I is a modified summary of past work as first described by Van der Zwan and Geiger.⁹ There is excellent agreement, within experimental errors, between Van der Zwan and Geiger and the present work for the total cross section. This was very significant, because both the thin target (Van der Zwan and Geiger) and thick targets (present work) techniques gave similar results. Overall the present work agrees well with all their results except at zero degrees, where there was a 26% difference. The reason for this discrepancy is not known. However, Marion et al.⁵ zero degree cross section at $E_p = 3.46$ MeV, which was obtained using thin target techniques, was in excellent agreement with present results.

Careful study of zero degree cross sections from B_2O_3 and B metal targets revealed that there is excellent agreement between the two at low energies. The investigation of the angular dependence of the cross section showed that the largest cross sections occurred at 0° in the laboratory. Therefore, we decided that 0° would be used in the feasibility study of boron profiling at $E_p \sim 3.2$ MeV. Further we decided that the B metal target would be used as a standard in the profiling experiments.

TABLE I. Published Cross Section for the $^{11}\text{B}(p,n)^{11}\text{C}$ Reaction.

<u>First Author</u>	<u>Ref</u>	<u>Year</u>	$\frac{\sigma_T(\text{mb})}{(E_p = 3.58 \text{ MeV})}$	$\frac{\sigma(0^\circ)(\text{mb/sr})}{(E_p = 3.58 \text{ MeV})}$	$\frac{\sigma(0^\circ)(\text{mb/sr})}{(E_p = 3.46 \text{ MeV})}$
Blaser	2	1951	58	--	--
Marion	5	1955	--	--	15
Legge	6	1961	195 ± 20	--	--
Segel	7	1965	45	--	--
Van der Zwan	9	1978	114 ± 11	11.8 ± 1.1	11.5
Present Work		1979	119 ± 11	16.0 ± 1.5	15.2 ± 1.4

VI. PROFILING

A. Theory.

The purpose of this chapter is to discuss the feasibility of using the $^{11}\text{B}(p,n)^{11}\text{C}$ reaction to determine concentrations of boron in solids. As used here, profiling means determining concentrations of boron as a function of depth below the surface of a target of otherwise known composition. The profiling is accomplished by comparing neutron time-of-flight spectra from two targets, one of pure boron and the other of an unknown concentration.

One example of neutron TOF spectra for a profiling experiment is shown in Fig. 12. The two TOF spectra were obtained with the same experimental set up used in the cross section determination. The upper TOF spectrum (squares) was obtained from a pure boron metal target with an incident proton energy of 4.517 MeV, flight path of 2.197 m and an integrated beam charge of 200 μC . The lower TOF spectrum (circles) was from a boro-silicate glass target with the $^{18}\text{O}(p,n)^{18}\text{F}$ TOF spectrum from pure SiO_2 (Fig. 4) subtracted from it. The lower spectrum was obtained with the same incident proton energy and flight path, but an integrated charge of 100 μC . Statistical fluctuations are more noticeable in the lower spectrum because the pure boron spectrum has been divided by two to normalize the integrated charge to 100 μC . However, it is very evident that the boro-silicate glass TOF spectrum shows a strong resemblance to the pure boron TOF spectrum. The two spectra have the same general characteristics.

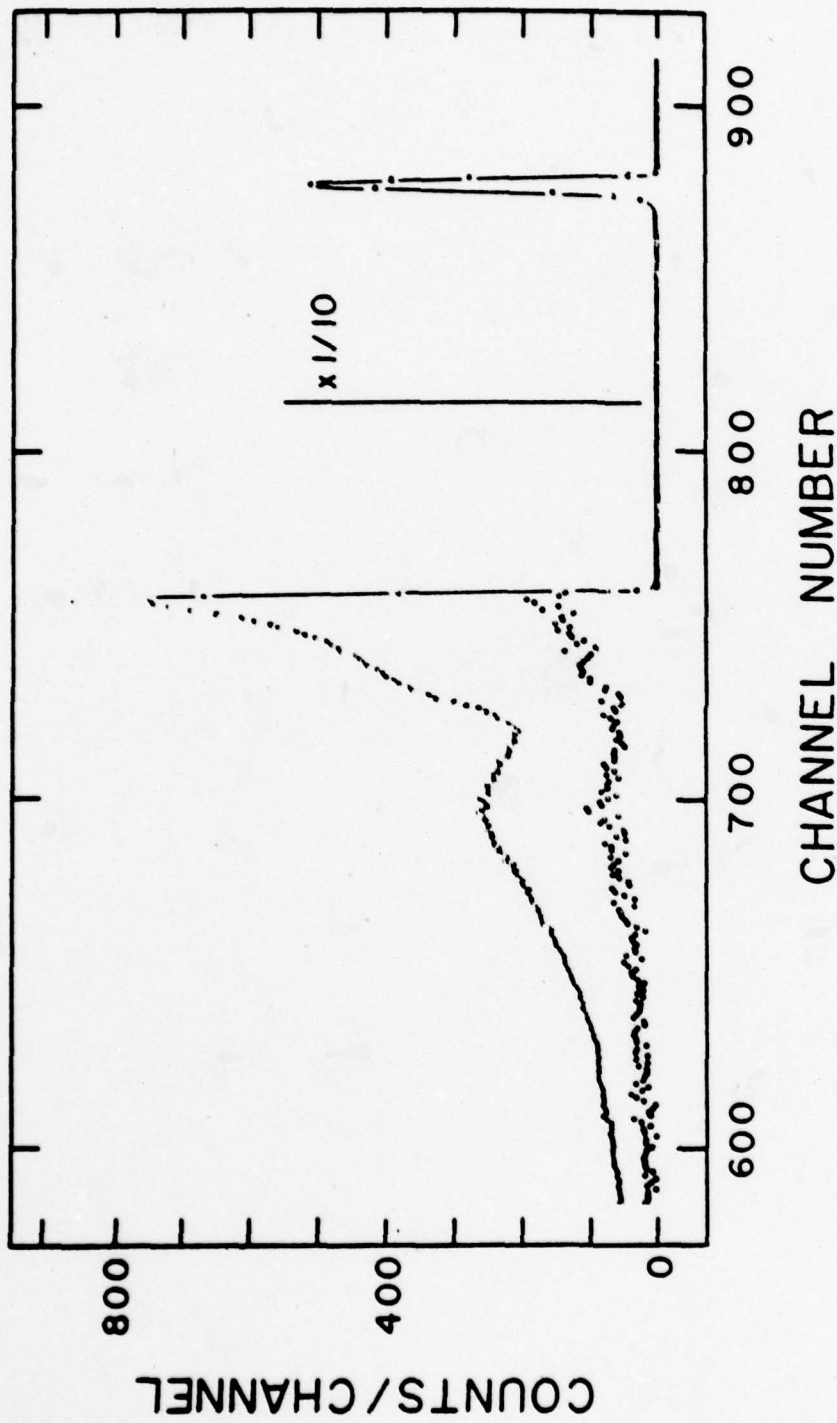


Fig. 12. Neutron time-of-flight spectra for the $^{11}\text{B}(p,n)^{11}\text{C}$ reaction. The squares represent the pure boron target. The circles represent a boro-silicate glass target with the $^{18}\text{O}(p,n)^{18}\text{F}$ TOF spectrum (Fig. 4) subtracted from it. Both targets had an incident proton energy of 4.517 MeV and flight path of 2.197 meters.

The theory and application of profiling elements by neutron time-of-flight has been studied in the past.^{10,22-23} The method used in this thesis was based on the article by Overley and Lefevre.²³ The concentration of boron atoms as a function of depth can be determined in the following manner. Let ψ_i be the atomic stopping cross section for an atom of type i . Assuming the sample of unknown concentration of boron consists of boron in a host material, one can then define ψ_H as the molecular stopping cross section for the host material,

$$\psi_H = \frac{\sum n_i \psi_i}{n_H} \quad 6.1$$

where n_H is the number density of host molecules and n_i is the number density of atoms of type i in the host material. Eq. 6.1 is related to Eq. 2.3 where the stopping cross section per ^{11}B atom is,

$$\psi = \frac{(n_{11} + n_{10})\psi_B + n_H\psi_H}{n_{11}}, \quad 6.2$$

where n_{11} is the number density of ^{11}B atoms and n_{10} is the number density of ^{10}B atoms. Expressing the two TOF spectra, taken at the same laboratory angle, in terms of their differential cross section (Eq. 2.2) one obtains,

$$N_{\text{det}}(t)_H dt = \sigma(\theta) \frac{n'_{11}}{(n'_{10} + n'_{11})\psi_B + n_H\psi_H} N_p \cdot \Delta E_p \cdot \Delta\Omega \cdot \varepsilon(E_n), \quad 6.3$$

$$N_{\text{det}}(t)_B dt = \sigma(\theta) \frac{n_{11}}{(n_{10} + n_{11})_B} N_p \cdot \Delta E_p \cdot \Delta\Omega \cdot \varepsilon(E_n), \quad 6.4$$

where the n' indicate the number densities of boron atoms in the host material. Taking the ratio of the two TOF spectra as expressed above and assuming experimental parameters are identical, one obtains the atomic concentration of boron as a function of depth x ,

$$\frac{n_B(x)}{n_B(x) + n_H(x)} = \left[1 + \left(\frac{N_{\text{det}}(t)_B(1 + \chi)}{N_{\text{det}}(t)_H(1 + \chi')} - 1 \right) \frac{\psi_B}{\psi_H} \right]^{-1}, \quad 6.5$$

where $n_B(x)$ is the number density of all boron atoms and $\chi = n_{10}/n_{11}$. For a pure boron sample χ is equal to 0.2/0.8 and for an implanted sample of ^{11}B atoms χ' is equal to zero.

Integrating the stopping cross section for the implanted sample one can calculate the depth x ,²²

$$x = - \int_{t_{\text{min}}}^t \frac{1}{n_B \psi_B + n_H \psi_H} \frac{dE_p}{dE_n} \frac{dE_n}{dt} dt, \quad 6.6$$

where t_{min} is the time corresponding to the flight time of neutrons produced at the front surface of the target, dE_p/dE_n is obtained as discussed in Chapter IV and dE_n/dt is obtained from the neutron flight time and energy relationships mentioned briefly in Chapter II.

The depth and corresponding concentration (Eq. 6.5 and 6.6) were evaluated by numerical approximations. The technique outlined by Overlay and Lefevre²² was used in this thesis. Basically, this involved taking a depth x and a depth interval Δx and calculating the ratio of the number of counts in the corresponding time interval in the TOF spectra.

B. Resolution Analysis.

The resolution as defined by Overley et al.¹⁰ is the uncertainty Δx in the depth at which the reaction occurs,

$$\Delta x = \Delta E_p (\Sigma n_i \psi_i)^{-1} , \quad 6.7$$

where ΔE_p is a proton energy interval and $n_i \psi_i$ is as defined previously. Assuming the front surface of the target to be smooth, there are three main effects that can contribute to the resolution: incident beam energy spread, energy straggling, and finite time resolution which gives rise to a spread in neutron energy and hence in proton energy.

Klystron beam bunching introduces a 5 KeV spread in incident beam energy. For a SiO_2 target with $E_p = 4.5$ MeV and a Si target with $E_p = 3.2$ MeV the associated depth uncertainties are $0.26 \mu\text{m}$ and $0.31 \mu\text{m}$ respectively. The values of $\Sigma n_i \psi_i$ in Eq. 6.7 were calculated with Eq. 2.4 in units of $\text{MeV}/\mu\text{m}$ from Janni's¹³ values. For a SiO_2 target with a molecular number density of $2.326 \times 10^{22} \text{cm}^{-3}$ the calculation constants of Eq. 2.4 were $C_1 = 1.776 \times 10^{-2} \text{MeV}^2/\mu\text{m}$ and $C_2 = 2.568$. The values for a Si target with a number density of 4.997×10^{22} atoms cm^{-3} were, $C_1 = 1.738 \times 10^{-2} \text{MeV}^2/\mu\text{m}$ and $C_2 = 2.322$.

Straggling has an effect only below the surface of the target. As the proton penetrates further into the target the straggling becomes more important. Utilizing Bohr's expression for energy straggling²⁴ one can solve for the uncertainty Δx_s (FWHM) due to straggling,

$$x_s = \frac{c}{\Sigma n_i \psi_i} \sqrt{x} , \quad 6.8$$

where Δx_s and x are in microns and $n_i \psi_i$ is evaluated at the energy the proton has at depth x . The constant c is equal to $2.355 [4\pi e^4 \Sigma(z_i n_i)]^{1/2}$ where z_i is the atomic number of atom i .

Differentiation of the basic relationship between neutron energy and flight time leads to the depth uncertainty Δx_t (FWHM) due to time resolution Δt ,

$$\Delta x_t = \frac{E_n^{3/2} \Delta t}{\Sigma n_i \psi_i \cdot X} \left(\frac{8}{m_n} \right)^{1/2}, \quad 6.9$$

where X is the flight path, m_n is the mass of the neutron and Δt is the time resolution (≈ 1.5 nsec). The stopping power $\Sigma n_i \psi_i$ is again evaluated at the energy the proton has when it produces a neutron of energy E_n . Eq. 6.9 assumes $\Delta E_p \approx \Delta E_n$ as discussed in Chapter V. Unlike the other two effects, Δx_t can be minimized experimentally by increasing X or decreasing the neutron energy. Neutron energy can be decreased by decreasing the incident proton energy, so long as the proton energy at any given depth remains above threshold.

The results of quadratically combining the three contributions to depth resolution for a SiO_2 and Si target are shown in Fig. 13. The incident proton energies and flight paths are indicated below the respective curves. The curves end at that depth where the proton energy has reached threshold, 10.1 μm for Si and 79.6 μm for SiO_2 . When the curve rises with depth straggling is dominant and where the curve falls with depth flight time resolution dominates.

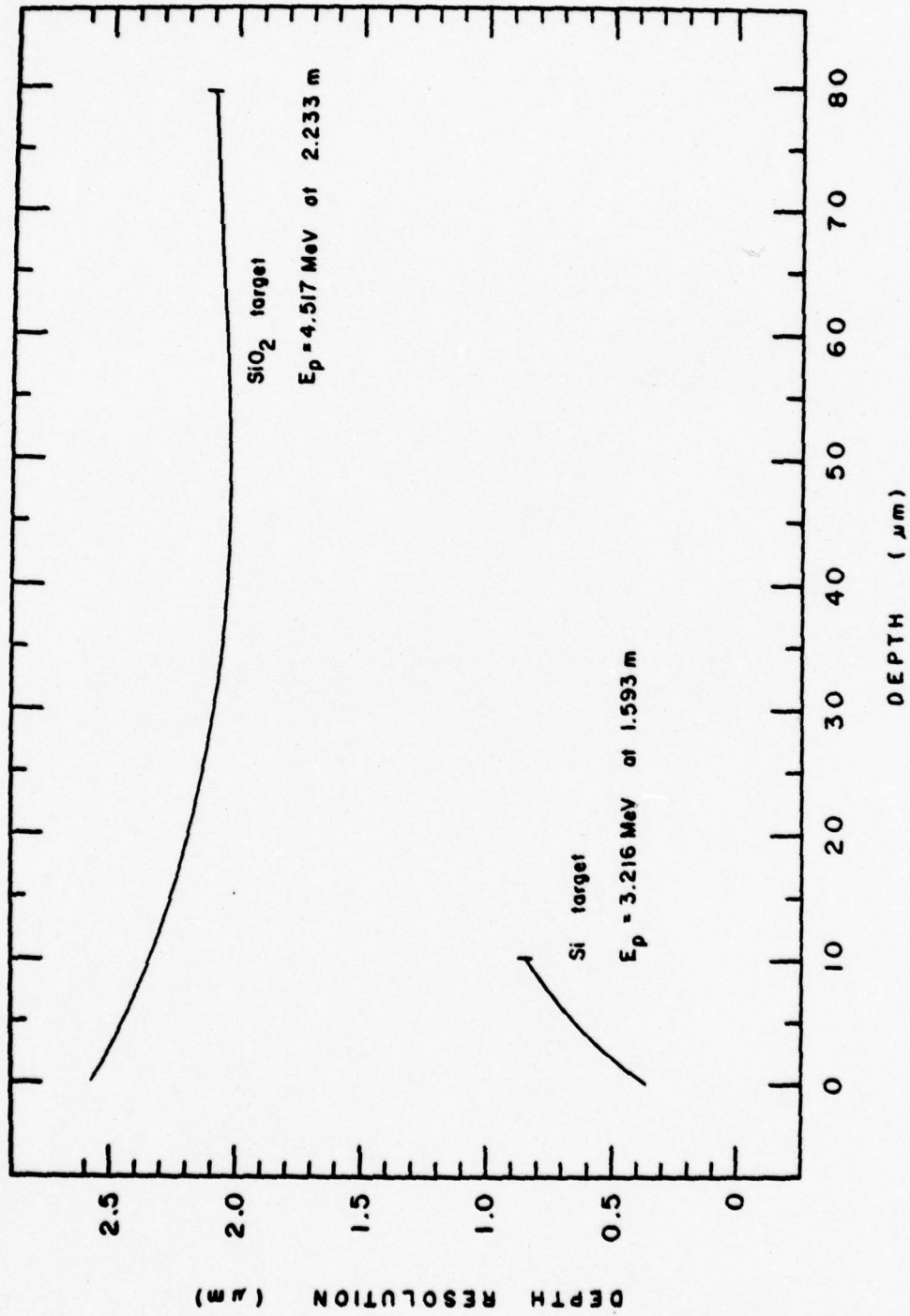


Fig. 13. Depth resolution versus depth in Si and SiO₂ targets with incident proton energy and flight path as indicated.

A computer code for calculating lithium concentrations in niobium¹² was modified for boron in silicon and for boron in silicon dioxide. (The program for silicon, SIBPRP is in Appendix F.) The second code was applied to the two spectra of Fig. 12 to calculate the concentration of boron atoms as a function of depth in the borosilicate glass sample. The results of the calculation are shown in Fig. 14. As expected, the concentration of boron is constant at about 5 atoms per 100 SiO₂ molecules. The error bars are based on the statistical uncertainty in the number of counts in the neutron TOF spectra. The negative concentration values are due to statistical fluctuations in the two TOF spectra. A front surface resolution of ~4 μm is experimentally obtained. This is in contrast to a calculated resolution of 2.6 μm. One reason the experimental resolution for the borosilicate target might be worse than calculated could be due to impurities near the target front surface. This particular target had been used for a number of years to align the accelerator's charged particle beam, as such has been bombarded with a lot of protons and α particles over the years.

C. Sensitivity Analysis.

To determine the minimum concentration of boron atoms one can detect using the $^{11}\text{B}(p,n)^{11}\text{C}$ reaction, the sensitivity of the method must be investigated. The sensitivity, defined as the number of boron atoms per unit area $n_B \Delta x$, which can be detected can be determined from Eq. 2.2 and Eq. 6.7 as,

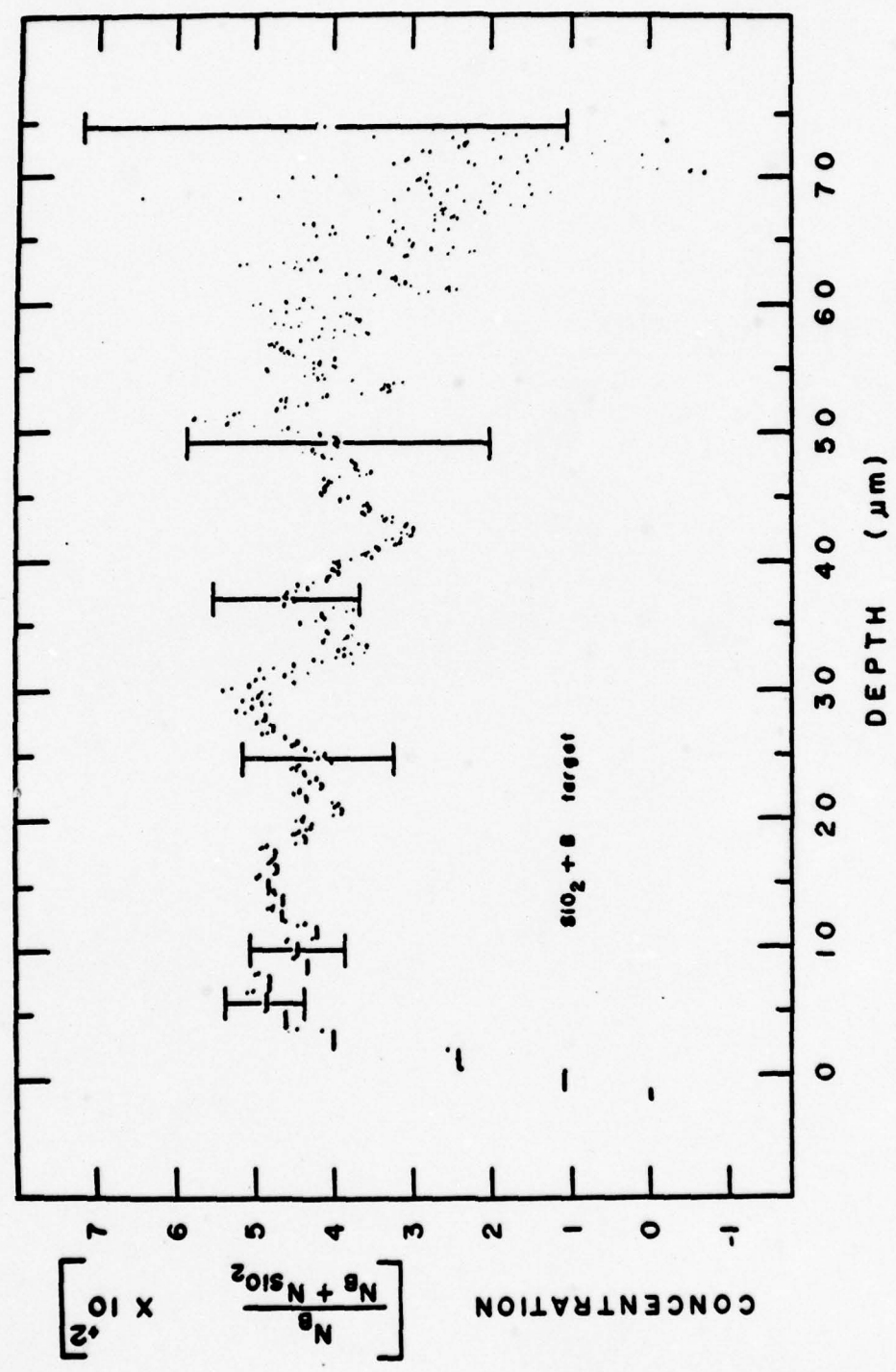


Fig. 14. Concentration of boron atoms versus depth in the borosilicate glass target. The incident proton energy was 4.517 MeV and the flight path was 2.233 meters. Error bars are based on statistical uncertainty in the number of counts in the neutron TOF spectra.

$$n_B \Delta x = \frac{N_{\text{det}}(t) \Delta t}{\sigma \cdot N_p \cdot \Delta \Omega \cdot \epsilon(E_n)} \quad . \quad 6.10$$

Overley et al.¹⁰ solved for the limit of the sensitivity in the following manner. If the areal density of boron atoms is to be determined to $\pm 10\%$, then the number of counts $N_{\text{det}}(t) \Delta t$ must be greater than 100. If one assumes a beam current of $1.5 \mu\text{A}$ is incident on the target for 1 hour, that a detector 11.43 cm in diameter with an efficiency of 30% is located 1.593 m from the target, and that the reaction cross section is 9.5 mb/sr, then the minimum boron content which can be measured is $n_B \Delta x = 2.8 \times 10^{14} \text{ cm}^{-2}$. Thus, if it is desired to determine the boron content to $\pm 10\%$ in a $0.1 \mu\text{m}$ depth interval, the density of boron atoms must be greater than $2.8 \times 10^{19} \text{ cm}^{-3}$. For boron in otherwise pure Si this represents 560 atomic parts per million (ppm) and in otherwise pure SiO_2 this represents a concentration of 1200 boron atoms per million SiO_2 molecules.

In practice one cannot expect to obtain the above calculated lower limit of sensitivity because of several types of background effects. There are three main background effects that can reduce the sensitivity.¹⁰ The first is a time uncorrelated background cosmic rays, natural radioactivity, and from room-thermalized neutrons inducing (n, γ) reactions. These effects can be minimized by building a better shielding system and by using a pulse shape discriminator to distinguish between neutron and γ ray signals from the scintillator. Other sources of background are time-correlated. These can result, for example, from (p, n) reactions

from light nuclei target constituents with low (p,n) threshold values. An example of this is the boro-silicate glass target where ^{18}O was present and neutrons from the $^{18}\text{O}(p,n)^{18}\text{F}$ reaction had to be subtracted. The third main effect is from scattered neutrons. If boron atoms are localized at one depth in the target, then there will be neutrons emitted with a very well defined energy. These neutrons can then be scattered in the room and be detected at lower energies, thereby producing a low energy tail in the TOF spectrum. This tail then tends to mask the effect of any other boron concentration at greater depths, thereby reducing the sensitivity.

To investigate the sensitivity experimentally, basically the same experimental set up was employed, but with the detection system used by Lunnon.¹⁶ To reduce time-uncorrelated background effects the scintillator system was shielded and pulse shape discrimination was used. A block diagram of the electronics is shown in Fig. 15. The scintillator was a 11.43 cm diameter by 2.54 cm thick NE 218 (Nuclear Enterprise) liquid scintillator. This scintillator was chosen by Lunnon because of its good discrimination between neutrons and γ rays. The scintillator shielding consisted mainly of a 1 meter long by 1 meter diameter doughnut shaped tank filled with boric acid and water. The scintillator was mounted inside the doughnut hole and shielded by lead blocks. The pulse shape discriminator used in this investigation is described in detail by Lunnon.¹⁶ The neutron window was set with a single channel analyzer (SCA) using an Am-Be neutron source. The SCA was adjusted to eliminate as many γ rays as possible without losing

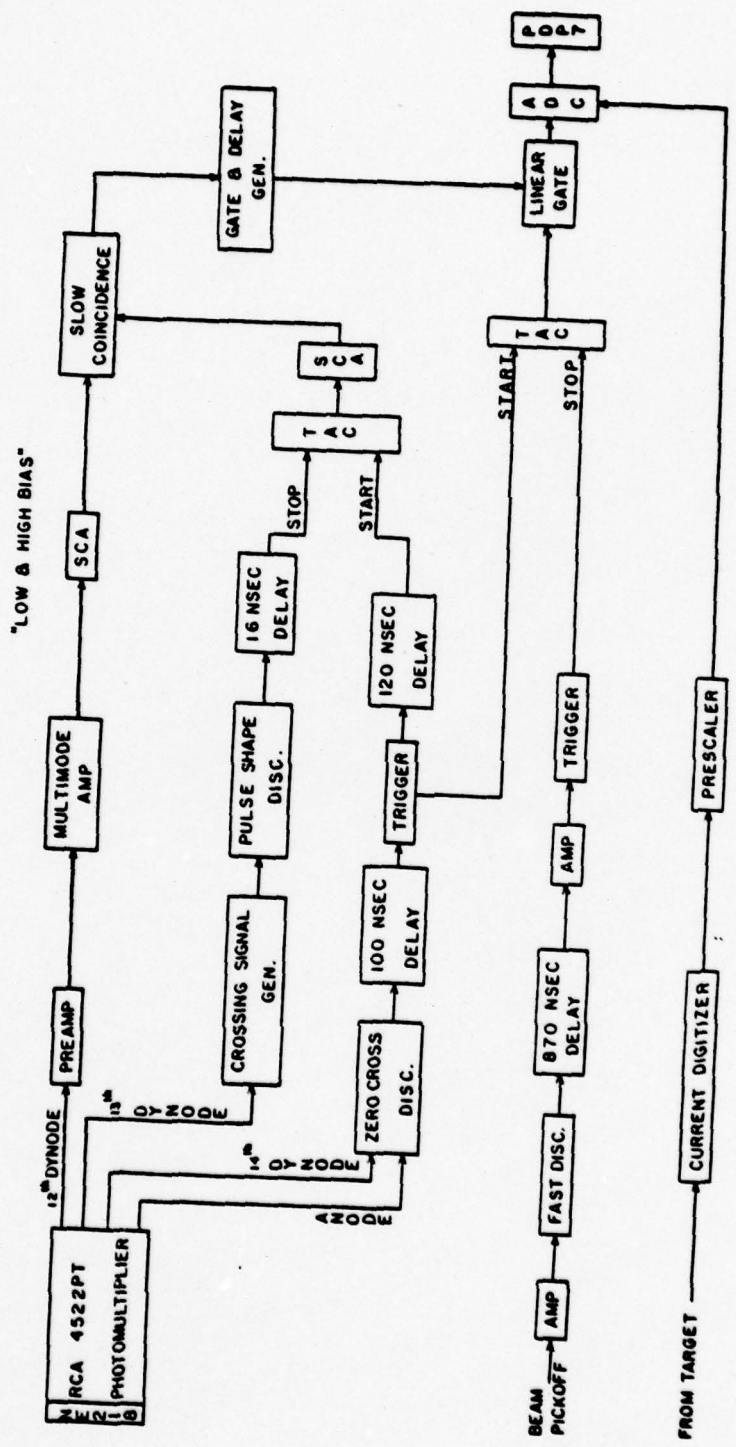


Fig. 15. Block diagram of electronics used in sensitivity profiling.

too many neutrons. The resulting signal was placed in coincidence with the SCA setting a low and a high pulse height bias. The low bias pulse height spectrum was set to 1/5 of the ^{241}Am 60-KeV γ ray full energy peak. The timing bias was adjusted to the low bias pulse height spectrum as described in Chapter II. The high bias was used to reduce background effects as much as possible, and was adjusted each time the incident proton energy was changed. The high bias was set to cut off pulses greater than those produced by 1.69 MeV or 0.31 MeV neutrons for incident proton energies of 4.517 MeV or 3.216 MeV respectively.

In order to maximize the sensitivity limits of this experiment one must have a high cross section and a large solid angle (small flight path). To maximize resolution one should have low neutron energy and long flight path. Thus to give a reasonable depth resolution and the best sensitivity an incident proton energy of 3.2 MeV was used and neutrons were observed at 0° with a 1.593 m flight path. This gave a maximum neutron energy of 0.31 MeV, a fairly high cross section of 9.5 mb/sr and a minimal flight path consistent with the constraints imposed by the shielding. Neutron TOF spectra were taken either at 1 or 1.5 μA beam current for around one hour on a boron-implanted $\langle 100 \rangle$ silicon target* doped with either As or P. Each targets' TOF spectrum was taken for a total of 5 mC integrated beam charge. The targets were silicon wafers implanted at 200 KeV with 1×10^{15} atoms of ^{11}B cm^{-2}

*The targets were supplied by Dr. Dean Casey, Manager, Material Research Laboratory, Tektronic, Inc.

(isotopically separated). An example of a neutron TOF spectrum is shown in Fig. 16. The small peak (~ 120 counts) near channel 420 corresponds to neutrons emitted from the implanted boron. The large γ ray peak lies beyond channel 650. Again the channel width was approximately 0.97 nsec/channel.

Immediately following the boron-implanted target run, a background spectrum was taken under the same experimental conditions. The boron-implanted Si target was turned over and the back of the target was bombarded with protons. Fig. 17 shows the background TOF spectrum obtained for a total integrated charge of 5 mC. The flat background below channel 550 indicates that the peak in Fig. 16 near channel 420 was indeed due to the implanted boron. The peaks in both Figs. 16 and 17 are basically the same in channels beyond 550. The two smaller peaks in Figs. 16 and 17 near channel 600 are thought to be a result of higher beam mass or gating difficulties as described in Chapter III. The peaks in channels beyond 700 are thought to be due to the 24 MHz bunching rate for the proton beam. Careful investigation of these peaks reveals that the peak near channel 710 is indeed separated by 40 nsec from the prompt γ ray. Further, one can see in Fig. 17 another peak 40 nsec earlier near channel 750. These peaks are very small as compared to the main γ ray peak and are seen only in runs of long time duration.

The spectrum of Fig. 16 was corrected for background (Fig. 17) and was analyzed in much the same way as the boro-silicate glass data. A TOF spectrum from a pure B metal target, obtained under the same experi-

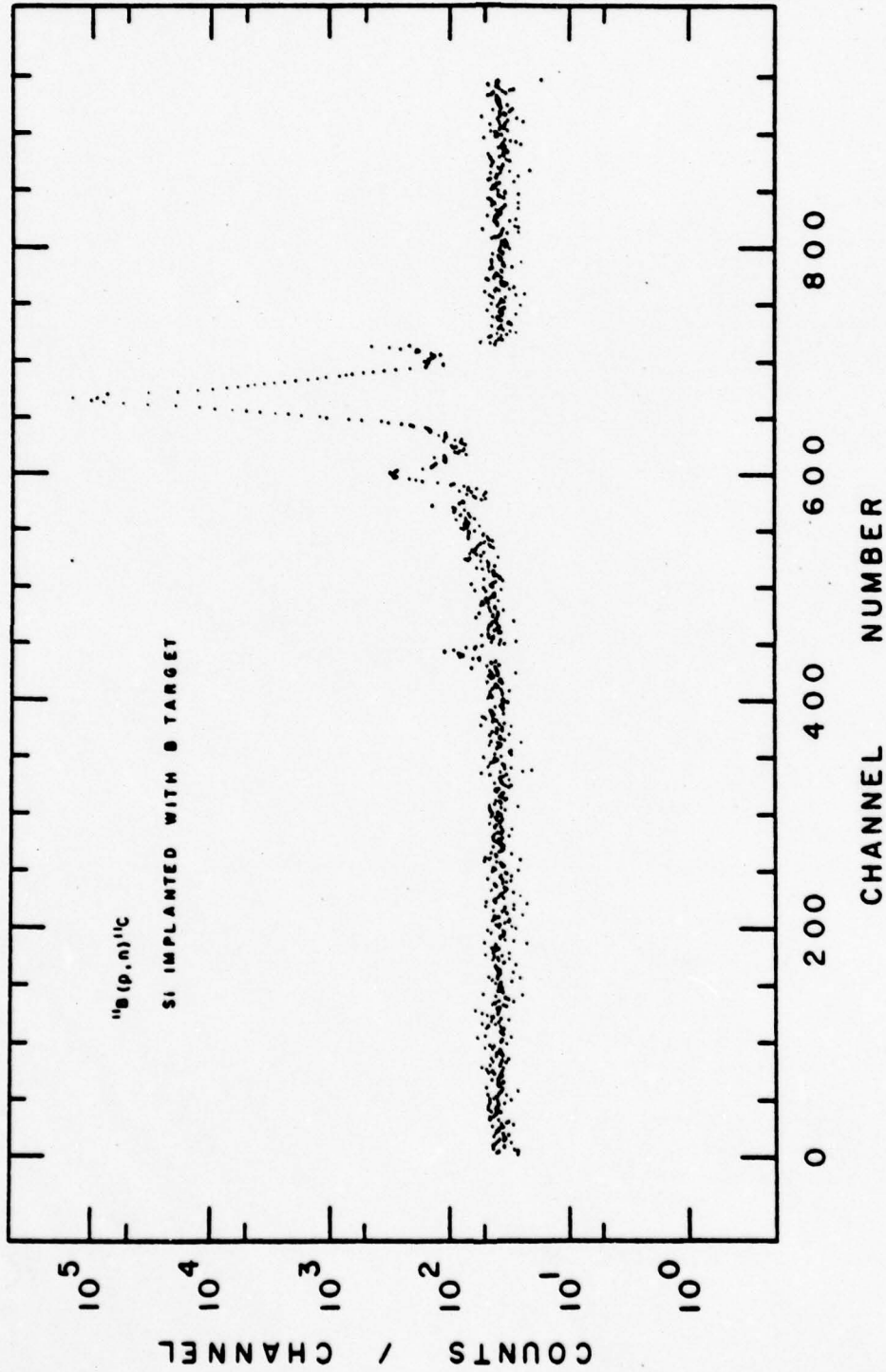


Fig. 16. Time-of-flight spectrum for boron profiling. The incident proton energy was 3.216 MeV, with a flight path of 1.593 meter and integrated beam current of 5 mc.

Neutrons from the $^{11}\text{B}(p,n)^{11}\text{C}$ reaction are confined to the small peak near channel 420.

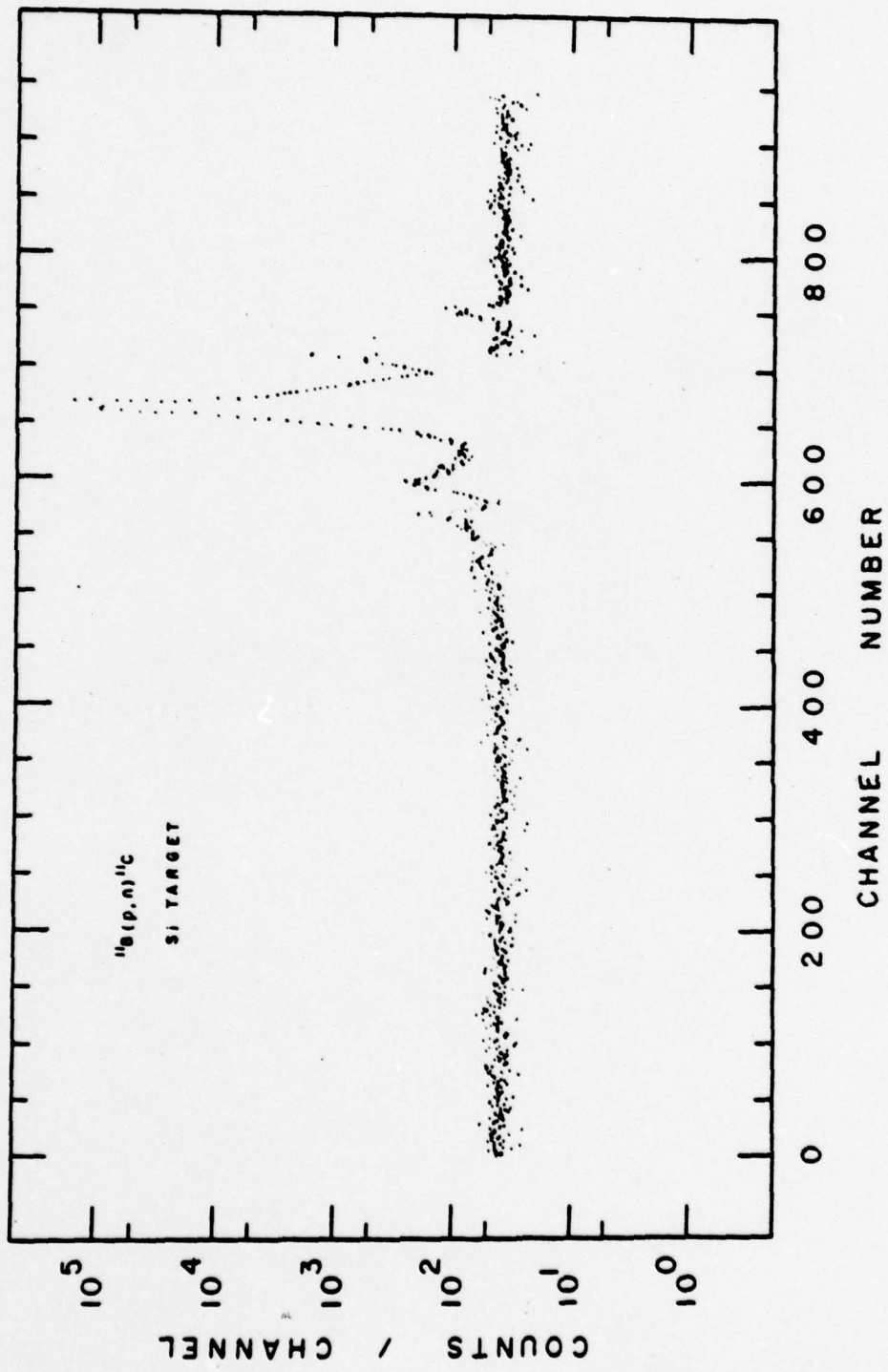


Fig. 17. Background time-of-flight spectrum from a silicon target. Experimental conditions were the same as described in Fig. 13.

mental conditions was used as the standard. The program SIBPRP (Appendix F) was used to obtain the concentration of boron atoms as a function of depth. Three Si targets were investigated, two As doped and one P doped. Their respective concentration profiles are shown in Fig. 18. The data points at less than zero depth are due to calculation of the concentration in front of the target and give an indication of the background fluctuations. If the backgrounds were identical the concentration would be zero in this region. The solid curves in Fig. 18 are drawn only to aid the reader's eye in determining the general shape of the peak.

In general all three targets show a peak near a depth of 1 μm and have a maximum ^{11}B concentration of ~ 225 ppm in a 0.1 μm depth interval. The actual concentration is undoubtedly much higher. It appears to be decreased by resolution effects. Integrating the concentration in each of the three peaks produces areal ^{11}B densities of $9.94 \pm 1.32 \times 10^{14} \text{ cm}^{-2}$, $9.25 \pm 1.39 \times 10^{14} \text{ cm}^{-2}$, and $8.33 \pm 1.27 \times 10^{14} \text{ cm}^{-2}$ for the top, middle and bottom profiles respectively. The error represents the combined uncertainties in the terms of Eq. 6.5 assuming the stopping cross sections have an uncertainty of $\sim 6\%$. The combined uncertainty was $\sim 15\%$ due mainly to counting statistics. The experimental ^{11}B areal densities for the two As-doped targets agree with the implanted densities of 10^{15} cm^{-2} to within the experimental uncertainty. The density for the P-doped target lies just outside the uncertainty limit. If the sensitivity limit of concentration is calculated for a measurement with 15% precision, one obtains 199 atomic ppm. This is

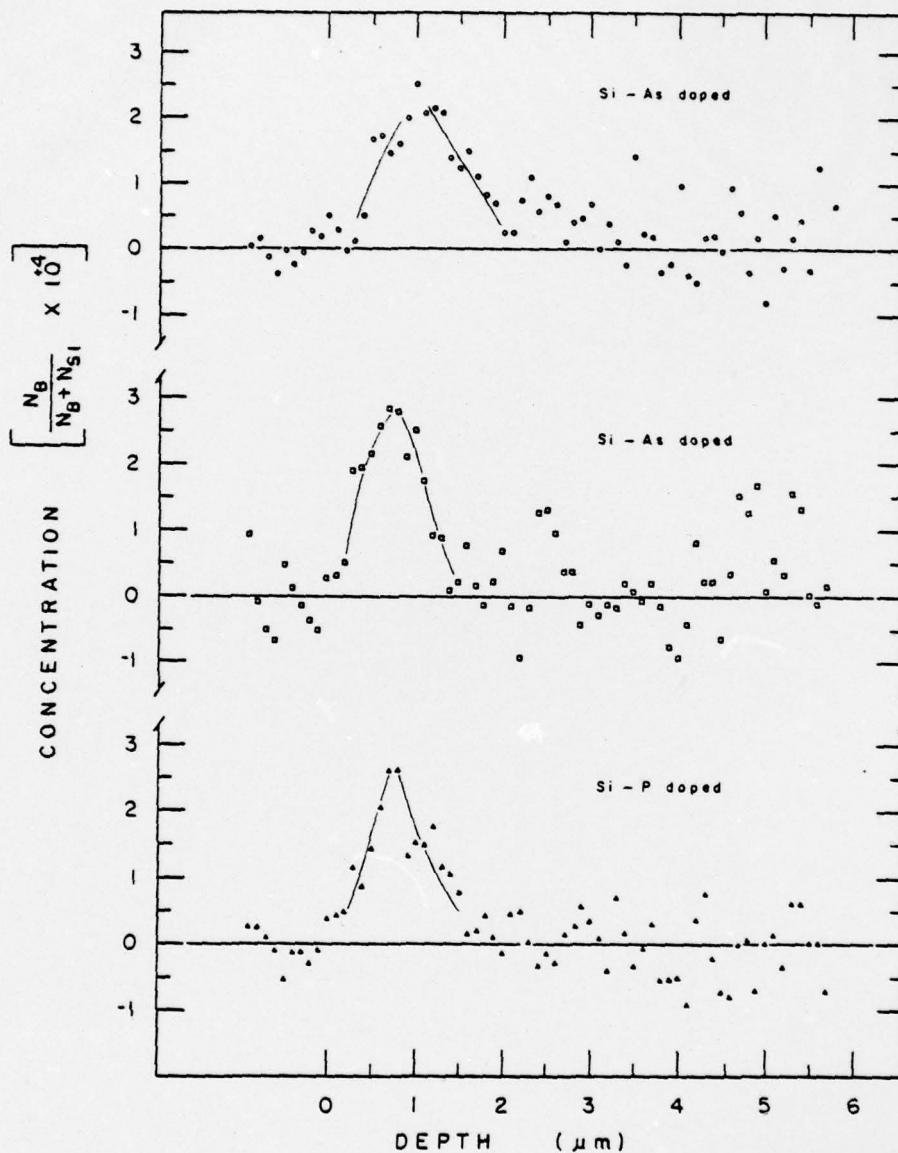


Fig. 18. Concentration of boron atoms versus depth for silicon implanted with boron. The silicon targets were doped with either As or P as indicated. Isotopically separated ^{11}B was implanted in the Si at an energy of 200 KeV. The concentration was calculated assuming a natural abundance of boron isotopes. The ordinate must therefore be multiplied by 0.8 since only ^{11}B is present.

close to the experimental value of 225 ppm. An analysis of the depth resolution of Fig. 18 shows a FWHM of 0.8 μm . This is in contrast to a calculated depth resolution of 0.4 μm (Fig. 13). The difference in depth resolution could be an indication of the limit of the technique, but more likely it is due to an underestimation of the straggling effects as calculated in Eq. 6.8. Bohr's formula is a fairly crude approximation of straggling due only to electronic stopping.

D. Conclusions.

The final objective of this thesis has been met. The $^{11}\text{B}(p,n)^{11}\text{C}$ reaction can be used to determine boron atomic concentration to ~ 225 ppm with a precision of 15%. The theoretical limit of resolution was not achieved in either of the two experiments, 0.35 μm for Si and 2.6 μm for SiO_2 . However, this could be due to target front surface problems and straggling estimations. We find that 200 KeV ^{11}B atoms implanted in silicon reside at a depth of ~ 1 μm with a FWHM of 0.8 μm .

The ^{11}B atom implantation depth in Si has been studied in the past using secondary ion mass spectroscopy,^{25,26} differential capacitance,²⁷⁻²⁹ and Hall effect and sheet-resistivity^{30,31} techniques. Boron implantation at three silicon crystalline configurations have been investigated; $\langle 110 \rangle$ which involves channeling and $\langle 111 \rangle$ and $\langle 100 \rangle$ where the effect of channeling is reduced. Further studies have been made on amorphous silicon where there is no crystalline structure present. Implanting ^{11}B atoms along the $\langle 110 \rangle$ configuration, maximizes the

effects of channeling and a depth of $1.7 \pm 0.2 \mu\text{m}$ with a FWHM of $0.6 \mu\text{m}$ at an implantation energy of 200 KeV was reported by Lecrosnier et al.²⁷ These authors also investigated the $\langle 111 \rangle$ configuration at the same energy and obtained a depth of $0.8 \mu\text{m}$. Davis^{28,29} and Lecrosnier et al.²⁷ have studied the mis-alignment of the crystal off the $\langle 111 \rangle$ axis with ^{11}B atom implantation energies of 200 KeV and obtained values of $0.66 \mu\text{m}$ with a FWHM of $0.6 \mu\text{m}$ and $0.6 \mu\text{m}$, respectively. Ohmura et al.³¹ studied the mis-alignment of the $\langle 100 \rangle$ crystal axis and further reduced channeling effects by growing a thin film of SiO_2 over the crystal surface. At an implantation energy of 200 KeV, ^{11}B atoms were reported to have a depth of $0.58 \mu\text{m}$ with a FWHM of $0.25 \mu\text{m}$. However, it should be noted that the samples are still crystalline and effects of channeling can still be there.²⁸ Amorphous silicon was also studied and values of $0.5 \pm 0.1 \mu\text{m}$ have been reported.^{26,29,32}

We could not locate a report specifically on the unobstructed Si $\langle 100 \rangle$ configuration at an energy of 200 KeV, but conclusions based on the above data can be drawn. One would expect the $\langle 100 \rangle$ and $\langle 111 \rangle$ configuration of silicon to have an implantation depth of ^{11}B atoms, at the same energy, to be greater than that in the amorphous sample and less than that observed in the $\langle 100 \rangle$ configuration. Based on this conclusion, which holds true for the $\langle 111 \rangle$ configuration, our results of the $\langle 100 \rangle$ oriented silicon sample seems reasonably consistent. Further, Wittmaack et al.²⁶ have reported that the depth distribution is not gaussian in shape at implantation energies greater than 40 KeV.

This also fit our data, as can be seen in Fig. 18. The reason for the non-gaussian shape is being investigated.

The $^{11}\text{B}(p,n)^{11}\text{C}$ reaction offers a non-destructive technique for determining boron atomic concentration as a function of depth. However, this technique probably is too limited in resolution and sensitivity to be of practical use to the semiconductor industry, where depth resolutions of less than $0.1\ \mu\text{m}$ are desirable.

Throughout this profiling investigation the main limiting factor was in the counting statistics of the foreground and background TOF spectra. These can be improved by counting for longer times, but a factor of 10 improvement in sensitivity would require counting for about four days, and the resolution would still be limited to about $0.35\ \mu\text{m}$ FWHM.

APPENDIX A

TABLE A.1. Differential Cross Sections and Associated Statistical Uncertainty for the $^{11}\text{B}(p,n)^{11}\text{C}$ Reaction.

E _p , lab MeV	$\sigma(0^\circ)$		$\sigma(20^\circ)$		$\sigma(31^\circ)$		$\sigma(50^\circ)$		$\sigma(69.8^\circ)$		$\sigma(80.3^\circ)$	
	mb/sr	$\Delta\sigma$	mb/sr	$\Delta\sigma$	mb/sr	$\Delta\sigma$	mb/sr	$\Delta\sigma$	mb/sr	$\Delta\sigma$	mb/sr	$\Delta\sigma$
3.03	3.756	0.117	5.877	0.122	6.666	0.666	6.666	0.666	6.666	0.666	6.666	0.666
3.04	5.661	0.113	5.545	0.114	6.666	0.666	6.666	0.666	6.666	0.666	6.666	0.666
3.05	5.597	0.116	5.327	0.111	4.668	0.666	3.869	0.666	6.666	0.666	6.666	0.666
3.05	6.033	0.115	5.686	0.113	4.555	0.102	3.461	0.666	6.666	0.666	6.666	0.666
3.07	6.126	0.113	6.615	0.114	5.619	0.156	4.615	0.666	11.561	0.583	6.666	0.666
3.08	6.177	0.114	6.345	0.115	5.483	0.166	4.766	0.666	4.819	0.124	7.812	0.179
3.09	6.706	0.117	6.683	0.119	6.666	0.113	5.264	0.666	3.766	0.166	1.275	0.052
3.10	7.723	0.124	7.244	0.126	6.466	0.116	5.666	0.166	2.752	0.166	1.938	0.061
3.11	9.675	0.136	8.171	0.127	7.128	0.116	6.361	0.166	4.616	0.166	2.286	0.066
3.12	9.616	0.133	8.535	0.132	7.424	0.123	6.469	0.166	4.356	0.113	2.783	0.071
3.13	9.965	0.146	9.363	0.135	8.645	0.124	6.766	0.166	4.358	0.112	3.645	0.075
3.14	10.213	0.143	9.693	0.139	7.971	0.125	6.696	0.166	4.551	0.114	3.563	0.080
3.15	10.354	0.144	9.725	0.139	8.268	0.126	6.963	0.166	4.661	0.114	3.625	0.080
3.16	10.141	0.142	9.717	0.140	8.236	0.125	6.278	0.666	4.794	0.114	3.616	0.077
3.17	10.038	0.141	9.797	0.140	8.163	0.127	6.372	0.666	4.519	0.166	3.649	0.078
3.19	9.866	0.139	9.893	0.135	8.076	0.127	6.421	0.666	4.566	0.166	3.875	0.080
3.19	9.612	0.137	9.618	0.132	8.046	0.125	6.485	0.666	4.517	0.166	3.497	0.076
3.20	9.413	0.136	9.666	0.133	8.042	0.125	6.576	0.666	4.222	0.166	3.763	0.077
3.21	9.567	0.137	8.916	0.132	7.786	0.123	6.646	0.666	4.458	0.166	3.574	0.075
3.22	9.437	0.146	9.134	0.134	7.772	0.123	6.599	0.666	4.288	0.166	3.756	0.077
3.23	9.648	0.136	9.436	0.135	8.222	0.127	6.875	0.666	4.566	0.166	3.623	0.074
3.24	9.807	0.146	9.264	0.136	8.252	0.127	6.635	0.666	4.622	0.166	3.762	0.076
3.25	10.021	0.142	9.451	0.137	8.465	0.136	6.832	0.666	4.937	0.113	3.849	0.077
3.26	10.156	0.145	9.745	0.139	8.417	0.129	7.083	0.666	4.937	0.112	4.165	0.079
3.27	10.312	0.142	9.761	0.142	8.607	0.132	7.288	0.666	5.227	0.116	4.163	0.080
3.28	10.854	0.153	10.179	0.146	8.661	0.133	7.336	0.666	5.272	0.115	4.469	0.083
3.29	11.132	0.156	10.232	0.147	8.643	0.136	7.529	0.666	5.255	0.115	4.469	0.084
3.30	10.983	0.156	10.538	0.151	8.316	0.139	7.761	0.666	5.256	0.114	4.838	0.087
3.31	10.920	0.157	10.992	0.155	8.556	0.142	8.019	0.666	5.256	0.117	4.606	0.085
3.32	10.617	0.156	10.866	0.155	10.057	0.147	8.216	0.666	5.621	0.117	4.861	0.086
3.33	10.521	0.156	10.685	0.156	10.612	0.147	8.429	0.666	5.682	0.121	4.836	0.085
3.34	11.294	0.163	10.772	0.157	9.949	0.149	8.676	0.666	6.167	0.123	4.967	0.087

TABLE A.1. (Continued)

$E_{p,lab}$	$\sigma(0^\circ)$	$\Delta\sigma$	$\sigma(20^\circ)$	$\Delta\sigma$	$\sigma(31^\circ)$	$\Delta\sigma$	$\sigma(50^\circ)$	$\Delta\sigma$	$\sigma(69.8^\circ)$	$\sigma(80.3^\circ)$	mb/sr
MeV	mb/sr	mb/sr	mb/sr	mb/sr	mb/sr	mb/sr	mb/sr	mb/sr	mb/sr	mb/sr	mb/sr
3.67	14.152	0.197	14.075	0.202	15.112	0.205	14.637	0.180	12.563	0.209	10.878
3.69	13.232	0.194	14.532	0.199	14.502	0.203	14.463	0.178	12.564	0.210	10.825
3.70	13.445	0.191	14.007	0.196	14.410	0.199	14.287	0.177	12.594	0.207	10.822
3.71	13.102	0.189	13.559	0.193	14.079	0.196	13.918	0.175	12.403	0.207	10.773
3.71	12.731	0.186	13.141	0.189	13.801	0.191	13.459	0.172	12.259	0.206	10.794
3.72	12.352	0.183	12.585	0.185	13.467	0.191	13.190	0.170	12.203	0.206	10.947
3.73	11.905	0.180	12.280	0.182	13.053	0.189	12.978	0.169	11.942	0.204	10.946
3.74	11.422	0.176	11.867	0.180	12.685	0.184	12.588	0.166	11.830	0.203	10.818
3.75	11.087	0.173	11.646	0.177	12.266	0.181	12.397	0.165	11.733	0.202	10.872
3.76	10.806	0.171	11.298	0.174	11.852	0.178	12.006	0.154	11.678	0.202	10.879
3.77	10.511	0.169	10.987	0.172	11.515	0.177	12.015	0.162	11.490	0.200	10.361
3.78	10.058	0.165	10.711	0.170	11.257	0.175	11.665	0.159	11.302	0.198	10.283
3.79	9.674	0.161	10.488	0.169	10.988	0.171	11.363	0.157	11.007	0.196	10.123
3.80	9.310	0.158	10.095	0.166	10.587	0.166	10.993	0.154	10.755	0.194	9.280
3.81	9.005	0.156	9.702	0.161	10.259	0.162	10.727	0.152	10.621	0.191	9.733
3.82	8.784	0.155	9.267	0.158	9.879	0.162	10.440	0.149	10.553	0.191	9.632
3.83	8.435	0.152	9.165	0.156	9.796	0.162	10.250	0.148	10.366	0.190	9.581
3.84	8.186	0.150	8.929	0.155	9.547	0.159	10.101	0.148	10.174	0.188	9.592
3.85	7.580	0.148	8.733	0.154	9.317	0.157	9.944	0.146	10.113	0.187	9.498
3.86	7.336	0.147	8.575	0.153	9.088	0.155	9.756	0.144	10.030	0.187	9.350
3.87	7.749	0.146	8.415	0.152	8.989	0.156	9.664	0.144	9.795	0.184	9.177
3.88	7.661	0.146	8.377	0.152	8.797	0.154	9.567	0.142	9.606	0.182	9.132
3.89	7.622	0.146	8.346	0.151	8.700	0.154	9.436	0.142	9.546	0.180	9.158
3.90	7.664	0.146	8.263	0.150	8.570	0.153	9.282	0.141	9.595	0.181	9.202
3.91	7.751	0.147	8.243	0.151	8.463	0.151	9.179	0.141	9.493	0.179	9.144
3.92	7.878	0.147	8.249	0.151	8.360	0.151	9.040	0.140	9.350	0.178	9.099
3.93	8.048	0.149	8.261	0.151	8.277	0.151	8.964	0.140	9.264	0.177	9.040
3.94	8.228	0.152	8.446	0.153	8.156	0.149	8.822	0.140	9.163	0.176	8.993
3.95	8.561	0.155	8.519	0.153	8.079	0.149	8.706	0.140	9.026	0.176	9.151
3.96	8.730	0.156	8.524	0.154	7.989	0.149	8.581	0.140	8.864	0.176	9.141
3.97	8.831	0.157	8.737	0.157	7.913	0.147	8.459	0.140	8.737	0.175	9.102
3.98	7.537	0.162	8.974	0.158	7.823	0.146	8.333	0.140	8.616	0.175	8.978

TABLE A.1. (Continued)

E _{p,lab} MeV	σ(0°)		σ(20°)		σ(31°)		σ(50°)		σ(69.8°)		σ(80.3°)		Δσ mb/sr
	mb/sr	Δσ	mb/sr	Δσ	mb/sr	Δσ	mb/sr	Δσ	mb/sr	Δσ	mb/sr	Δσ	
3.35	11.947	0.168	11.147	0.161	9.718	0.142	8.864	0.121	6.329	0.127	5.133	0.689	
3.36	12.056	0.170	11.629	0.166	9.770	0.149	8.864	0.125	6.320	0.127	5.420	0.690	
3.37	12.211	0.172	12.122	0.171	10.516	0.156	9.509	0.127	6.529	0.129	5.522	0.692	
3.38	12.362	0.177	12.359	0.173	11.032	0.161	9.258	0.127	6.763	0.131	5.776	0.694	
3.39	12.508	0.182	12.591	0.175	11.636	0.162	9.313	0.129	7.002	0.134	6.033	0.697	
3.40	12.655	0.186	12.817	0.182	11.462	0.166	9.596	0.132	7.243	0.135	6.191	0.698	
3.41	12.821	0.188	13.503	0.185	11.777	0.170	10.193	0.137	7.476	0.141	6.328	0.699	
3.42	12.967	0.191	13.636	0.187	12.194	0.173	10.501	0.139	7.537	0.142	6.416	0.699	
3.43	12.485	0.186	13.919	0.189	12.622	0.178	10.845	0.143	7.929	0.142	6.551	0.702	
3.44	12.827	0.199	14.250	0.193	12.520	0.181	11.171	0.146	8.189	0.150	6.942	0.705	
3.45	12.959	0.200	14.785	0.198	13.406	0.185	11.452	0.149	8.351	0.152	7.050	0.706	
3.46	13.217	0.202	15.163	0.202	13.822	0.189	11.776	0.151	8.539	0.155	7.282	0.709	
3.47	13.643	0.206	15.351	0.204	14.068	0.192	12.242	0.154	8.827	0.157	7.571	0.713	
3.48	14.091	0.211	15.544	0.205	14.428	0.196	12.750	0.159	9.159	0.158	7.802	0.715	
3.49	14.252	0.213	15.623	0.207	14.759	0.199	13.116	0.163	9.507	0.157	8.122	0.719	
3.50	14.653	0.210	15.502	0.209	15.152	0.202	13.405	0.165	9.660	0.163	8.122	0.719	
3.51	14.101	0.211	16.061	0.210	15.382	0.203	13.766	0.167	9.545	0.169	8.154	0.718	
3.52	14.213	0.212	16.360	0.212	15.573	0.204	13.615	0.170	9.673	0.171	8.185	0.718	
3.53	14.130	0.211	16.364	0.213	15.866	0.205	13.246	0.174	9.878	0.174	8.061	0.720	
3.54	14.116	0.211	16.495	0.214	16.116	0.211	14.762	0.177	10.194	0.177	8.250	0.721	
3.55	14.086	0.212	16.417	0.213	15.999	0.210	14.905	0.179	10.688	0.183	8.668	0.726	
3.56	14.157	0.212	16.399	0.213	15.988	0.209	14.936	0.179	10.904	0.185	9.012	0.729	
3.57	14.159	0.212	16.570	0.213	15.941	0.209	15.052	0.181	11.175	0.189	9.352	0.732	
3.58	14.990	0.211	16.450	0.214	15.767	0.208	15.235	0.183	11.476	0.192	9.411	0.733	
3.59	14.862	0.202	16.549	0.213	15.669	0.209	15.368	0.184	11.476	0.194	9.524	0.734	
3.60	15.941	0.210	16.508	0.215	15.820	0.210	15.361	0.184	11.723	0.196	9.573	0.737	
3.61	15.824	0.209	16.192	0.212	16.178	0.210	15.242	0.184	11.909	0.199	10.266	0.742	
3.62	15.607	0.209	15.925	0.209	16.092	0.210	15.265	0.183	12.153	0.202	10.309	0.742	
3.63	15.406	0.206	15.759	0.210	15.950	0.209	15.130	0.182	12.600	0.207	10.486	0.744	
3.64	15.259	0.206	15.564	0.209	15.645	0.207	14.929	0.181	12.659	0.208	10.609	0.745	
3.65	14.821	0.202	15.280	0.206	15.401	0.205	14.907	0.182	12.540	0.207	10.708	0.747	
3.66	14.533	0.199	15.173	0.205	15.364	0.206	14.910	0.182	12.400	0.206	10.884	0.748	

TABLE A.1. (Continued)

E _{p,lab} MeV	σ(0°)		σ(20°)		σ(31°)		σ(50°)		σ(69.8°)		σ(80.3°)	
	mb/sr	Δσ	mb/sr	Δσ	mb/sr	Δσ	mb/sr	Δσ	mb/sr	Δσ	mb/sr	Δσ
3.99	9.550	0.163	9.629	0.158	7.770	0.146	7.055	0.123	8.724	0.172	8.793	0.134
4.06	9.727	0.164	9.623	0.156	7.742	0.146	6.683	0.120	8.611	0.170	8.698	0.134
4.01	10.181	0.168	9.155	0.150	7.692	0.146	6.436	0.118	8.498	0.169	8.547	0.132
4.02	10.415	0.170	9.098	0.150	7.650	0.145	6.224	0.116	8.325	0.167	8.482	0.132
4.03	10.494	0.170	9.046	0.150	7.576	0.145	5.872	0.113	8.119	0.165	8.304	0.132
4.04	10.779	0.172	9.168	0.160	7.445	0.144	5.655	0.111	7.868	0.162	8.285	0.131
4.05	10.800	0.173	9.131	0.159	7.318	0.142	5.447	0.109	7.644	0.160	8.172	0.130
4.06	11.019	0.174	9.119	0.158	7.183	0.140	5.064	0.105	7.473	0.158	8.043	0.129
4.07	11.232	0.175	9.146	0.159	7.050	0.139	4.850	0.103	7.314	0.157	7.887	0.128
4.08	11.235	0.175	9.073	0.158	6.951	0.138	4.690	0.101	7.074	0.155	7.728	0.126
4.09	11.340	0.177	9.069	0.158	6.809	0.137	4.476	0.099	6.893	0.154	7.536	0.124
4.10	11.394	0.177	9.008	0.158	6.646	0.135	4.259	0.098	6.674	0.151	7.377	0.123
4.11	11.430	0.177	8.946	0.156	6.501	0.133	4.106	0.095	6.410	0.148	7.260	0.122
4.12	11.429	0.177	8.810	0.155	6.316	0.131	3.974	0.094	6.242	0.146	7.045	0.120
4.13	11.339	0.177	8.712	0.154	6.124	0.129	3.732	0.091	6.091	0.144	6.891	0.119
4.14	11.412	0.178	8.676	0.154	6.009	0.128	3.516	0.088	5.797	0.141	6.691	0.117
4.15	11.320	0.177	8.530	0.153	5.794	0.126	3.325	0.085	5.668	0.139	6.429	0.115
4.16	11.256	0.177	8.424	0.152	5.652	0.124	3.131	0.083	5.506	0.138	6.291	0.114
4.17	11.308	0.178	8.343	0.152	5.472	0.122	3.046	0.082	5.321	0.136	6.149	0.113
4.18	11.336	0.178	8.266	0.151	5.256	0.121	2.834	0.079	5.161	0.133	5.958	0.111
4.19	11.396	0.178	8.135	0.150	5.239	0.119	2.774	0.078	4.922	0.131	5.810	0.110
4.20	11.325	0.178	8.021	0.149	5.069	0.118	2.593	0.075	4.857	0.129	5.624	0.109
4.21	11.352	0.177	8.029	0.149	4.950	0.117	2.519	0.074	4.648	0.127	5.497	0.107
4.22	11.245	0.177	7.951	0.149	4.915	0.116	2.336	0.071	4.566	0.126	5.429	0.107
4.23	11.222	0.176	7.984	0.148	4.862	0.116	2.292	0.071	4.460	0.124	5.344	0.106
4.24	11.115	0.176	7.784	0.146	4.763	0.114	2.121	0.068	4.376	0.123	5.272	0.105
4.25	11.211	0.176	7.798	0.147	4.722	0.114	2.051	0.067	4.299	0.123	5.185	0.104
4.26	11.102	0.175	7.745	0.146	4.675	0.113	1.945	0.065	4.175	0.120	5.051	0.103
4.27	11.125	0.175	7.763	0.146	4.618	0.113	1.926	0.065	4.097	0.119	4.956	0.102
4.28	11.001	0.174	7.706	0.146	4.531	0.111	1.782	0.062	3.894	0.115	4.810	0.101
4.29	11.133	0.175	7.731	0.146	4.484	0.111	1.762	0.062	3.859	0.115	4.757	0.100
4.30	11.066	0.175	7.754	0.145	4.451	0.110	1.687	0.061	3.687	0.113	4.643	0.099

TABLE A.1. (Continued)

$E_{p,lab}$	$\sigma(0^\circ)$	$\Delta\sigma$	$\sigma(20^\circ)$	$\Delta\sigma$	$\sigma(31^\circ)$	$\Delta\sigma$	$\sigma(50^\circ)$	$\Delta\sigma$	$\sigma(69.8^\circ)$	$\Delta\sigma$	$\sigma(80.3^\circ)$	$\Delta\sigma$
MeV	mb/sr	mb/sr	mb/sr	mb/sr	mb/sr	mb/sr	mb/sr	mb/sr	mb/sr	mb/sr	mb/sr	mb/sr
4.31	11.150	0.175	7.699	0.145	4.405	0.110	1.664	0.060	3.607	0.111	4.587	0.079
4.32	11.054	0.174	7.732	0.145	4.377	0.109	1.645	0.060	3.483	0.109	4.494	0.098
4.33	11.085	0.174	7.734	0.145	4.323	0.109	1.622	0.060	3.441	0.109	4.439	0.097
4.34	11.061	0.174	7.786	0.146	4.288	0.108	1.637	0.060	3.366	0.107	4.389	0.096
4.35	11.025	0.173	7.693	0.145	4.226	0.107	1.646	0.060	3.318	0.107	4.338	0.095
4.36	11.076	0.174	7.772	0.146	4.240	0.108	1.634	0.060	3.237	0.105	4.301	0.095
4.37	10.955	0.173	7.662	0.144	4.192	0.107	1.652	0.060	3.204	0.105	4.287	0.095
4.38	11.097	0.173	7.826	0.146	4.265	0.108	1.624	0.059	3.125	0.103	4.305	0.095
4.39	11.061	0.173	7.718	0.144	4.231	0.107	1.663	0.060	3.082	0.102	4.246	0.094
4.40	11.105	0.173	7.746	0.145	4.260	0.107	1.655	0.060	3.052	0.102	4.197	0.094
4.41	11.156	0.174	7.707	0.144	4.265	0.107	1.647	0.060	3.027	0.102	4.164	0.093
4.42	11.143	0.174	7.686	0.144	4.273	0.106	1.639	0.060	3.012	0.102	4.150	0.093
4.43	11.424	0.176	7.722	0.144	4.385	0.109	1.614	0.059	2.956	0.101	4.097	0.092
4.44	11.312	0.175	7.652	0.144	4.340	0.108	1.546	0.054	2.981	0.101	4.080	0.092
4.45	11.461	0.176	7.362	0.141	4.387	0.108	1.328	0.054	2.971	0.101	4.041	0.092
4.46	11.415	0.176	7.267	0.140	4.369	0.108	1.096	0.049	2.946	0.101	4.028	0.092
4.47	11.316	0.175	6.820	0.136	4.226	0.107	0.868	0.043	2.922	0.101	4.011	0.091
4.48	11.226	0.174	5.922	0.127	4.139	0.105	0.560	0.043	2.896	0.100	3.878	0.090
4.49	11.138	0.174	5.939	0.127	4.086	0.105	0.445	0.031	2.830	0.095	3.812	0.089
4.50	9.925	0.164	4.294	0.108	3.145	0.092	0.402	0.029	2.477	0.092	3.448	0.085

TABLE A.2. Differential Cross Section and Associated Statistical Uncertainties for the $^{11}\text{B}(p,n)^{11}\text{C}$ Reaction.

E_p , lab MeV	$\sigma(90^\circ)$		$\sigma(100^\circ)$		$\sigma(114^\circ)$		$\sigma(138^\circ)$		$\sigma(155^\circ)$		$\Delta\sigma$ mb/sr
	mb/sr	$\Delta\sigma$ mb/sr	mb/sr	$\Delta\sigma$ mb/sr	mb/sr	$\Delta\sigma$ mb/sr	mb/sr	$\Delta\sigma$ mb/sr	mb/sr	$\Delta\sigma$ mb/sr	
3.10	2.461	0.080	0.000	0.000	0.000	0.000	0.000	0.000	0.000	0.000	0.000
3.11	2.241	0.066	0.116	0.000	0.000	0.000	0.000	0.000	0.000	0.000	0.000
3.12	2.429	0.068	0.066	17.819	0.000	0.000	0.000	0.000	0.000	0.000	0.000
3.13	2.648	0.070	0.067	2.521	0.087	0.000	0.000	0.000	0.000	0.000	0.000
3.14	2.894	0.072	0.070	1.959	0.062	0.000	0.000	0.000	0.000	0.000	0.000
3.15	3.169	0.076	0.070	2.036	0.063	0.000	0.000	0.000	0.000	0.000	0.000
3.16	3.312	0.077	0.069	2.129	0.063	1.915	0.068	7.138	0.000	0.000	0.000
3.17	3.352	0.077	0.072	2.357	0.066	1.759	0.059	2.560	0.095	0.000	0.000
3.18	3.304	0.075	0.072	2.418	0.072	1.879	0.066	1.886	0.061	0.000	0.000
3.19	3.388	0.075	0.075	2.412	0.066	1.882	0.066	1.785	0.056	0.000	0.000
3.20	3.399	0.075	0.071	2.513	0.067	1.974	0.067	1.596	0.061	0.000	0.000
3.21	3.607	0.078	0.072	2.588	0.062	2.112	0.061	2.097	0.062	0.000	0.000
3.22	3.246	0.072	0.071	2.823	0.070	2.303	0.064	2.037	0.060	0.000	0.000
3.23	3.401	0.073	0.074	2.837	0.070	2.401	0.065	2.218	0.063	0.000	0.000
3.24	3.440	0.074	0.072	2.965	0.070	2.573	0.067	2.292	0.063	0.000	0.000
3.25	3.643	0.075	0.072	2.962	0.069	2.588	0.067	2.363	0.065	0.000	0.000
3.26	3.639	0.074	0.071	3.165	0.072	2.729	0.069	2.495	0.066	0.000	0.000
3.27	3.699	0.076	0.074	3.095	0.071	2.663	0.067	2.624	0.068	0.000	0.000
3.28	3.714	0.075	0.072	3.130	0.070	2.838	0.068	2.623	0.067	0.000	0.000
3.29	3.981	0.078	0.073	3.244	0.071	2.898	0.058	2.867	0.069	0.000	0.000
3.30	4.163	0.080	0.074	3.382	0.074	2.971	0.069	2.916	0.069	0.000	0.000
3.31	4.243	0.081	0.075	3.312	0.071	3.150	0.072	3.079	0.070	0.000	0.000
3.32	4.428	0.083	0.075	3.493	0.072	2.986	0.069	3.058	0.070	0.000	0.000
3.33	4.524	0.084	0.079	3.492	0.073	3.157	0.070	3.281	0.073	0.000	0.000
3.34	4.547	0.084	0.079	3.653	0.075	3.353	0.071	2.912	0.068	0.000	0.000
3.35	4.597	0.084	0.081	3.741	0.075	3.370	0.072	3.295	0.071	0.000	0.000
3.36	4.773	0.084	0.083	3.961	0.077	3.357	0.072	3.310	0.071	0.000	0.000
3.37	4.519	0.086	0.084	4.077	0.079	3.446	0.071	3.257	0.070	0.000	0.000
3.38	4.868	0.086	0.084	4.190	0.080	3.612	0.073	3.544	0.073	0.000	0.000
3.39	5.045	0.087	0.084	4.246	0.081	3.638	0.074	3.418	0.071	0.000	0.000
3.40	5.393	0.090	0.084	4.258	0.084	3.734	0.074	3.623	0.072	0.000	0.000
3.41	5.547	0.092	0.086	4.556	0.083	3.836	0.075	3.836	0.075	0.000	0.000
3.42	5.835	0.095	0.086	4.452	0.082	3.990	0.077	3.636	0.073	0.000	0.000
3.43	5.935	0.096	0.088	4.681	0.084	4.169	0.079	3.783	0.075	0.000	0.000
3.44	5.866	0.095	0.090	4.734	0.083	4.208	0.080	3.889	0.075	0.000	0.000
3.45	6.125	0.097	0.093	4.737	0.084	4.372	0.081	4.070	0.077	0.000	0.000

TABLE A.2. (Continued)

E_p, lab MeV	$\sigma(90^\circ)$		$\sigma(100^\circ)$		$\sigma(114^\circ)$		$\sigma(138^\circ)$		$\sigma(155^\circ)$		$\Delta\sigma$ mb/sr
	mb/sr	$\Delta\sigma$ mb/sr	mb/sr	$\Delta\sigma$ mb/sr	mb/sr	$\Delta\sigma$ mb/sr	mb/sr	$\Delta\sigma$ mb/sr	mb/sr	$\Delta\sigma$ mb/sr	
3.46	6.321	0.099	5.767	0.094	4.946	0.086	4.416	0.082	4.154	0.079	0.082
3.47	6.494	0.101	5.841	0.095	4.948	0.086	4.667	0.084	4.260	0.080	0.084
3.48	6.525	0.102	5.802	0.094	5.106	0.087	4.735	0.084	4.358	0.081	0.081
3.49	6.799	0.105	6.283	0.097	5.488	0.091	4.528	0.083	4.459	0.082	0.082
3.50	7.009	0.107	6.262	0.098	5.531	0.091	4.707	0.083	4.529	0.082	0.082
3.51	7.290	0.110	6.275	0.099	5.652	0.093	4.916	0.084	4.674	0.083	0.083
3.52	7.479	0.111	6.357	0.100	5.650	0.093	4.928	0.085	4.693	0.083	0.083
3.53	7.723	0.114	6.685	0.103	5.745	0.093	4.964	0.085	4.647	0.082	0.082
3.54	7.760	0.115	6.891	0.105	6.006	0.095	4.941	0.084	4.753	0.084	0.084
3.55	7.826	0.117	6.942	0.107	6.138	0.096	5.181	0.087	4.858	0.084	0.084
3.56	7.709	0.116	7.198	0.109	6.091	0.096	5.497	0.090	4.828	0.084	0.084
3.57	7.712	0.116	7.309	0.110	6.162	0.097	5.420	0.089	4.840	0.083	0.083
3.58	7.789	0.118	7.432	0.111	6.270	0.099	5.431	0.090	4.831	0.083	0.083
3.59	8.033	0.120	7.423	0.113	6.473	0.101	5.365	0.091	5.104	0.086	0.086
3.60	8.490	0.124	7.315	0.113	6.609	0.103	5.536	0.091	5.235	0.087	0.087
3.61	8.644	0.126	7.170	0.112	6.714	0.105	5.632	0.091	5.223	0.087	0.087
3.62	8.706	0.127	7.224	0.113	6.827	0.106	5.600	0.091	5.328	0.089	0.089
3.63	8.828	0.128	7.434	0.114	6.882	0.107	5.698	0.092	5.370	0.089	0.089
3.64	8.876	0.129	7.768	0.118	6.821	0.106	5.923	0.094	5.270	0.088	0.088
3.65	9.011	0.132	7.869	0.120	6.754	0.107	5.868	0.094	5.197	0.087	0.087
3.66	9.078	0.133	7.954	0.120	6.700	0.107	5.761	0.094	5.221	0.088	0.088
3.67	9.222	0.134	8.121	0.122	6.629	0.107	5.870	0.095	5.459	0.090	0.090
3.68	9.334	0.136	8.139	0.122	6.674	0.107	5.949	0.096	5.409	0.090	0.090
3.69	9.479	0.136	8.112	0.123	6.740	0.109	6.059	0.098	5.370	0.090	0.090
3.70	9.388	0.137	8.175	0.124	6.895	0.110	5.981	0.097	5.442	0.091	0.091
3.71	9.371	0.138	8.360	0.126	7.058	0.112	5.848	0.097	5.438	0.091	0.091
3.72	9.415	0.138	8.443	0.127	7.029	0.112	5.906	0.097	5.436	0.092	0.092
3.73	9.423	0.139	8.347	0.127	6.982	0.112	5.937	0.099	5.528	0.093	0.093
3.74	9.426	0.140	8.272	0.127	7.007	0.113	5.712	0.097	5.475	0.093	0.093
3.75	9.436	0.140	8.364	0.128	7.080	0.114	5.547	0.097	5.362	0.092	0.092
3.76	9.421	0.139	8.354	0.129	7.026	0.115	5.582	0.097	5.375	0.092	0.092
3.77	9.369	0.140	8.269	0.129	6.991	0.115	5.577	0.097	5.240	0.092	0.092
3.78	9.278	0.140	8.283	0.129	6.975	0.114	5.497	0.097	5.151	0.092	0.092
3.79	9.059	0.139	8.334	0.130	7.028	0.115	5.626	0.098	5.151	0.092	0.092
3.80	8.936	0.138	8.244	0.129	6.983	0.116	5.552	0.099	5.031	0.092	0.092
3.81	8.898	0.137	8.137	0.129	6.922	0.116	5.492	0.098	4.971	0.091	0.091

TABLE A.2. (Continued)

E_p , lab MeV	$\sigma(90^\circ)$		$\Delta\sigma$		$\sigma(100^\circ)$		$\Delta\sigma$		$\sigma(114^\circ)$		$\Delta\sigma$		$\sigma(138^\circ)$		$\Delta\sigma$		$\sigma(155^\circ)$		$\Delta\sigma$	
	mb/sr	mb/sr	mb/sr	mb/sr	mb/sr	mb/sr	mb/sr	mb/sr	mb/sr	mb/sr	mb/sr	mb/sr	mb/sr	mb/sr	mb/sr	mb/sr	mb/sr	mb/sr	mb/sr	mb/sr
4.18	6.373	0.113	6.272	0.112	5.682	0.107	4.643	0.096	4.494	0.094										
4.19	6.223	0.112	6.173	0.111	5.600	0.106	4.626	0.096	4.448	0.094										
4.20	6.048	0.111	6.067	0.110	5.554	0.105	4.606	0.095	4.424	0.093										
4.21	5.937	0.110	5.938	0.109	5.450	0.104	4.585	0.095	4.427	0.093										
4.22	5.792	0.109	5.892	0.109	5.344	0.103	4.545	0.095	4.444	0.094										
4.23	5.672	0.108	5.809	0.108	5.246	0.102	4.522	0.095	4.469	0.094										
4.24	5.561	0.107	5.692	0.106	5.156	0.101	4.492	0.094	4.515	0.094										
4.25	5.357	0.105	5.617	0.106	5.072	0.100	4.470	0.094	4.497	0.094										
4.26	5.257	0.104	5.554	0.105	5.014	0.100	4.459	0.094	4.513	0.094										
4.27	5.136	0.103	5.380	0.104	4.962	0.099	4.466	0.094	4.534	0.094										
4.28	5.028	0.102	5.326	0.103	4.911	0.099	4.459	0.094	4.540	0.094										
4.29	4.954	0.101	5.274	0.103	4.842	0.098	4.461	0.093	4.643	0.096										
4.30	4.933	0.101	5.184	0.103	4.807	0.098	4.532	0.094	4.640	0.096										
4.31	4.891	0.101	5.108	0.102	4.770	0.097	4.500	0.094	4.647	0.095										
4.32	4.860	0.100	5.050	0.101	4.796	0.097	4.471	0.093	4.673	0.095										
4.33	4.826	0.100	5.004	0.101	4.780	0.097	4.477	0.093	4.656	0.095										
4.34	4.803	0.099	4.960	0.100	4.800	0.097	4.466	0.093	4.658	0.095										
4.35	4.788	0.100	4.950	0.100	4.811	0.097	4.453	0.093	4.668	0.095										
4.36	4.780	0.100	4.937	0.100	4.785	0.097	4.497	0.093	4.724	0.095										
4.37	4.760	0.100	4.958	0.101	4.757	0.097	4.520	0.093	4.764	0.096										
4.38	4.726	0.100	4.935	0.101	4.736	0.097	4.523	0.093	4.786	0.096										
4.39	4.712	0.099	4.947	0.100	4.733	0.097	4.575	0.094	4.822	0.096										
4.40	4.670	0.099	4.894	0.100	4.730	0.097	4.602	0.094	4.802	0.096										
4.41	4.683	0.099	4.944	0.100	4.700	0.097	4.636	0.094	4.788	0.095										
4.42	4.645	0.098	4.903	0.100	4.771	0.098	4.701	0.095	4.842	0.096										
4.43	4.680	0.099	4.980	0.101	4.750	0.097	4.684	0.095	4.824	0.096										
4.44	4.660	0.098	4.967	0.101	4.777	0.098	4.708	0.095	4.837	0.096										
4.45	4.690	0.098	5.039	0.102	4.746	0.097	4.690	0.095	4.833	0.096										
4.46	4.682	0.099	5.000	0.102	4.810	0.098	4.658	0.095	4.791	0.095										
4.47	4.609	0.098	4.983	0.102	4.767	0.097	4.614	0.094	4.772	0.095										
4.48	4.554	0.097	4.896	0.100	4.726	0.097	4.552	0.093	4.684	0.094										
4.49	4.501	0.094	4.597	0.097	4.604	0.096	4.179	0.089	4.581	0.093										
4.50	3.951	0.090	4.513	0.096	4.328	0.094	3.926	0.086	4.020	0.087										

APPENDIX B

TABLE B.1. Legendre Power Series Coefficients and Associated Statistical Errors.

E _p , lab MeV	σ_{TOT}		A ₁ mb/sr	ΔA_1		A ₂ mb/sr	ΔA_2		A ₃ mb/sr	ΔA_3		A ₄ mb/sr	ΔA_4	
	mb	mb		mb/sr	mb/sr		mb/sr	mb/sr		mb/sr	mb/sr		mb/sr	mb/sr
3.05	13.140	3.283	1.031	0.519	-0.665	0.732	-0.177	0.922	0.522	0.658				
3.06	13.620	3.536	1.229	0.605	-0.214	0.826	-0.703	0.970	0.594	0.641				
3.07	18.640	3.975	1.433	0.640	-1.347	0.985	0.683	1.176	-0.051	0.716				
3.08	24.320	4.180	1.435	0.659	-1.347	0.926	1.229	1.081	-0.252	0.727				
3.09	25.310	4.027	1.637	0.673	-1.230	0.865	-0.084	0.858	0.402	0.675				
3.10	30.670	3.982	1.562	0.638	-1.258	0.833	0.236	0.847	0.215	0.707				
3.11	36.130	3.979	1.327	0.630	-0.714	0.819	0.293	0.826	-0.110	0.726				
3.12	39.840	4.097	1.234	0.654	-0.522	0.858	0.336	0.853	-0.237	0.739				
3.13	43.690	3.899	1.144	0.588	-0.146	0.774	0.305	0.820	-0.351	0.756				
3.14	45.050	3.763	1.224	0.543	-0.434	0.722	0.756	0.790	-0.458	0.767				
3.15	49.560	3.960	0.782	0.591	0.232	0.775	0.014	0.867	-0.015	0.804				
3.16	51.170	3.709	0.249	0.541	0.977	0.705	-0.681	0.810	0.499	0.804				
3.17	51.570	3.519	0.369	0.475	0.893	0.617	-0.501	0.694	0.241	0.760				
3.18	51.240	3.430	0.412	0.450	0.697	0.588	-0.250	0.642	0.111	0.712				
3.19	50.750	3.399	0.474	0.445	0.700	0.572	-0.190	0.634	-0.117	0.707				
3.20	51.170	3.393	0.467	0.448	0.790	0.570	-0.347	0.639	-0.070	0.703				
3.21	52.000	3.421	0.383	0.452	0.798	0.571	-0.328	0.648	0.010	0.711				
3.22	52.110	3.414	0.396	0.453	0.957	0.571	-0.286	0.641	-0.079	0.714				
3.23	53.960	3.460	0.435	0.462	1.006	0.572	-0.424	0.656	-0.171	0.726				
3.24	54.370	3.461	0.412	0.463	1.097	0.578	-0.388	0.653	-0.097	0.732				
3.25	56.040	3.516	0.495	0.467	0.937	0.583	-0.396	0.662	-0.023	0.745				
3.26	57.570	3.547	0.492	0.473	1.060	0.589	-0.437	0.669	0.003	0.754				
3.27	59.160	3.605	0.595	0.478	1.026	0.594	-0.510	0.684	0.072	0.770				
3.28	60.150	3.623	0.667	0.470	1.040	0.597	-0.437	0.683	0.126	0.774				
3.29	63.680	3.685	0.638	0.488	1.112	0.603	-0.468	0.698	0.161	0.786				
3.30	63.760	3.747	0.693	0.494	1.038	0.609	-0.489	0.705	0.083	0.797				
3.31	65.250	3.793	0.755	0.502	1.184	0.614	-0.637	0.714	-0.025	0.805				
3.32	66.840	3.828	0.872	0.504	0.972	0.612	-0.628	0.717	-0.197	0.812				
3.33	68.380	3.895	0.772	0.514	0.985	0.618	-0.720	0.736	-0.152	0.824				
3.34	69.250	3.940	0.909	0.516	0.897	0.620	-0.511	0.736	-0.185	0.833				
3.35	71.050	3.999	0.849	0.524	0.983	0.631	-0.554	0.755	0.117	0.851				
3.36	72.920	4.065	0.805	0.532	0.907	0.635	-0.441	0.766	0.054	0.862				
3.37	75.210	4.129	1.060	0.539	0.940	0.640	-0.373	0.773	-0.204	0.877				
3.38	77.170	4.192	1.063	0.549	1.110	0.653	-0.460	0.787	-0.062	0.900				
3.39	78.280	4.240	1.146	0.552	0.958	0.660	-0.310	0.789	0.021	0.909				
3.40	80.660	4.327	1.237	0.563	1.043	0.669	-0.340	0.804	0.092	0.922				

TABLE B.1. (Continued)

E _p , lab MeV	σ _{TOT} mb	σ _{TOT} mb	A ₁ mb/sr	ΔA ₁ mb/sr	A ₂ mb/sr	ΔA ₂ mb/sr	A ₃ mb/sr	ΔA ₃ mb/sr	A ₄ mb/sr	ΔA ₄ mb/sr
3.41	4.437	84.130	1.315	0.578	1.048	0.682	-0.489	0.829	0.034	0.946
3.42	4.485	85.580	1.503	0.582	0.958	0.687	-0.452	0.830	-0.066	0.949
3.43	4.606	88.710	1.534	0.597	1.011	0.701	-0.451	0.851	-0.154	0.972
3.44	4.682	90.890	1.677	0.606	1.019	0.710	-0.522	0.864	-0.118	0.986
3.45	4.757	93.690	1.724	0.616	1.021	0.722	-0.598	0.878	-0.121	1.001
3.46	4.858	96.270	1.825	0.628	1.004	0.734	-0.599	0.895	-0.190	1.023
3.47	4.943	98.660	1.899	0.638	1.014	0.748	-0.716	0.907	-0.099	1.037
3.48	5.030	100.780	2.049	0.649	1.091	0.755	-0.816	0.922	-0.167	1.054
3.49	5.105	103.230	2.033	0.658	1.020	0.758	-0.563	0.941	-0.419	1.073
3.50	5.186	105.740	2.149	0.666	0.898	0.770	-0.791	0.949	-0.427	1.084
3.51	5.265	108.100	2.188	0.675	0.930	0.780	-0.941	0.964	-0.461	1.098
3.52	5.315	108.840	2.261	0.681	0.946	0.783	-0.924	0.972	-0.507	1.103
3.53	5.405	111.420	2.368	0.689	0.777	0.790	-0.913	0.981	-0.686	1.113
3.54	5.483	113.820	2.441	0.698	0.707	0.795	-0.979	0.995	-0.829	1.125
3.55	5.559	115.900	2.379	0.705	0.573	0.810	-1.109	1.010	-0.676	1.141
3.56	5.604	117.200	2.341	0.709	0.519	0.820	-1.116	1.015	-0.629	1.148
3.57	5.646	118.240	2.394	0.711	0.534	0.825	-1.144	1.021	-0.518	1.156
3.58	5.694	119.190	2.403	0.716	0.214	0.829	-1.148	1.030	-0.553	1.163
3.59	5.759	120.820	2.281	0.725	0.236	0.839	-1.251	1.045	-0.491	1.177
3.60	5.810	122.490	2.282	0.729	0.069	0.850	-1.294	1.055	-0.294	1.192
3.61	5.853	123.580	2.305	0.731	-0.073	0.859	-1.388	1.059	-0.251	1.203
3.62	5.870	124.050	2.254	0.733	-0.192	0.863	-1.441	1.067	-0.169	1.212
3.63	5.888	124.880	2.126	0.734	-0.334	0.868	-1.419	1.070	-0.098	1.215
3.64	5.902	124.990	1.969	0.734	-0.452	0.873	-1.242	1.071	-0.087	1.214
3.65	5.931	124.710	1.922	0.735	-0.651	0.875	-1.215	1.073	-0.090	1.213
3.66	5.943	124.820	1.915	0.736	-0.755	0.876	-1.338	1.075	0.028	1.215
3.67	5.951	125.000	1.775	0.736	-0.811	0.882	-1.395	1.077	0.110	1.216
3.68	5.945	124.480	1.618	0.734	-0.960	0.884	-1.323	1.076	0.154	1.215
3.69	5.941	123.550	1.430	0.733	-1.060	0.885	-1.268	1.076	0.152	1.213
3.70	5.917	122.280	1.216	0.730	-1.078	0.882	-1.148	1.080	0.153	1.212
3.71	5.890	121.140	1.009	0.727	-1.193	0.879	-0.931	1.081	0.140	1.211
3.72	5.889	120.480	0.841	0.724	-1.340	0.882	-0.904	1.081	0.238	1.211
3.73	5.868	119.230	0.684	0.722	-1.363	0.882	-0.976	1.081	0.311	1.207
3.74	5.821	117.240	0.588	0.715	-1.483	0.876	-0.894	1.076	0.345	1.197
3.75	5.791	115.820	0.490	0.711	-1.634	0.869	-0.737	1.073	0.327	1.189
3.76	5.766	114.530	0.377	0.708	-1.655	0.865	-0.713	1.072	0.336	1.183

TABLE B.1. (Continued)

E_b , lab MeV	σ_{TOT}		A_1 mb/sr	ΔA_1 mb/sr	A_2 mb/sr	ΔA_2 mb/sr	A_3 mb/sr	ΔA_3 mb/sr	A_4 mb/sr	ΔA_4 mb/sr
	mb	mb								
3.77	113.660	5.741	0.321	0.705	-1.684	0.861	-0.667	1.069	0.289	1.179
3.78	111.440	5.698	0.218	0.599	-1.741	0.858	-0.571	1.060	0.225	1.176
3.79	109.980	5.667	0.010	0.598	-1.659	0.854	-0.463	1.060	0.079	1.163
3.80	107.790	5.616	-0.125	0.693	-1.647	0.847	-0.342	1.052	0.047	1.155
3.81	105.710	5.562	-0.182	0.586	-1.693	0.937	-0.313	1.044	0.082	1.144
3.82	104.550	5.529	-0.329	0.683	-1.708	0.835	-0.271	1.043	0.102	1.141
3.83	103.880	5.514	-0.461	0.682	-1.692	0.834	-0.251	1.044	0.064	1.137
3.84	102.890	5.494	-0.558	0.681	-1.675	0.832	-0.289	1.045	0.106	1.134
3.85	101.860	5.476	-0.626	0.680	-1.670	0.829	-0.261	1.046	0.080	1.131
3.86	100.570	5.447	-0.660	0.677	-1.701	0.824	-0.141	1.041	0.048	1.125
3.87	99.480	5.418	-0.668	0.674	-1.687	0.818	-0.057	1.034	-0.047	1.118
3.88	98.720	5.397	-0.722	0.673	-1.646	0.815	-0.064	1.033	-0.008	1.114
3.89	98.410	5.393	-0.786	0.673	-1.595	0.816	-0.067	1.034	0.025	1.116
3.90	97.530	5.384	-0.834	0.673	-1.595	0.818	-0.068	1.035	0.149	1.116
3.91	97.080	5.355	-0.904	0.671	-1.540	0.816	-0.067	1.036	0.210	1.118
3.92	96.210	5.329	-1.000	0.669	-1.470	0.813	0.245	1.036	0.214	1.119
3.93	95.610	5.319	-1.105	0.669	-1.423	0.813	0.461	1.035	0.237	1.120
3.94	95.280	5.298	-1.149	0.667	-1.406	0.813	0.628	1.032	0.347	1.119
3.95	95.170	5.294	-1.158	0.665	-1.452	0.816	0.684	1.029	0.589	1.121
3.96	94.920	5.289	-1.199	0.666	-1.426	0.817	0.733	1.031	0.653	1.124
3.97	94.430	5.280	-1.270	0.666	-1.361	0.817	0.938	1.031	0.694	1.125
3.98	94.040	5.261	-1.354	0.666	-1.214	0.816	1.189	1.033	0.792	1.128
3.99	93.130	5.226	-1.424	0.663	-1.067	0.814	1.299	1.030	0.813	1.126
4.00	92.560	5.207	-1.567	0.663	-0.982	0.815	1.506	1.032	0.879	1.129
4.01	91.860	5.187	-1.605	0.662	-0.883	0.812	1.717	1.031	0.984	1.130
4.02	90.820	5.151	-1.612	0.657	-0.848	0.809	1.840	1.026	1.069	1.127
4.03	89.410	5.111	-1.584	0.653	-0.766	0.806	1.971	1.019	1.140	1.122
4.04	88.240	5.068	-1.712	0.649	-0.630	0.801	2.084	1.016	1.216	1.113
4.05	86.930	5.023	-1.745	0.645	-0.534	0.796	2.172	1.009	1.272	1.113
4.06	85.160	4.954	-1.793	0.636	-0.472	0.790	2.229	0.996	1.383	1.103
4.07	83.630	4.901	-1.760	0.630	-0.361	0.785	2.388	0.987	1.463	1.095
4.08	82.050	4.855	-1.778	0.626	-0.284	0.779	2.419	0.982	1.502	1.090
4.09	80.480	4.810	-1.772	0.621	-0.208	0.773	2.510	0.978	1.539	1.085
4.10	78.570	4.758	-1.751	0.615	-0.141	0.763	2.576	0.969	1.502	1.075
4.11	77.050	4.692	-1.753	0.608	-0.053	0.756	2.632	0.955	1.558	1.065
4.12	75.490	4.637	-1.750	0.602	0.007	0.748	2.656	0.946	1.554	1.054
4.13	73.590	4.574	-1.778	0.595	0.094	0.741	2.561	0.936	1.608	1.044

TABLE B.1. (Continued)

E _{p,lab} MeV	σ _{TOT}		A ₁ mb/sr	ΔA ₁ mb/sr	A ₂		ΔA ₂ mb/sr	A ₃ mb/sr	ΔA ₃ mb/sr	A ₄		ΔA ₄ mb/sr
	mb	mb			mb/sr	mb/sr						
4.14	71.726	4.561	-1.748	0.596	0.165	0.733	2.707	0.922	1.685	1.032		
4.15	70.020	4.444	-1.770	0.570	0.210	0.726	2.735	0.912	1.704	1.020		
4.16	63.426	4.361	-1.781	0.573	0.270	0.722	2.695	0.903	1.904	1.011		
4.17	67.136	4.342	-1.767	0.568	0.330	0.715	2.670	0.897	1.945	1.003		
4.18	65.650	4.285	-1.800	0.562	0.428	0.700	2.720	0.888	1.872	0.992		
4.19	64.500	4.243	-1.730	0.558	0.501	0.703	2.722	0.886	1.828	0.985		
4.20	62.080	4.187	-1.830	0.552	0.576	0.696	2.742	0.871	1.852	0.976		
4.21	62.066	4.151	-1.810	0.549	0.672	0.691	2.708	0.865	1.863	0.969		
4.22	60.976	4.105	-1.845	0.543	0.725	0.690	2.710	0.857	1.926	0.961		
4.23	60.080	4.076	-1.831	0.541	0.793	0.685	2.648	0.852	1.940	0.955		
4.24	58.636	4.025	-1.872	0.535	0.848	0.681	2.605	0.844	2.027	0.948		
4.25	58.100	3.994	-1.831	0.533	0.933	0.677	2.572	0.839	2.041	0.943		
4.26	57.136	3.954	-1.866	0.530	1.008	0.673	2.582	0.833	2.033	0.935		
4.27	56.426	3.927	-1.842	0.528	1.104	0.670	2.500	0.820	2.011	0.920		
4.28	55.340	3.882	-1.882	0.524	1.185	0.665	2.543	0.823	2.011	0.920		
4.29	55.030	3.866	-1.893	0.523	1.276	0.665	2.470	0.823	2.002	0.910		
4.30	54.430	3.848	-1.832	0.522	1.356	0.663	2.487	0.818	2.042	0.913		
4.31	53.900	3.828	-1.910	0.520	1.447	0.660	2.460	0.815	2.076	0.908		
4.32	53.630	3.808	-1.922	0.519	1.474	0.654	2.475	0.811	2.015	0.901		
4.33	53.310	3.789	-1.914	0.517	1.504	0.651	2.480	0.800	1.990	0.899		
4.34	53.126	3.785	-1.910	0.516	1.507	0.649	2.466	0.800	1.955	0.895		
4.35	52.940	3.783	-1.921	0.516	1.577	0.650	2.462	0.810	1.958	0.895		
4.36	52.810	3.783	-1.935	0.517	1.578	0.649	2.410	0.800	1.942	0.892		
4.37	52.850	3.780	-1.962	0.517	1.578	0.649	2.442	0.800	1.971	0.891		
4.38	52.780	3.775	-1.938	0.516	1.645	0.648	2.442	0.800	1.912	0.891		
4.39	52.810	3.770	-1.960	0.518	1.668	0.648	2.401	0.800	1.890	0.889		
4.40	52.640	3.760	-1.951	0.517	1.717	0.646	2.416	0.800	1.890	0.889		
4.41	52.640	3.768	-1.957	0.517	1.722	0.645	2.440	0.807	1.890	0.888		
4.42	52.750	3.776	-1.900	0.520	1.774	0.645	2.433	0.810	1.858	0.880		
4.43	52.840	3.771	-1.960	0.518	1.803	0.646	2.513	0.800	1.876	0.880		
4.44	52.176	3.754	-2.077	0.515	1.813	0.645	2.623	0.803	1.950	0.883		
4.45	52.050	3.726	-2.087	0.513	1.866	0.642	2.636	0.802	1.950	0.883		
4.46	51.400	3.682	-2.162	0.509	1.758	0.643	2.788	0.796	2.010	0.870		
4.47	50.100	3.634	-2.252	0.500	1.706	0.638	2.793	0.788	2.100	0.860		
4.48	48.116	3.600	-2.297	0.495	1.593	0.620	2.675	0.778	2.014	0.862		
4.49	48.050	3.438	-2.340	0.474	1.622	0.616	2.703	0.751	2.200	0.837		
4.50	41.940	3.311	-2.280	0.452	1.128	0.581	2.531	0.715	1.700	0.799		

APPENDIX C

Program TOF-NE

```

C TOF-NE SRC      TIME OF FLIGHT TO NEUTRON ENERGY TRANSFORMATION
C PROGRAM:      (#N=10+Q)/(#C.P.*MEV*SP) VS ENERGY
C              FOR 2 1/2" SCINT. (OMEGA)
C EXPERIMENTAL PARAMETERS & TOF DATA ON TAPE UNIT #1, WITH EFFICIENCY
C TABLE (IF USED) IN BLOCK 1
C NEUTRON ENERGY SPECTRUM OUTPUT ON TAPE UNIT #2
C MODIFIED 7/11/71 FOR 1024 CHANNEL INPUT SPECTRUM -- ON CAR 59 - 3
C
C DOUBLE PRECISION BTL,BTU
C DIMENSION EFTABL(50),NTOF(1024),NNE(1024),TOF(4)
C COMMON EFTABL,NTOF,NNE
C DATA MLI,M2,M3/5H TOF-,5HNE 7/,5H11/71/
C DATA A,B,C,D/5HTYPE ,5H1 FOR,5H EFF=,5H 1.0,/
C DATA E,F,G/5H 2.0 ,5HFOR T,5HABLE /
C DATA Q,R,S,T,U/5HLEN =,5HINPUT,5H TOF ,5HSW# =,5HRCN#=/
C DATA P1,P2,53/5H ENMA,5HX = ,5HONE /
C DATA PI,E0/3.1416,939.505/
C
C IDENTIFY PROGRAM
C CALL ASCII(HLI,3)
C
C ASK EFFICIENCY TO BE USED:  EFF= 1.0 TYPE 1.0: = FIT(EFTABL) TYPE 2
C EFTABL (EFFICIENCY TABLE IS F.P. W/ ENLOW 1ST ENTRY, ENINC 2ND)
100 CALL ASCII(A,7)
   CALL ANYINP(EFFLG)
   K = EFFLG
   GO TO (200,300), K
   GO TO 100
C EFFICIENCY = 1.0
200 EFF = 1.0
   GO TO 400
C EFFICIENCY = EFTABL ON BLOCK 1, READ AND SET PROGRAM FLAG
300 CALL DTAPE(1,1,0,256,EFTABL(1))
C NEUTRON ENERGY INCREMENT IN MEV
400 CALL ASCII(C,1)
   CALL ANYINP(DE)
C DATA TAPE SWITCH # (2 TO 16) AND 1024 CHNL. REGION # (1 TO 5)
500 CALL ASCII(F,3)
   CALL ANYINP(SWI)
600 CALL ASCII(U,1)
   CALL ANYINP(RGN)
   JB = 20.*(SWI-1.)+4.*(RGN-2.)
C ZERO TOF & NE REGIONS
DO 800 I=1,1024
  NTOF(I) = 0
800 NNE(I) = 0
C MAXIMUM NEUTRON ENERGY IN MEV
CALL ASCII(P1,2)
CALL ANYINP(EMAX)
J = EMAX/DE
C LOAD THE TOF SPECTRUM
CALL DTAPE(1,JB,0,1024,NTOF(1))
DO 900 I=1,4
  NNE(I) = NTOF(I)

```

THIS PAGE IS BEST QUALITY PRINT
FROM COPY FURNISHED TO DDC

```

900      TOF(I) = NTOF(I)
C EXPERIMENTAL PARAMETERS:      DT(NSEC/CHANNEL), GAMMA(CHANNEL #),
C      EL(FLIGHT PATH IN METERS), UCOUL(CHARGE IN MICROCOULOMBS)
      DT = TOF(1)/10000.
      GAMMA = TOF(2)/100.
      EL = TOF(3)/1000.
      UCOUL = TOF(4)/100.
      OMEGA = PI*(0.0315/EL)*(0.0315/EL)
      ZERO = GAMMA + 3.34*EL/DT
      FNU = DE*0.5
C GENERATE THE NEUTRON ENERGY SPECTRUM
DO 999 I=1,J
      IPI = I+1
      XI = I
      EN = DE*XI
C EFFICIENCY OF DETECTOR
      GO TO (920,910), X
C '910' IS EFFICIENCY FROM TABLE (CUBIC FIT)
910      CALL FIT2(EN,EFF)
      IF(EFF.LE.0.0) GO TO 999
920      ENL = ENU
      FNU = DE*(XI+0.5)
C RELATIVISTIC CALCULATION OF HISTOGRAM BOUNDARIES
      GL = ENL/EO
      GU = FNU/EO
      RTL = 2.*GL*(1.-3./2.*GL*(1.-4./3.*GL))
      RTU = 2.*GU*(1.-3./2.*GU*(1.-4./3.*GU))
      BETAL = DSORT(RTL)
      BETAU = DSORT(RTU)
      TL = EL/(0.299793*BETAL)
      TU = EL/(0.299793*BETAU)
      CIL = ZERO-TL/DT
      CIU = ZERO-TU/DT
C CALCULATE THE HISTOGRAM
      I1 = CIL+.5
      I2 = CIU+.5
      DELTA = CIU-CIL
      N = I2-I1
      SUM = 0.0
      IF(I1)999,999,1
      IF(DELTA-1.)2,2,3
2      IF(X)4,4,3
3      IF(X-1)4,7,5
4      F1 = DELTA
      F2 = 0.0
      GO TO 5
5      NI = I1+1
      N2 = I2-1
      DO 6 L=NI,N2
      ICH = L+1
      YDATA = NTOF(ICH)
6      SUM = SUM+YDATA
7      YI1 = I1
      YI2 = I2
      F1 = 0.5-(CIL-YI1)
      F2 = 0.5+(CIU-YI2)
9      ICH = I1+1

```

THIS PAGE IS BEST QUALITY PRACTICABLE
 FROM COPY FURNISHED TO DDC

```
YDATA = VTOF(ICH)
SUM = SUM+F1*YDATA
ICH = I2+1
YDATA = VTOF(ICH)
SUM = SUM+F2*YDATA
C CALCULATION OF  $4N \cdot 10^{19} / (INC. PARTICLES \cdot MEV \cdot SP)$ 
NNE(IPI) = SUM*1.602E-4/(UCOUL*DE*DCMEGA*EFF)
CALL LITES(I)
999 CONTINUE
C WRITE OUT NEUTRON ENERGY SPECTRUM ON UNIT #2
CALL ASCII(T,1)
CALL ANYIMP(SVI)
CALL ASCII(U,1)
CALL ANYIMP(RGN)
JB = 20.*(SVI-1.)+4.*(RGN-2.)
CALL CTAPE(2,JB,1,1024,NNE(I))
C TYPE 'DONE'
CALL ASCII(R3,1)
C TYPING 1. RESTARTS, 2. RESTARTS WITH EFF AND DEN SET, OTHER STOPS
CALL ANYIMP(X)
IX = Y
GO TO (100,500), IX
STOP
END
```

THIS PAGE IS BEST QUALITY PRACTICABLE
FROM COPY FURNISHED TO DDC

APPENDIX D

Program B11PNX, Subroutines KINSUB and FIT2

```

C      B11PNX SRC
C      FOR 118CP, V) IIC RXN ONLY, CALC TOF TO X-SECT
C      MODIFIED JAN 78 FOR BORON RYN FROM LITAN SPC BY SEALOCK
C      WHICH WAS MODIFIED FROM LITPN1 AND TFSTAT - CAP THESIS.
C      CALCULATES SIGMA IN MICROBARNES/SR
C      STATISTICS OUTPUT AS 10*4/SCRT(CNTE) (7=10*4)
C      FOR 2 1/2" SCINTILLATOR
C      FOR VARIABLE STOPPING CROSS SECTION - B203, EN, S TGTS.
C
C      DOUBLE PRECISION BTL, R2U, ARGLOG, DSORT
C      DIMENSION EFTABL(1024), XTOF(1024), XSIG(1024), TOF(9)
C      COMMON EFTABL, XTOF, XSIG
C      COMMON /XINCOM/A1, A2, A3, EPK, QO, TC, THETA, FNC, ENK, P, NO
C      COMMON /SCTCOM/EN, SR
C      DATA AB, AC/5H DE ,5H(XEV)/
C      DATA AA, BP/5H SW# =,5H RGN# =/
C      DATA CC, DD, EE, FF/5H INPUT, 5H DT1 ,5H OUTPU, 5H DT2/
C      DATA PI, ONEAMU/3.1416, 931.481/
C      DATA XI, Y2, X3, Y4, 7P/1.007825, 11.009350, 1.00865, 11.011432, 1./
C      DATA Z1, Z2, O/1., 5., -2.763/
C      DATA DD1, DD2, DD3/5H INPUT, 5H TGT ,5H# /
C      DATA DD4, DD5, DD6, DD7/5H 1=R20, 5H3 2=,5H R 3=,5H R 4/
C      DATA DD8, DD9, DD10/5H=3N=0, 5H 5=1, 5H VPUT /
C      DATA DD11, DD12, DD13, DD14/5H INPUT, 5H STOP, 5H PING ,5H CROSS/
C      DATA DD15, DD16, DD17/5H SECT, 5H ION (,5H A, R) /
C      NO = 1
C      A1 = X1
C      A2 = X2
C      A3 = X3
C      QO = 0
C      XIM = XI*ONEAMU
C      XIP = XIM
C      EU = Y3*ONEAMU
C      XEM = 0.511004
C      XRTU = 7P*7P*72*4.*PI*532.16E-40/(XEM*2.5667E-12)
C      CONST = 1.602E-19*1.E+06/(1.E-06*1.E-24)
C      CALL DTAPF(1,1,0,1024,EFTABL(1))
C      TRANSFORMATION CHANNEL WIDTH (MEV)
C      CALL ASCII(AB,2)
C      CALL ANYIMP(CE)
C      INPUT STOPPING CROSS SECTION VALUES
C      CALL ASCII(DD1,3)
C      CALL ASCII(DD4,7)
C      CALL ANYIMP(CCI)
C      C2 = 0.
C      IF(CCI.EQ.1.) C1=5.525E-21
C      IF(CCI.EQ.1.) C2=2.839
C      IF(CCI.EQ.2.) C1=1.644E-21
C      IF(CCI.EQ.2.) C2=2.982
C      IF(CCI.EQ.3.) C1=3.912E-21
C      IF(CCI.EQ.3.) C2=2.8758
C      IF(CCI.EQ.4.) C1=4.793E-21
C      IF(CCI.EQ.4.) C2=2.846
C      IF(CCI.EQ.5.) GO TO 4
C      GO TO 7
C      CALL ASCII(DD11,7)

```

THIS PAGE IS BEST QUALITY PRACTICABLE
FROM COPY FURNISHED TO DDG

```

C      CALL MNYINP(C1,C2,D1,D2,D3)
C      INPUT DECTAPE SWITCH #, REGION #
C      IF(C2.EQ.0.)GO TO 5
7      CALL ASCII(CC,2)
C      CALL ASCII(AA,1)
C      CALL ANYINP(SWN)
C      CALL ASCII(BB,1)
C      CALL ANYINP(RGN)
C      OUTPUT DECTAPE SWITCH #, REGION #
C      CALL ASCII(EE,2)
C      CALL ASCII(AA,1)
C      CALL ANYINP(SWO)
C      CALL ASCII(BB,1)
C      CALL ANYINP(RGO)
C      JBN = 20.*(SWN-1.) + 4.*(RGN-2.)
C      JBO = 20.*(SWO-1.)+4.*(RGO-2.)
C      CALCULATE PROTON THRESHOLD ENERGY
C      EPMIN = (X1+X2)*(-C)/X2
C      KTMIN = EPMIN/DE
C      ZERO DATA AND SIGMA MATRICES
C      DO 222 M=1,1024
C      KTOF(M) = 0
C      XSIG(M) = 0
222    CONTINUE
C      READ TOF SPECTRUM
C      WRITE TRANSFORMED SPECTRUM ONTO DECTAPE UNIT 2.
C      CALL DTAPE(1,JBN,0,1024,KTOF(1))
C      DO 224 IX = 1,7
C      TOF(IX) = KTOF(IX)
224    CONTINUE
C      READ PARAMETERS FROM DATA TAPE:DT(FLIGHT TIME,NANOSEC)
C      GAMMA(CHANNEL #),EL(NEUTRON FLIGHT PATH, METERS),
C      UCOUL(INTERGRATED BEAM CURRENT,MICRO COUL),THETA(DEG),
C      EMAX(INCIDENT PROTON ENERGY,MEV)
C      DT = TOF(1)/10000.
C      GAMMA = TOF(2)/100.
C      EL = TOF(3)/1000.
C      UCOUL = TOF(4)/10.
C      THETA = TOF(5)/100.
C      EMAX = TOF(6)/1000.
C      CCP = TOF(7)/100.
C      IF(CCP.EQ.0.0) CCP = 1.000
C      KTMAY = EMAX/DE
C      TOF SCATTERING CORRECTION--SLOPING LINE MWHM 50NSEC/METER
C      MAX CHANNEL AND MAX COUNTS INPUT WITH TOF DATA
C      MAXCHN = KTOF(8)
C      IF(MAXCHN.EQ.0) GO TO 230
C      CNTMAX = KTOF(9)
C      MINCHN = 100.*EL/DT
C      MINCHN = MAXCHN - MINCHN
C      IF(MINCHN-15.LE.0) MINCHN = 15
C      DO 227 ICHNL = MINCHN,MAXCHN
C      T = MAXCHN - ICHNL
C      T = T*DT/EL
C      ICNT = (100.-T) * CNTMAX/100.
C      IF(ICNT.LE.0) GO TO 227
C      VTOF(ICHNL) = VTOF(ICHNL) - ICNT

```

THIS PAGE IS BEST QUALITY PRINTING
 FROM COPY FURNISHED TO DDQ

```

227 CONTINUE
230 OMEGA = 3.1416*(.0315/EL)*(0.0315/EL)
ZERO = GAMMA+3.34*EL/DT
EPK = EPMIN - DE/2.
CALL XINSUB
ENU = ENK
C CALCULATE TRANSFORM
DO 800 XT=XTMIN,XTMAX
XT1 = XT + 1
C CALCULATE THE ENERGIES
XX=XT
EP=DE*XX
EPU=DE*(XX+.5)
ENL=ENU
EPK = EP
CALL XINSUB
EN = ENY
EPK = EPU
CALL XINSUB
ENU = ENY
C RELATIVISTIC CALCULATION OF HISTOGRAM BOUNDARIES
GL = ENL/EU
GU = ENU/EU
BTL = 2.*GL*(1.-3./2.*GL*(1.-4./3.*GL))
B2U = 2.*GU*(1.-3./2.*GU*(1.-4./3.*GU))
BETAL=DSORT(BTL)
BETAU=DSORT(B2U)
TL=EL/(.299793*BETAL)
TU=EL/(.299793*BETAU)
CIL=ZERO-TL/DT
CIU=ZERO-TU/DT
C GET SCATTERING CORRECTION FOR GIVEN EN,THETA -DISREGARD
C FOR B11PN RXN.
SR = 1.
C EFFICIENCY NOW DEFINED
CALL FIT2(EN,EFF)
IF(EFF.LE.0.0) GO TO 800
C CALCULATE DEAD/DY (MEV CM CY) FOR P11 FROM PN TGT CMPD USING
C EMPIRICAL EXPRESSION CALCULATED FROM JANNI VALUES FOR
C BORON AND NITROGEN.
DEADX = C1/EP *(ALOG(EP) + C2)
C CALCULATE THE HISTOGRAM
I1=CIL+.5
I2=CIU+.5
DELTA=CIU-CIL
N=I2-I1
SUM=0.
IF(I1)800,800,28
IF(DELTA-1.)1,1,2
1 IF(N)3,3,2
2 IF(N-1)3,26,6
3 F1=DELTA
F2=.0
GO TO 27
6 N=I1+1
M=I2-1
CO 200 L=V,4

```

THIS PAGE IS BEST QUALITY PRACTICABLE
FROM COPY FURNISHED TO DDC

```

      ICH = I+1
      XDATA = KTOF(ICH)
      SUM = SUM + XDATA
260  CONTINUE
26   XII = I1
      XI2 = I2
      F1 = 0.5 - (CIL-XI1)
      F2 = 0.5 + CIU - XI2
27   ICH = I1+1
      XDATA = KTOF(ICH)
      SUM = SUM + F1*XDATA
      ICH = I2+1
      XDATA = KTOF(ICH)
      SUM = SUM + F2*XDATA
C    UNCERTAINTIES
C    SOURCE SCATTERING UNCERTAINTIES-- % OF INITIAL DATA CORRECTION
C    USE CHANNEL AS AVERAGE OF TWO LIMITS
      SSPR = 0.
      ICHSS = (CIL + CIU)/2.
      TC = MAXCHN - ICHSS
      TC = TC*DT/EL
      IF(TC.LE.0.0) GO TO 733
      IF(TC.GE.100.0) GO TO 733
      TC = (100.-TC)*CNTMAX/100.
      SSPR = KTOF(ICHSS)
      SSPR = TC/(TC+SSPR)
      SSPR = SSPR*SSPR
C    BORON SCATTERING RESONANCE UNCERTAINTIES AS %
733  XLRPR = ABS(1.00 - SR)
      XLRPR = XLRPR*XLRPR
C    COUNTING STATISTICS UNCERTAINTY AS %
      STATPR = 1.0 / SUM
C    COMBINE AND OUTPUT UNCERTAINTIES AS % * 10^4
      KTIP = KT1 + 400
      BTL = STATPR + 0.3*(SSPR + XLRPR)
      KSIG(KTIP) = 1.0E+04*DSQRT(BTL)
C    CALCULATE SIGMA AND DEPOSIT IN KSIG MATRIX
      KSIG(KT1) = DEADX*COR*SR*SUM*CONST/(UCOUL*EFF*DO*EGA*DE)
800  CONTINUE
      DO 850 KL=1,6
      KSIG(KL) = KTOF(KL)
850  CONTINUE
C    WRITE SIGMA ONTO DECTAPE UNIT #2
      CALL DTAPE(2,JBO,1,1024,KSIG(1))
      GO TO 5
      END

```

THIS PAGE IS BEST QUALITY PRACTICABLE
FROM COPY FURNISHED TO DDC

```

C      KINSUB SPC
C      KINEMATICS SUBROUTINE
C      (WITH NAMED COMMON = KINCOM FOR PARAMETER PASSING)
C      MODIFIED 21 SEPT. 1970, CA2
C      PHIL BEVINGTON, STANFORD UNIVERSITY 6/11/65
C      TRANSFORMS ENERGIES, ANGLES, AND CROSS SECTIONS
C      BETWEEN CM AND LAB SYSTEMS
C      SEE NUCLEAR DATA TABLES, PAGES 161,162 FOR NOTATION
C      A1, A2, A3 ARE MASSES (IN AMU) OF INCIDENT, TARGET,
C      AND EMITTED PARTICLES
C      E1 = INCIDENT ENERGY (IN MEV) IN LAB SYSTEM
C      Q = Q OF REACTION (IN MEV)
C      THETACM AND THETALAB ARE EMISSION ANGLE (IN DEGREES)
C      E3CM AND E3LAB ARE ENERGIES OF EMITTED PARTICLE (IN MEV)
C      RATIO = CM CROSS SECTION / LAB CROSS SECTION
C      MODE < 0: INPUT = A1, A2, A3, E1, Q, THETACM
C      MODE = 0: INPUT = A1, A2, A3, E1, THETALAB, E3LAB
C      MODE > 0: INPUT = A1, A2, A3, E1, Q, THETALAB
C      SUBROUTINE KINSUB
C      DOUBLE PRECISION AC, ECEL, FLEC, F3, RT, AAEF
C      COMMON /KINCOM/A1, A2, A3, E1, Q, THETAC, THETAL, E3CM, E3LAB,
C      1 RATIO, MODE
11      IF (MODE) 13, 12, 12
12      SINLAB = SIN(THETAL * 0.0174532925)
13      COSLAB = COS(THETAL * 0.0174532925)
14      A4 = A1 + A2 - A3
15      IF (MODE) 31, 21, 31
16      Q = Q
17      DO 25 I = 1, 3
18      A4 = A4C - Q/931.478
19      AAEF = A1*A3*E1+E3LAB
20      Q = ((A3+A4)*E3LAB + (A1-A4)*E1 - 2.*DSORT(AAEF)
21      1 *COSLAB) / A4
22      ET = E1 + Q
23      IF (ET) 32, 32, 41
24      E3CM = -Q.
25      E3LAB = -0.000
26      RATIO = -Q.
27      IF (MODE.GT.0) THETAC = 0.0
28      RETURN
29      A4 = A4C - Q/931.478
30      DENOM = (A1+A2) * (A3+A4)
31      A = E1 * A1*A4/DENOM
32      B = A * A3/A4
33      C = (ET + C*A1/A2) * A2*A3/DENOM
34      IF (C.LT.0.0) GO TO 32
35      E3CM = C * A4/A3
36      AC = A*C
37      SORTAC = DSORT(AC)
38      IF (MODE) 51, 61, 61
39      SINCM = SIN(THETAC * 0.0174532925)
40      E3LAB = E3CM + B + 2.0*SORTAC*COS(THETAC*0.0174532925)
41      ECEL = E3CM/E3LAB
42      SINLAB = SINCM * DSORT(ECEL)
43      RT = E3CM/B - SINLAB*SINLAB
44      IF (RT) 32, 62, 62

```

THIS PAGE IS BEST QUALITY FRAGMENTS
FROM COPY FURNISHED TO DDC

```

62      ROOT = DSORT(RT)
        IF (MODE) 91, 95, 94
91      CONTINUE
        IF (SINLAB) 92, 92, 93
92      CONTINUE
        THETA = THETAC
        GO TO 100
93      CONTINUE
        ER = E3LAB/R
        COSLAB = DSORT(ER) - ROOT
        THETA = 90. + ATAN(-COSLAB/SINLAB) / 0.0174532925
        GO TO 100
94      CONTINUE
        E3LAB=B*(COSLAB+ROOT)*(COSLAB+ROOT)
95      CONTINUE
        IF (SINLAB) 96, 96, 97
96      CONTINUE
        THETAC = THETA
        GO TO 100
97      CONTINUE
        ELEC = E3LAB/E3CM
        SINCM = SINLAB * DSORT(ELEC)
        COSCM = (E3LAB - E3CM - B) * 0.5/SORTAC
        THETAC = 90. + ATAN(-COSCM/SINCM) / 0.0174532925
100     CONTINUE
        RATIO = SORTAC*ROOT/E3LAB
        RETURN
        END

```

C FIT2

```

SUBROUTINE FIT2(EIN, SIG)
DIMENSION S(250)
COMMON S
EL = S(1)
EC = S(2)
IF(EIN-(EL+EC))20, 21, 21
20     SIG=0.
        RETURN
21     ENTRY=1.+(EIN-EL)/EC
        K=ENTRY+2.
C      FIRST 2 ENTRIES ARE ELOW AND EINC, SO ADD TWO TO POINTERS
        YK=K
        Y0=S(Y-1)
        Y1=S(Y)
        Y2=S(Y+1)
        Y3=S(Y+2)
        Y=ENTRY-YK+3.
        A=(-Y0+3.*Y1-3.*Y2+Y3)
        B=(6.*Y0-15.*Y1+12.*Y2-3.*Y3)
        C=(-11.*Y0+18.*Y1-9.*Y2+2.*Y3)
        SIG=Y0+X*(C+Y*(B+Y*A))/S.
30     RETURN
        END

```

THIS PAGE IS BEST QUALITY PRACTICE
FROM COPY FURNISHED TO DDC

APPENDIX E

Program LSQFT3, Subroutines CBFIT8, LEGPOL and MINV7

```

C      LSQFT3 SRC
C      A LEAST SQUARES PROGRAM THAT FITS A SERIES
C      OF LEGENDE POLYNOMIALS TO BORON 11(P,N) ANGULAR DISTRIBUTIONS
C      INPUT: SIGMA (THETALAB) IN MICROBARN/SP, NO. OF POLYNOMIALS
C      (NPOL, MAX = 6), NO. OF ANGLES (NANGLE, MAX = 11)
C      DE IS ENERGY INTERVAL OF THE INPUT CROSS SECTION IN MEV.
C      INPUT CROSS SECTION MUST BE IN AN INCREASING SEQUENCE OF
C      ANGLES BY SWITCH AND REGION NO. UPPER & LOWER EI LEVELS, PYN
C      MASS & Q VALUES ARE VARIABLE. MODIFIED FROM LSRFIT AUG 78.
C      TOTAL X SECTION ( JO(LG) ) IS DIVIDED BY 10.
C      LEG COEF : JO(L1)*10 + E4 AND ERROR JO(L2)*10
C      USES MODIFIED CBFIT8 AUG 78.
C
C      COMMON JD(5632),JO(3072),ELSD(20,4),A(6,2)
C      COMMON /KINCOM/ A1,A2,A3,EAK,Q,TC,THETA,FNC,ENK,P,MO
C      DATA C1,C2,C3/5HINPUT,5H SW,F,5HEG /
C      DATA B1,B2,B3,B4/5H SW,RE,5HG FOR,5H OUTP,5HUT /
C      DATA B5,B6,B7/5HARRAY,5H STAR,5H TS AT/
C      DATA B8,B9,B10,B11/5H -SWI,5H TCH ,5H -REG,5H ION /
C      DATA C4,C5,C6/5H BORON,5H I1(PN,5H) PYN/
C      DATA C7,C8,C9,C10,C11/5HINPUT,5H O IF,5H NO C,5H HANGE,5H TO * /
C      DATA C12,C13/5H I1,M2,,5H M3,Q /
C      DATA D1,D2,D3,D4,D5/5H NPOL ,5H I MAX ,5H S1, N,5H ANGLE,5H (MAX/
C      DATA D6,D7/5H I11,,5H DE /
C      DATA D8,D9,D10,D11,D12/5H TO E,5H I LIM,5H I TS (,5H J04,4,5H S1) /
C      DATA D12A/5H EI /
C      DATA D13,D14,D15,D16,D17/5H COS(T,5H C) PA,5H D, ER,5H POS. ,5H X SECT
C      DATA D18,D19,D20/5H, CAL,5H LEG ,5H X SECT/
C      DATA C14,C15,C16,C17/5H ANGL,5H E TOO,5H LARG,5H FOR /
C      DATA C18,C19,C20,C21,C22/5H EI RA,5H NGE ,5H TTY C,5H UTPUT,5H DES?
C      DATA C23,C24,C25/5H PED?,5H I O =,5H NO 1/
C      DATA Y1,X2,Y3,X4/1.007825,11.008350,1.008665,-2.763/
C      GIVES PYN & ALLOWS FOR CHANGE OF MASS & Q VALUE.
40      CALL ASCII(C4,3)
C      CALL ASCII(C7,7)
C      CALL MNYINP(AA1,AA2,AA3,GGG,D1)
C      ALLOWS FOR TTY OUTPUT OF X-SECTION.
C      CALL ASCII(C20,6)
C      CALL MNYINP(A DATA,D1,D2,D3,D4)
C      INPUT THE LOCATION OF THE FIRST ANGLE OF THE SERIES.
C      CALL ASCII(C1,3)
C      CALL MNYINP(SW,REG,D3,D1,D2)
C      INPUT THE STARTING LOCATION FOR OUTPUT DATA.
C      CALL ASCII(B1,4)
C      CALL MNYINP(SVO,REGO,D1,D2,D3)
C      INPUT # OF POLYNOMIALS, # OF ANGLES IN SERIES & THE ENERGY INTERVAL
545      CALL ASCII(D1,7)
C      CALL MNYINP(XPOL,YANGLE,DE,D1,D2)
C      NPOL=XPOL+.5
C      NANGLE=YANGLE+.5
C      MO=1
C      A1=Y1
C      A2=Y2
C      A3=Y3

```

THIS PAGE IS BEST QUALITY PRINTING
FROM COPY FURNISHED TO DDC

```

      Q=X4
C   CHANGE OF MASS & Q VALUE IF REQUESTED.
      IF(AA1.EQ.0.) GO TO 541
      A1 = AA1
      A2 = AA2
      A3 = AA3
      Q = Q00
541  CALL ASCII(C7,4)
      IDUM = 311
C   ALLOWS FOR CHANGE OF ENERGY LIMITS.
      CALL ASCII(D8,5)
      CALL MNYINP(XEIL,YEIU,D1,D2,D3)
      IEIL = 304
      IEIU = 451
      IF (XEIL.EQ.0.) GO TO 801
      IEIL = YEIL+.5
      IEIU = YEIU+.5

C
C   CALCULATION OF THE MATRIX REFERENCE #.
C   IEIL & IEIU = ENERGY OF MI LOWER AND UPPER WRT X-SECTION.
C   CONSTANTS ICC1 TO ICC10 ARE FIXED FOR THE GIVEN ENERGY REGION.
C
501  ICC1 = IEIU - IEIL
      ICC2 = 2 + ICC1
      ICC3 = ICC2 + 1 + ICC1
      ICC4 = ICC3 + 1 + ICC1
      ICC5 = ICC1 + 1
      ICC6 = IEIL - ICC3 - 1
      ICC7 = IEIL - ICC2 - 1
      ICC8 = IEIL - 2
      ICC9 = 1025-IEIL
      ICC10 = 2049-IEIL
C   CALCULATION OF MATRIX DIMENSION FOR JD.
      ICC11 = 512*WANGLE
      ICC12 = 512
      ICA = ICC4+2
      IF (ICCA.GT.512) GO TO 601
      GO TO 602
601  ICC11 = 1024 * WANGLE
      ICC12 = 1024
602  IF (ICC11.GT.5632) GO TO 543
      GO TO 544
543  CALL ASCII(C14,6)
      GO TO 545
C   ZERO THE MATRIX AND READONE ANGLE AT A TIME (Y-SECTION, FPROP).
544  RAD = 3.14159/180.
      DO 201 I=1,5632
201  JD(I)=0
      DO 202 I= 1,3072
202  JO(I)=0
      DO 100 IOA=1,WANGLE
      JC=20.*(SW-1.)+4.*(PEG-2.)
      JC=JC+(IOA-1)*4
      CALL DTAPF(1,JC,0,1024,JO(I))
      V=(IOA-1)*ICC12+1
      DO 203 I=IEIL,IEIU
      XD=X+I-IEIL+1

```

THIS PAGE IS BEST QUALITY PRACTICABLE
FROM COPY FURNISHED TO DDG

```

                JD(YD)=JO(I)
                LA = XD + ICC5
203          JD(LA)=JO(I+400)
          C
          C      CONVERT TO CENTER OF MASS SYSTEM
          C
                JD(X)=JO(5)
                THETA=JO(5)/100
                DO 100 I=1,ICC5
                KS=X+I
                EAK=FLOAT(I+ICCR)*DE
                IF(JD(XS).NE.0) GO TO 50
                JD(XS)=10
                LB = XS+ICC5
                JD(LP)=100000
          50          CALL XINSUB
                KDS=XS+ICC5
                XTH=XS+ICC5+ICC5
                JD(XS)=FLOAT(JD(XS))*P
                JD(XDS)=FLOAT(JD(XS))*FLOAT(JD(XDS))/100.
                JD(XTH)=TC*100.
          100         CONTINUE
          C
          C      OUTPUT ON TAPE: X-SECTION CM,ERROR*E4, THETA CM.
          C
                JB=20.*(SWO-1.)+4.*(REGO-2.)
                JP2 = NANGLE*2-1
                CALL DTAPE(2,JB,1,ICC11,JD(1))
          C
          C      CREATE ARRAYS AND DO LEAST SQUARES FIT
          C
                DO 200 I =1,3072
          200         JO(I)=0
                DO 30 L=IE1L,IE1H
                DO 20 I=1,NANGLE
                X=L+(I-1)*ICC12
                LC = X - ICC6
                THETC=FLOAT(JD(LC))/100.
                ELSD(I,1)=COS(THETC*RAD)
                LD = X - ICC7
                ELSD(I,2)=FLOAT(JD(LD))/10.
                LE = X - ICC8
                ELSD(I,3)=FLOAT(JD(LE))
                ELSD(I,2)=ELSD(I,2)*ELSD(I,2)
                IF(ELSD(I,2).EQ.0.0) GO TO 30
                IF(ELSD(I,3).EQ.0.0) GO TO 30
          20          CONTINUE
          25          CALL CBFIT(ELSD, A, XI, NPOL, NANGLE)
                IF (ADATA.EQ.0.) GO TO 22
          C
          C      TTY OUTPUT OF COS(), ERROR, X-SECTION, CALC POLY X-SECTION.
          C
                IF(L .EQ. IDU*) GO TO 205
                GO TO 22
          205         CALL ITYPE(L)
                IDU* = IDU* + 10
                CALL ASCII(C12A,9)

```

THIS PAGE IS BEST QUALITY PRACTICABLE
FROM COPY FURNISHED TO DDC

```

DO 21 IO=1,NANGLE
D1=ELSD(IO,1)
D2=ELSD(IO,2)
D3=ELSD(IO,3)
D4=ELSD(IO,4)
21 CALL XNYOUT(4,D1,D2,D3,D4)
C
C
C
22 CREATE OUTPUT ARRAYS (XI*XI, TOTAL X-SECTION, X-SECTION ERROR).

A4P=4.*3.14159*A(1,1)
LF = L - IEIL + 1
JO(LF)=XI*1000.
LG = L - ICC7 - 1
JO(LG)=A4P/10.
LH = L - ICC6 - 1
JO(LH)=A(1,2)*40.*3.14159
DO 30 J1=2,NPOL
L1=L+ICC9+(J1-2)*ICC5
L2=L+ICC10+(J1-2)*ICC5
JO(L1)=A(J1,1)*10.+50000.
JO(L2)=A(J1,2)*10.
30 CONTINUE
C
C
C
CALCULATION OF THE BLOCK, SW & PEG NO. FOR OUTPUT OF ARRAYS.
JBA = ICC11/256 + 1
JB = JB + JBA
AJB = JB
ISW5 = 1.+(AJB + 4.)/20.
SW5 = ISW5
IRG5 = 2.+(AJB - 20.)*(SW5-1.)/4.
RG5 = IRG5
JB5 = 20.*(SW5 - 1.) + 4.*(RG5 - 2.) + 4.
CALL DTAPE(2,JB5,1,3072,JO(1))
C OUTPUT SW & PEG# FOR START OF OUTPUT ARRAYS - 3 PECIONS - .
CALL ASCII(83,5)
AJB5 = JB5
ISW6 = 1.+(AJB5+4.)/20.
SW6 = ISW6
IPG6 = 2.+(AJB5-20.)*(SW6-1.)/4.
CALL ITYPE(ISW6)
CALL ASCII(88,2)
CALL ITYPE(IPG6)
CALL ASCII(810,2)
LGI = IEIL-ICC7-2
CALL ITYPE(LGI)
CALL ASCII(D20,1)
GO TO 40
END

```

THIS PAGE IS BEST QUALITY FRAGMENT
FROM COPY FURNISHED TO DDC

```

SUBROUTINE CBFITS(ELSD,A,XI,NPOL,ANGLE)
PROGRAM ACCEPTS A VARIABLE NPOL .LE.6 & ANGLE .LE.15 .
C NPOL IS # OF POLYNOMIALS. IF INCREASING IT OVER 6, MUST INCREASE
C DIM'S BELOW. ANGLE IS # OF ANGLES OF INPUT DATA. (DIM FOR 15).
C PROGRAM MODIFIED FROM CBFITS AUG 78, RENAMED THE SAME.
C DIMENSION OF M2(*) MUST = X*Y WHERE M(X,Y).
C DIMENSION OF ELSD & A MUST BE SAME AS IN THE MAIN PROGRAM.
C
DOUBLE PRECISION M,U,DET,M2(36),DEORT
DIMENSION ARG(11),EG(6),L(6),Y(6),U(11)
DIMENSION ELSD(20,4),A(6,2),M(6,6),POLY(11,6)
EQUIVALENCE (M2(1),M(1,1))
DATA SINGU,SINGU2/5M SING,5MULAR /
XNORM=ANGLE/NPOL
DO 10 J=1,ANGLE
ARG(J) = ELSD(J,1)
CALL LEGPOL(EG,ARG(J),NPOL)
DO 10 Y=1,NPOL
POLY(J,Y) = EG(Y)
10
C
C POLY NOW STORES VALUES OF P0 THROUGH P(NPOL-1) AT EACH OF 15 ANGLES
C POLY(15,NPOL)
C
DO 20 J=1,NPOL
DO 20 Y=1,NPOL
20 M(J,Y) = 0.
DO 21 I=1,NPOL
DO 21 J=1,NPOL
DO 21 Y=1,ANGLE
21 M(I,J) = M(I,J) + POLY(K,I)*POLY(Y,J)/ELSD(Y,2)
DO 22 J=1,NPOL
DO 22 I=1,NPOL
K = 1+(J-1)*NPOL
22 M2(Y) = M(I,J)
CALL MINV7(M2,NPOL,DET,L,Y)
IF(DET) 27,25,27
25 CALL ASCII(SINGU,2)
GO TO 100
C
C M IS NOW INVERTED, CALCULATE U
C
27 Y = Y+1
DO 23 J2 = 1,NPOL
DO 23 I2 = 1,NPOL
Y = Y-1
I = NPOL-I2+1
J = NPOL-J2+1
23 M(I,J) = M2(Y)
DO 30 I=1,ANGLE
30 U(I) = 0.0
DO 31 I=1,NPOL
DO 31 J=1,ANGLE
31 U(I) = U(I) + POLY(J,I)*ELSD(J,J)/ELSD(J,2)
C
C CALCULATE THE COEFFS, YI, AND CROSS SECTION
C

```

THIS PAGE IS BEST QUALITY FRAGMENTABLE
FROM GPOY PUBLISHED TO DDC

```

      YISC = 0.
      DO 35 I=1, NPOL
35      A(I,1) = 0.0
      DO 40 I=1, NPOL
      DO 40 J=1, NPOL
40      A(I,1) = A(I,1) + U(J)*H(J,I)
      C
      C NOW XI
      C
      DO 45 I=1, NANGLE
      SIGCLC = 0.
      DO 44 J=1, NPOL
44      SIGCLC = SIGCLC + A(J,1)*POLY(I,J)
      ELSD(I,4) = SIGCLC
      IF(I.GT.NANGLE) GO TO 45
      XI = ELSD(I,3) - ELSD(I,4)
      XI = XI * XI
      YISC = YISC + XI/ELSD(I,2)
45      CONTINUE
      XI = YISC/XNORM
      DO 50 J=1, NPOL
      IF(H(J,J).LT.0.0) H(J,J) = 0.0
      A(J,2) = DSORT(H(J,J))
50      CONTINUE
      C PROGRAM RETURNS WITH CALCULATED YSECT IN ELSD(I,4), COEFFS
      C AND ERRORS IN A(I,J), AND XI
100     RETURN
      END

```

```

      C SUBROUTINE LEGPOL RECURSIVE EVALUATION OF LEGENDRE
      C POLYNOMIALS NPOL = # OF POLYNOMIALS TO RETURN
      SUBROUTINE LEGPOL(POL, ARG, NPOL)
      DIMENSION POL(6)
      XI = ARG
      POL(1) = 1.0
      POL(2) = XI
      N = NPOL - 1
      DO 99 L=2, N
      FL = L
99     POL(L+1) = ((2.*FL-1.)*XI)*POL(L) - (FL-1.)*POL(L-1) / FL
      RETURN
      END

```

THIS PAGE IS BEST QUALITY PRINTING
FROM COPY FURNISHED TO DDC

```

C SUBROUTINE MINV7 -- TAKEN FROM SUBROUTINE MINV OF 300 SCIENTIFIC
C SUBROUTINE PACKAGE
C NOTE DOUBLE PRECISION VARIABLES
C DESCRIPTION OF PARAMETERS
C A - INPUT MATRIX, DESTROYED IN COMPUTATION AND REPLACED
C BY RESULTANT INVERSE
C N - ORDER OF MATRIX A
C D - RESULTANT DETERMINANT
C L - WORK VECTOR OF LENGTH N
C M - WORK VECTOR OF LENGTH N
C
C SUBROUTINE MINV7(A,N,D,L,M)
C DOUBLE PRECISION A,BIGA,HOLD,C,CABS
C DIMENSION A(1),L(6),M(6)
C SEARCH FOR LARGEST ELEMENT
D = 1.0D00
NK = -N
DO 20 K=1,N
  MW = 'W + N
  L(K) = K
  M(K) = K
  MK = MW + K
  BIGA = A(MK)
  DO 20 J=K,N
    IZ = MW(J-1)
    DO 20 I=K,N
      IJ = IZ + I
      IF( DABS(BIGA) - DABS(A(IJ)) ) 15,20,20
15  BIGA = A(IJ)
      L(K) = I
      M(K) = J
20  CONTINUE
C
C INTERCHANGE ROWS
C
C J = L(K)
IF(J-M) 35,35,25
25  MI = M - N
  DO 30 I=1,N
    NI = MI + I
    HOLD = -A(NI)
    JI = MI - K + J
    A(NI) = A(JI)
    A(JI) = HOLD
30  C
C INTERCHANGE COLUMNS
C
C I = M(K)
IF(I-M) 45,45,35
35  JP = M(I-1)
  DO 40 J=1,N
    JV = MW + J
    JI = JP + J
    HOLD = -A(JV)
    A(JV) = A(JI)
    A(JI) = HOLD
40

```

THIS PAGE IS BEST QUALITY PRACTICABLE
FROM COPY FURNISHED TO DDC

```

C
C   DIVIDE COLUMN BY MINUS PIVOT ( VALUE OF PIVOT ELEMENT IS
C   CONTAINED IN B1GA )
C
45  IF(B1GA) 48,46,48
46  D = 0.0000
    RETURN
48  DO 55 I=1,N
    IF(I-K) 50,55,50
50  IK = NW + I
    A(IK) = A(IK) / (-B1GA)
55  CONTINUE
C
C   REDUCE MATRIX
C
    DO 65 I=1,N
    IV = NW + I
    HOLD = A(IK)
    IJ = I - N
    DO 65 J=1,N
    IJ = IJ + N
    IF(I-K) 60,65,60
50  IF(J-K) 62,65,62
62  VJ = IJ - I + K
    A(IJ) = HOLD*A(VJ) + A(IJ)
65  CONTINUE
C
C   DIVIDE ROW BY PIVOT
C
    VJ = V - N
    DO 75 J=1,N
    VJ = VJ + N
    IF(J-K) 70,75,70
70  A(KJ) = A(VJ) / B1GA
75  CONTINUE
C
C   PRODUCT OF PIVOTS
C
    D = D*B1GA
C
C   REPLACE PIVOT BY RECIPROCAL
C
    A(KK) = (1.0000) / B1GA
    CONTINUE
80  C
C
C   FINAL ROW AND COLUMN INTERCHANGE
C
    K = N
    K = K - 1
100  IF(V) 150,150,105
    I = L(V)
105  IF(I-K) 120,120,108
108  JC = NW(V-1)
    JP = NW(I-1)
    DO 110 J=1,N
    JK = JC + J
    HOLD = A(JV)

```

THIS PAGE IS BEST QUALITY PRACTICES
FROM GUY F. PUBLISHED TO DDC

```
JI = JP + J
A(JM) = -A(JI)
110 A(JI) = HOLD
120 J = M(N)
IF(J-N) 100,100,125
125 NI = N - N
DO 130 I=1,N
NI = NI + N
HOLD = A(NI)
JI = NI - N + J
130 A(NI) = -A(JI)
A(JI) = HOLD
GO TO 100
150 RETURN
END
```

THIS PAGE IS BEST QUALITY PRACTICABLE
FROM COPY FURNISHED TO DDC

APPENDIX F

Program SIBPRP and Subroutine HISTO

```

C      SIBPRP SRC
C      MODIFIED APRIL 1979 FROM NBLPRC, PROF. QUEFLEY 4-75
C      CALCULATES BORON PROFILING IN PURE SILICON TARGETS
C      USING B11(PN)11C REACTION.
C      ORDINATE IS CONCENTRATION (#BORON/(#BORON + #SI)) *EE
C      ABSCISSA IS IN MICRONS (PX)
C
C      DIMENSION NTE(1024), NTSAM(1024), IBPRO(1024),RPS(5),RPP(5)
C      COMMON NTE, NTSAM, IBPRO
C      DATA A1,A2,A3,A4/5HSIBPR,5HP P(P,5HN)C ,5H 4/79/
C      DATA B1,B2,B3,B4/5H INPU,5HT SAM,5HMLE S,5HV # =/
C      DATA C1,C2/5HRGN#=#,5H DY= /
C      DATA D1,D2,D3,D4/5H INPU,5HT BOP,5HON ,5H5W#=# /
C      DATA E1,E2,E3/5H OUTP,5HUT S,5HV # =/
C      DATA CC1,CC2,CC3,CC4/0.007036,120.2858,355.7498,110.2858/
1     CALL ASCII(A1,4)
C     INPUT TIME OF FLIGHT SPECTRUM FROM DT1
C     CALL ASCII(B1,4)
C     CALL ANYINP(SVI)
C     CALL ASCII(C1,1)
C     CALL ANYINP(RGN)
C     INPUT SAMPLE DEPTH INCREMENT IN MICRONS (DY).
C     CALL ASCII(C2,1)
C     CALL ANYINP(DY)
C     DY=DY/10000.
C     JS=20.+(SVI-1.)+4.+(RGN-2.)
C     INPUT STANDARD (PURE) BORON TOF SPECTRUM FROM DECTAPE 1
C     CALL ASCII(D1,4)
C     CALL ANYINP(SVI)
C     CALL ASCII(D1,1)
C     CALL ANYINP(RGN)
C     JL=20.+(SVI-1.)+4.+(RGN-2.)
C     INITIALIZE INPUT AND OUTPUT ARRAYS TO ZERO
C     DO 100 I=1,1024
C     NTE(I)=0
C     NTSAM(I)=0
C     IBPRO(I)=0
100    CONTINUE
C     CALL STAPE(1,JS,0,1024,NTSAM(1))
C     CALL STAPE(1,JL,0,1024,NTE(1))
C     INPUT TIME OF FLIGHT SPECTRA SHOULD BE LABELED WITH PUNNING
C     PARAMETERS AS FOLLOWS: CH 0=CHANNEL WIDTH IN PSEC; CH 1 =
C     GAMMA RAY CHANNEL TIMES TEN; CH 2= FLIGHT PATH IN CM; CH 3=
C     INTEGRATED PROTON BEAM CURRENT IN UCOUL; CH4=PROTON ENERGY MEV * 1000
C     DO 200 I=1,5
C     RPP(I)=NTE(I)
C     RPS(I)=NTSAM(I)
200    IBPRO(I)=NTSAM(I)
C     CALCULATE ZERO TIME FOR EACH TOF SPECTRUM
C     ?R=RPP(2)/10.+33.4+RPP(3)/RPP(1)
C     ?SAM=NTSAM(2)/10.+33.4+RPP(3)/RPP(1)
C     FPM=RPP(5)/1000.
C     SET CONCENTRATION EQUAL TO ZERO.
C     R=0.
C     SAMPLE NUMBER DENSITY FOR SILICON (BORON = 128.14 E+21)

```

THIS PAGE IS BEST QUALITY PRACTICABLE
FROM COPY FURNISHED TO DDC

```

201   SND=49.97E+21
C   START ENERGY OF PROTON TEN STEPS INFRONT OF TARGET.
DO 150 I=1,10
   EPSAM=3.481E-21*(ALOG(EPH)+2.319)/EPH
150   EPH=EPH+SND*(EPSAM)*DX
C   CALCULATE CONCENTRATION AS A FUNCTION OF DEPTH (DX)
DO 300 I=11,1024
C   CALCULATE STOPPING POWER FOR BORON & SILICON
C   NOT PER 11B ATOM AS WAS DONE IN X-SECT.
202   EPSB=1.324E-21*(ALOG(EPH)+2.965)/EPH
   EPSAM=3.481E-21*(ALOG(EPH)+2.319)/EPH
   EPSBA=EPSB/EPSAM
C   CALCULATE THE NEW ENERGY OF THE PROTON BASED ON THE
C   CONCENTRATION OF THE BORON PRESENT USING CURRENT CONCENTRATION
C   AND STOPPING POWER.
220   IF(R-1.) 203,204,204
203   EPL=EPH-SND*(EPSAM+R*EPSB/(1.0-R))*DX
   GO TO 205
204   EPL=EPH-128.14E+21*EPSB*DX
205   IF(EPL-3.0R) 301,206,206
C   CALCULATE NEUTRON ENERGY FROM KINEMATICS FOR 0 DEG & GIVEN EP
206   ENL=CC1+EPL*(CC2-CC3/EPL+2.*SQRT(CC4-CC3/EPL))
   ENU=CC1+EPH*(CC2-CC3/EPH+2.*SQRT(CC4-CC3/EPH))
C   CALCULATE NEUTRON CHANNEL # (RELATIVISTICALLY) FOR SAMPLE
   TLS=0.7236*PPS(3)/SQRT(ENL)
   TUS=0.7236*PPS(3)/SQRT(ENU)
   CILS=75AM-TLS*1000./PPS(1)
   CIUS=75AM-TUS*1000./PPS(1)
   IF(CILS) 301,301,230
C   CALCULATE # OF COUNTS BETWEEN GIVEN CHANNELS, FOR SAMPLE SPECTRUM
230   CALL HISTO(CILS,CIUS,NTSAM,SUMSAM)
C   CALCULATE NEUTRON CHANNEL # (RELATIVISTICALLY), FOR BORON SPECTRUM
   TLB=0.7236*PPB(3)/SQRT(ENL)
   TUB=0.7236*PPB(3)/SQRT(ENU)
   CILB=7B-TLB*1000./PPB(1)
   CIUB=7B-TUB*1000./PPB(1)
   IF(CILB) 301,301,240
C   CALCULATE # OF COUNTS BETWEEN GIVEN CHANNELS, FOR BORON SPECTRUM
240   CALL HISTO(CILB,CIUB,NTB,SUMB)
C   CALCULATE CONCENTRATION
   R0=RPP(4)*EPSAM*SUMSAM/(RPP(3)*RPP(3))
   R2=RPS(4)*EPSB*SUMB/(RPS(3)*RPS(3))
   R1=R0/(R0-R0*EPSBA+R2)
   IF(R1) 1,200,200
208   IF(F1.GT.1.0) R1=1.0
   COMP=(R1-R)/R1
   R=R1
C   CHECK TO BE SURE THAT NEW R IS WITHIN 1% OF THE OLD R
   IF((COMP.GT.0.01).OR.(COMP.LT.-0.01)) GO TO 220
200   IERPRO(1)=R*1.0E+8
   EPH=EPL
300   CALL LITFS(1)
CONTINUE
C   OUTPUT SW & RGN ON DT1
301   CALL ASCII(F1,3)
   CALL ANYIMP(SYI)
   CALL ASCII(C1,1)

```

THIS PAGE IS BEST QUALITY PRACTICABLE
FROM COPY FURNISHED TO DDC

```

CALL ANYIN(PGN)
JC=20.*(SWI-1.)+4.*(RGN-2.)
CALL DTAPE(1,JC,1,1024,ISPRO(1))
C OUTPUT STARTS IN SPA CHANNEL 10. FRONT SURFACE OF TARGET IS
C NOMINALLY IN SPA CHANNEL 20. ORDINATE IS CONCENTRATION TIMES E+8.
GO TO 1
STOP
END

```

```

SUBROUTINE WISTO(CIL, CIU, NTOF, SUM)
DIMENSION NTOF(1024)
I1 = CIL+.5
I2 = CIU+.5
DELTA = CIU-CIL
M = I2-I1
SUM = 0.0
IF(I1)10,10,1
1 IF(DELTA-1.)2,2,3
2 IF(M)4,4,3
3 IF(N-1)4,7,5
4 F1 = DELTA
F2 = 0.0
GO TO 3
5 N1 = I1+1
N2 = I2-1
DO 6 L=N1, N2
ICM = L+1
YDATA = NTOF(ICM)
SUM = SUM+YDATA
7 YI1 = I1
YI2 = I2
F1 = 0.5*(CIL-YI1)
F2 = 0.5*(CIU-YI2)
ICM = I1+1
YDATA = NTOF(ICM)
SUM = SUM+F1*YDATA
ICM = I2+1
YDATA = NTOF(ICM)
SUM = SUM+F2*YDATA
10 RETURN
END

```

THIS PAGE IS BEST QUALITY PRACTICABLE
FROM COPY FURNISHED TO DDC

REFERENCES

1. F. Ajzenberg-Selvove, Nuclear Physics A 248, 1 (1975).
2. J. P. Blaser, F. Boehm, P. Marmier and P. Scherrer, Helv. Phys. Acta 24, 465 (1951).
3. J. K. Bair, J. D. Kington and H. B. Willard, Phys. Rev. 100, 21 (1955).
4. J. H. Gibbons and R. L. Macklin, Phys. Rev. 114, 571 (1959).
5. J. B. Marion, T. W. Bonner and C. F. Cook, Phys. Rev. 100, 91 (1955).
6. G. J. F. Legge and I. F. Bubb, Nucl. Phys. 26, 616 (1961).
7. R. E. Segel, S. S. Hanna and R. G. Allas, Phys. Rev. 139, B818 (1965).
8. J. C. Overley and R. R. Borchers, Nucl. Phys. 65, 156 (1965).
9. L. Van der Zwan and K. W. Geiger, Nucl. Phys. A 306, 45 (1978).
10. J. C. Overley, R. P. Ebright, and H. W. Lefevre, IEEE Transactions on Nuclear Science NS-26, 1624 (1979).
11. C. A. Burke, Ph. D. Thesis, University of Oregon, 1972 (unpublished).
12. J. C. Overley, private communication.

13. J. F. Janni, Air Force Weapons Laboratory Tech. Report No. AFWL-TR-150 (1966) (unpublished).
14. E. Segre, Experimental Nuclear Physics, John Wiley & Sons, Inc., New York, Vol. 1, 168 (1953).
15. Weast, Handbook of Chemistry and Physics, 52nd Ed., Chemical Rubber Co., Ohio, F 18 (1972).
16. M. T. Lunnon, Ph. D. Thesis, University of Oregon, 1974 (unpublished).
17. P. R. Bevington, W. W. Roland, and H. W. Lewis, Phys. Rev. 121, 871 (1961).
18. R. R. Borchers and C. H. Poppe, Phys. Rev. 129, 2679 (1963).
19. H. Liskien and A. Paulsen, Atomic Data and Nuclear Data Tables, 15-1, 58 (1975).
20. H. W. Lefevre, The Absolute Neutron Spectrum to $E_n = 2.4$ MeV from the (p,n) Reaction in Thick Lithium Metal Target, (unpublished).
21. D. J. Hughes and R. B. Schwartz, Neutron Cross Sections, 2nd Ed., Associated Universities, Inc., Brookhaven National Lab, New York, 38 (1958).
22. J. C. Overley and H. W. Lefevre, Proc. Symposium Radiation Effects on Solid Surfaces, N. Kaminsky, Ed., American Chemistry Society, Washington, D. C., 282 (1976).

23. J. C. Overley and H. W. Lefevre, Scientific and Industrial Applications of Small Accelerators, Fourth Conference-1976, J. Duggan and I. Morgan, Ed., IEEE, New York, NY, 76 CH 1175-9NPS, 557 (1976).
24. C. A. Barns, J. C. Overley, Z. E. Switkowski, and T. A. Tombello, App. Phys. Lett., 31, 239 (1977).
25. C. W. White, J. Narayan, R. T. Young, Science 204, 461 (1979).
26. K. Wittmaack, J. Maul and F. Schulz, Ion Implantation in Semiconductors and Other Materials, B. L. Crowder, Ed., Plenum Press, New York, 147 (1973).
27. D. Lecrosnier, J. Paugam and J. Gallou, Appl. Phys. Letters, 30, 323 (1977).
28. D. Eirug Davis, Appl. Phys. Letters, 13, 243, (1968).
29. D. Elrug Davis, Can. J. Phys., 47, 1750 (1969).
30. H. Ryssel, H. Kranz, K. Muller, R. Henkelmann and J. Biersach, Appl. Phys. Letters, 30, 399 (1977).
31. Y. Ohmura, K. Koike and H. Kobayashi, Ion Implantation in Semiconductors, Susumu Namba, Ed., Plenum Press, New York, 183 (1974).
32. Y. Akasaka and K. Horie, Ion Implantation in Semiconductors and Other Materials, B. L. Crowder, Ed., Plenum Press, New York, 183 (1974).

TYPIST: Laura Kay Littlejohn